MULTI-QUADRANT PERFORMANCE SIMULATION FOR SUBSONIC AXIAL FLOW COMPRESSORS

Werner van Antwerpen

B.Eng (Mechanical Engineering)

Thesis submitted in partial fulfilment of the requirements for the degree

Master of Engineering

School of Nuclear Engineering

at

North-West University

Potchefstroom Campus

Promoter: Prof. P.G. Rousseau

Mr. B. du Toit

Potchefstroom

2007

NORTH-WEST UNIVERSITY
YUNIBESITI YA BOKONE-BOPHIRIMA
NOORDWES-UNIVERSITEIT

EXECUTIVE SUMMARY

Name: Werner van Antwerpen

Title: Multi-Quadrant Performance Simulation for Subsonic Axial Flow Compressors

Date: May 2007

The emergence of closed–loop Brayton cycle power plants, such as the PBMR, resulted in the need to simulate start-up transients for industrial multi-stage axial flow compressors operating at subsonic conditions. This implies that the delivery pressure and power requirements must be predicted for different mass flow rates and rotational speeds while operating in the first and fourth quadrants on the compressor performance charts.

Therefore, an analytical performance prediction model for subsonic multi-stage axial flow compressors had to be developed that can be integrated into a generic network analysis software code such as Flownex. For this purpose, performance calculations based on one-dimensional mean-line analysis demonstrated good accuracy, provided that the correct models for losses, incidence and deviation are used. Such a model is therefore the focus of this study.

A preliminary analytical performance prediction code, with the capability of interchanging between different deviation and loss models is presented. Reasonably complex loss models are integrated in association with the correct incidence and deviation models in a software package called "Engineering Equation Solver" (EES). The total pressure loss calculations are based on a superposition of theoretically separable loss components that include the following: blade profile losses, secondary losses and annulus losses. The fundamental conservation equations for mass, momentum and energy for compressible "rotating pipe" flow were implemented into the performance prediction code. Performance prediction models were validated against experimental data and evaluated according to their ease of implementation. Verification was done by comparing simulation results with experimental work done by Von Backström. This includes a calculation to determine the uncertainty in the experimental results.

Furthermore, since the conventional definition of isentropic efficiency breaks down at the boundaries of quadrants on the performance charts, a new non-dimensional power formulation is presented that allows for the calculation of the compressor power in all of the relevant quadrants.

Good comparison was found between simulation results and measurements in the first and fourth quadrant of operation.

Keywords: Loss, axial flow compressor, quadrant, subsonic, mean-line, start-up, simulation

UITTREKSEL

Naam: Werner van Antwerpen

Titel: Multi-Kwadrant Werkverrigting Simulasie vir Subsoniese Aksiaal Vloei Kompressors

Datum: May 2007

Met die ontwikkeling van geslote Brayton siklus krag stasies, soos die PBMR, is die behoefte geïdentifiseer om transiente tydens die aanskakeling van multi-stadium aksiaal vloei kompressors by subsoniese kondisies te simuleer. Dit bring mee dat druk en drywing vereistes voorspel moet word vir verskillende massa vloeie en rotasionele spoede. Dit sal gedoen word tydens werking in die eerste en vierde kwadrant op die kompressor werkverrigtings kaarte.

'n Analitiese werkverrigting model vir subsonies multi-stadium aksiaal vloei kompressors moet dus ontwikkel word wat in 'n generiese netwerk analise sagteware pakket soos Flownex geïmplementeer kan word. Daar is gevind dat werkverrigtingsberekeninge gebaseer op elementêre eendimensionele voorspellings, by die gemiddelde radius, merkwaardige akkuraatheid kan oplewer, mits geskikte modelle vir die verliese en die afwykings hoeke by die inlaat en uitlaat gebruik word. Sulke modelle is dus die fokus van hierdie studie.

'n Voorlopige kode, vir die voorspelling van kompressor werkverrigting, is voorgestel en het die vermoë om tussen verskillende verlies en deviasie modelle te ruil. Redelike komplekse verlies en afwykings hoek modelle is geïmplementeer in 'n sagteware pakket genaamd "Engineering Equation Solver" (EES). Die totale druk verlies berekeninge is gebaseer op 'n superposisie van verskillende teoretiese komponente naamlik: lem profiel verliese, sekondêre verliese en annulus verliese. Die behoudswette vir massa, momentum en energie vir saamdrukbare "roterende pyp" vloei was in die werkverrigtings model geïmplementeer. Werkverrigtings modelle was gevalideer teen eksperimentele data en geëvalueer met betrekking tot graad van gemaklikheid tydens implementering in die simulasie kode. Resultate is verder vergelyk met eksperimentele werk gedoen deur Von Backström. 'n Berekening is ook gedoen om die onsekerheid in die eksperimentele data te kry.

Verder, omdat die konvensionele definisie van isentropiese effektiwiteit ongeldig raak naby die grense van die kwadrante op die werkverrigtings kaarte, is 'n nuwe dimensielose drywing geformuleer. Dit geld vir die akkurate berekening van kompressor drywing in al die kwadrante.

'n Goeie vergelyking was gevind tussen simulasie en eksperimentele resultate in die eerste en vierde kwadrant.

Sleutelwoorde: Verlies, aksiaal vloei kompressor, kwadrant, subsonies, simulasie

ACKNOWLEDGEMENTS

I thank my Heavenly Father who heard all my prayers as well as all the opportunities and talents he gave me. Without him nothing was possible!

I would also like to thank my parents who gave me the opportunity to go to university and all the love and guidance they gave me.

Furthermore, I would like to thank my two promoters for all their professional guidance and willingness to help making this study a great success.

Finally, a special thanks to Leandré for her love and understanding. Her prayers contributed greatly to the successful completion of this study.

INDEX

LIST OF FIGURES

LIST OF TABLES

NOMENCLATURE

Variables	
a	Factor in equation for equivalent diffusion ratio
A^*	Minimum loss area contraction ratio
A	Flow area
BF	Blockage Factor
C	Absolute velocity
c	Axial chord length
c_p	Specific heat
c_m	Cetin *et al.* off-design correction coefficient
D_{eq}	Equivalent diffusion ratio
Δp_{0L}	Stagnation pressure loss coefficient
g	Newton gravitational constant
H_2	Wake form factor
h	Enthalpy, Blade height
I_1, I_2, I_3	Coefficients used in throat width calculation
i	incidence angle
k_{CLA}	Centreline average of roughness particles
k_s	Equivalent sand roughness
L	Finite length
m, m_1, m_2	Coefficients for optimum deviation angle calculation Wright and Miller
$\dot{m}$	Mass flow rate
Ma	Mach number
n	Slope of variation in minimum loss incidence angle with camber
N	Rotational speed in revs per minute, Newton
o	Throat width
p	Pressure
$\dot{\mathbb{Q}}_c$	Power
$\dot{\mathbb{Q}}$	Non-dimensional power
r	Radius
R	Gas constant
Re	Reynolds number
s	Blade pitch length
t	Blade thickness
T	Temperature
U	Blade speed
V	Relative velocity
$\mathbb{V}$	Volume
Y	Tip/Hub diameter ratio (D_t/D_h)
Z	Torque
CE	Conservation equations
CFD	Computed Fluid Dynamics
EES	Engineering equation solver
HHT	High temperature nuclear reactor with helium gas turbines
I,DM	Incidence and deviation models
LE	Leading edge
LM	Loss Models
PBMR	Pebble bed modular reactor
TE	Trailing edge

VT	Velocity triangles
Greek symbols	
α	Relative outside flow angle, Angle of attack
β	Relative flow angle, Conservation equation
$\partial\beta$	Operating range
δ	Deviation angle
ϵ	Turning
δ^*	Boundary layer displacement thickness
Δ	Blockage
Φ	Correctional slope factor
Γ	Blade circulation
γ	Specific heat ratio
η_c	Compressor efficiency
μ	Viscosity
θ	Absolute flow angle, Boundary layer momentum thickness
θ_{camber} , φ	Blade camber angle
ρ	Density
σ	Blade solidity = c/s
ω	Pressure loss coefficient, Rotor angular velocity
Ω	Axial velocity ratio
ζ	Blade stagger angle
Subscripts	
-	Averaged value
0	Stagnation condition
1	Inlet into blade rotor or stage
2	Outlet from rotor and inlet to stator
3	Outlet from stator and stage
a	Annulus loss, Axial component
B	Blade metal angle, Bursting
c	Compressor, Chord
ch	Chocking
cr	Critical value
e	Outlet of bladerow
hb	Hub
i	Inlet of bladerow
inc	incidence
Ma	Mach number
max	Maximum condition or value
min	Minimum condition or value
opt	Optimum
p	profile
ps	Throat region
R	Rotor
r	Relative frame
Re	Reynolds number
ref	Reference values
r.m.s.	Root mean square
S	Stator
s	Secondary loss
st	Stall
t	Tip
te	Trailing edge

w	Tangential component
x,y,z	Cartesian coordinates with z in the axial direction
Superscripts	
*	Reference condition, Ideal condition

CHAPTER 1

INTRODUCTION

"We still do not know one thousandth of one percent of what nature has revealed to us."

(Albert Einstein)

1.1 BACKGROUND

Brayton cycle power plants such as the Pebble Bed Modular Reactor (PBMR) consist of a general network of components. One such component is the axial flow compressor which provides a pressure rise in the fluid. This ensures flow through the closed-loop Brayton cycle for cooling of the heat source (reactor) and generating of electricity (Figure 1.1).

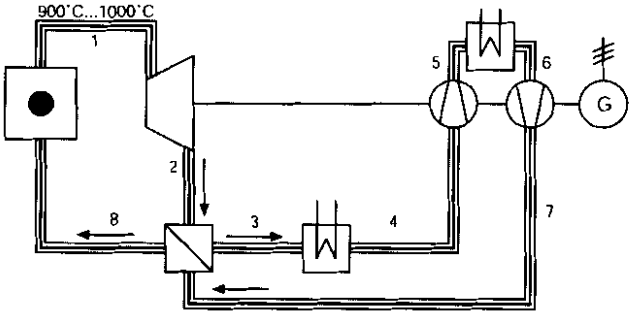

Figure 1.1 Gas turbine process (Brayton cycle) flow sheet, with one-shaft machine and a LP and HP axial flow compressor (Kugeler *et al.*, 2006:Ch.7,10)

Multi-stage axial flow compressors are generally used in a wide spectrum of engineering applications. Therefore it is critical that the simulation of compressor performance charts correspond to the latest technology of the day.

Turbomachines has a designed direction of rotation, a preferred flow direction and a positive or negative pressure difference across it. During abnormal operating conditions turbomachines can also operate at other off-design combinations of rotation, flow direction and pressure difference. This results in operation in all four quadrants of a general performance chart of pressure difference on the y-axis versus mass flow rate on the x-axis.

Gamache (1985:44) noticed in 1985 that during the past two decades, the development of the nuclear power industry has helped spark renewed interest in the phenomenon of reverse flow in turbomachinery. Most of this new interest was based in Germany in response to a German federal program from the 70's and 80's. The program's focus is to develop nuclear closed-loop gas turbine power generation technology. This cycle involves the use of a high temperature nuclear reactor and helium gas turbines. As a result, the German HHT conducted research in turbomachinery operating in reverse flow. This has been primarily directed towards the four quadrant performance of gas turbine stages. According to Bammert and Zehner (1980), all imaginable cases of operation can be described with the aid of a four-quadrant characteristic field which encompasses the range of positive and negative flow direction and rotation direction of the turbine rotor.

The PBMR technology originated from Germany, thus the motives for investigating turbomachinery in multiple quadrants are obvious. However, nuclear related research was ended after the Chernobyl accident in 1986. This is one of the main reasons for the limited literature on four quadrant operation of turbomachinery.

The normal designed operation of an axial flow compressor is confined to the positive direction of rotation and positive pressure difference across it. Varying the power output in a closed-loop Brayton cycle power plant due to electricity demands, often change the fluid conditions at the inlets of all the axial flow compressors. Therefore, design conditions of an axial flow compressor cannot be met at all instances. Thus, axial flow compressor performance charts are a graphical representation of the machine's performance over a range of ambient conditions, rotational speeds and mass flow rates.

Flownex (M-Tech Industrial (Pty) Ltd., 2006) is a general simulation network analysis code that solves the flow, pressure and temperature distribution in arbitrary-structured thermal-fluid networks. Flownex currently uses turbomachine performance charts obtained from the manufacturer to predict the performance of an axial flow compressor.

This method is, however not always satisfactory for two reasons:

- Turbomachine manufacturers are often reluctant to supply detail performance information about their products and therefore the required performance charts might not always be available.
- Details of abnormal operating conditions such as accidental or start-up transients in a closed-loop cycle can be shown in multiple quadrants, not supplied by the manufacturer.

To resolve these unforeseen issues, an analytical performance prediction model should be developed from fundamental principles. This gives the advantage that only the axial flow compressor and blade geometrical specifications needs to be known. The model can then be integrated into the generic Flownex source code.

Although fundamental axial flow compressor performance prediction models are routinely used within the gas turbine industry only few are discussed in open literature. Some examples of performance prediction models discussed in open literature are:

- Streamline curvature method.
- Matrix throughflow method.
- Mean-line prediction method.

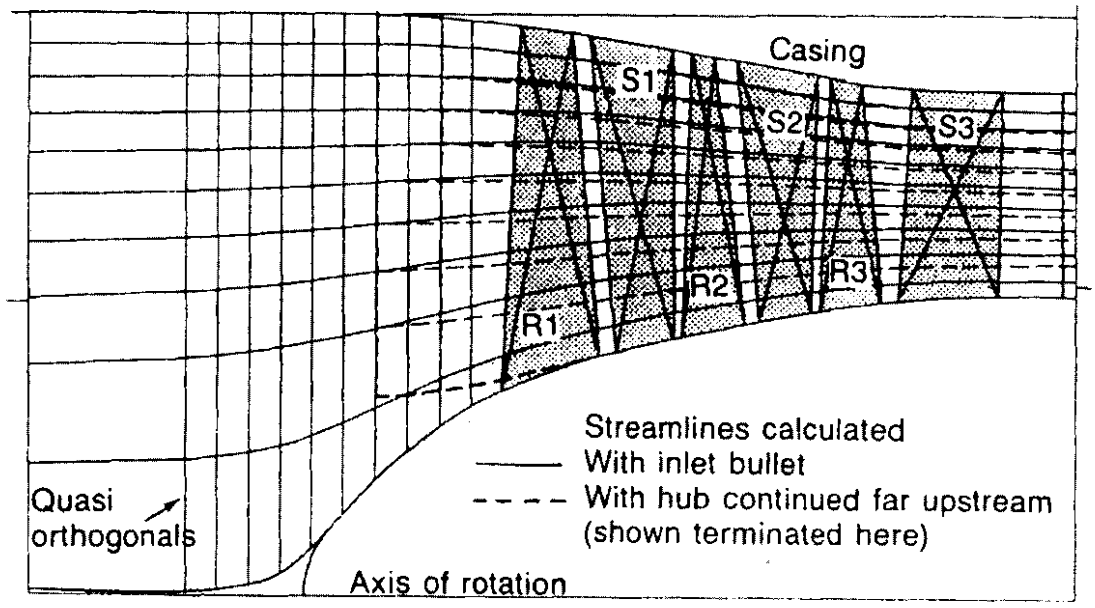

Figure 1.2 Computed meridional streamlines for a three-stage transonic compressor of low hub – casing ratio, with and without inlet bullet (Cumpsty, 1989:116)

The streamline curvature and matrix throughflow method calculates flow in two dimensions (axial – radial plane). It also average out the variations that occur in the circumferential direction. There appears to be little relative advantage (and indeed no fluid mechanical difference) between the streamline curvature and matrix throughflow methods, but it does appear that the streamline curvature method is overwhelmingly the more popular of the two according to Cumpsty (1989:112).

Figure 1.2 present some results from a throughflow calculation for a three – stage transonic axial flow compressor. Two geometries have been investigated, one with an inlet bullet (such as the front of a jet engine might have) and the other with an upstream annulus. A meridional view is given in Figure 1.2 for the two geometries together with the quasi-orthogonals and the computed streamline shapes (Cumpsty, 1989:115).

There are many methods to improve performance prediction of an axial flow compressor over the mean-line approach. However, each assumption that is removed from the mean-line approach brings two main disadvantages:

- Firstly, more data for the stage geometry must be specified, and not all of this data is always available (for example, variation of blade profile with radius and annulus shape).
- Secondly, additional correlations are required (for example, for the distribution of losses

and for streamtube contraction and secondary flow effects on the deviation angle).

These changes bring only a small improvement in accuracy for calculations involving well-designed blades.

Researchers (Lieblein 1959:387, Casey 1987:273 & Wright and Miller 1991:69) demonstrated that performance calculations based on an elementary one-dimensional mean-line prediction method could achieve good accuracy if used in certain boundaries. This is also the preferred method used in this thesis for simulation of the Rofanco axial flow compressor. The argument behind choosing this method is further elaborated in Chapter 2.

1.2 OUTCOMES OF THE STUDY

Axial flow compressor performance charts consist of four quadrants (Figure 1.7 (a)). A detailed study of the first and fourth quadrant was necessary to gain confidence in attempting performance prediction for axial flow compressors in a start-up transient or operation far removed from the design point. The following outcomes were subsequently identified:

1. To understand the operational modes of an axial flow compressor in the first and fourth quadrant of a four quadrant performance chart (Figure 1.7 (a)).
2. To comprehensively understand the mechanisms and sources that causes loss as well as the flow direction changes in each blade row for the first and fourth quadrant.
3. To generate a mean-line performance prediction code. The emphasis falls on subsequently generating a performance chart in the first and fourth quadrant with given axial flow compressor geometrical specifications. This code can also be used to predict and investigate axial flow compressor performance for any given number of stages, blade and physical axial flow compressor geometry.
4. To acquire physical data to compare simulation to experimental results, subsequently testing the validity of the loss and flow directional models obtained in open literature.
5. To introduce a new non-dimensional power term. Isentropic efficiency of a compressor breaks down at the boundaries of quadrants on the performance charts. Thus a new and more generically applicable representation of the work transfer rate to and/or from the axial flow compressor is established.

1.3 THE AXIAL FLOW COMPRESSOR

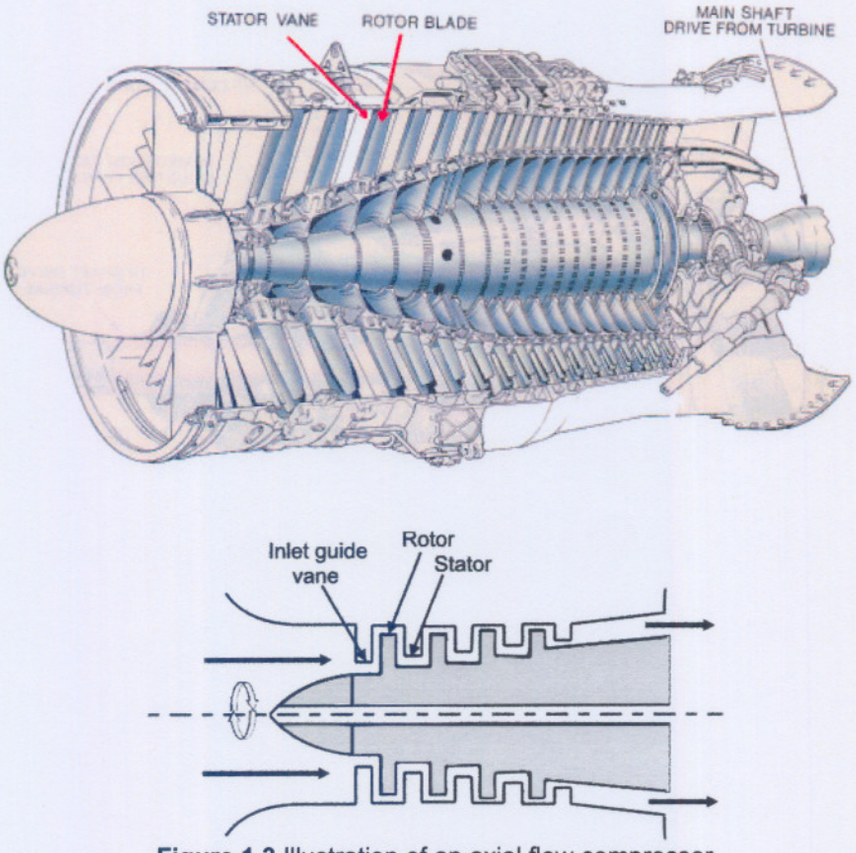

Figure 1.3 Illustration of an axial flow compressor

It is important to distinguish between a compressor and a turbine. A compressor does work on the fluid, while turbines extract work from the fluid. Thus, the difference is based on whether the torque applied to the rotor is in the direction of rotation (compressors) or against rotation (turbines) as explained by Von Backström (2005:P1,2). This implies that the angular momentum of the flow leaving the rotor increases with flow in either the direction of rotation (compressors) or in the opposite direction (turbines). In principle, a machine designed as a compressor can also operate as a turbine and vice versa.

The main function of an axial flow compressor is to transfer work to the fluid, resulting in a pressure and temperature rise. Modern industrial axial flow compressors consist of a rotating rotor and stationary stator blades. A stage consists of a combined rotor and stator blade row. The rotating blade row (rotor) is attached to a central rotating shaft, while the stationary blade row (stator) is fastened to the inner compressor casing. Work is done on the fluid by means of the rotor that changes the tangential velocity and swirl component as described by Lieblein

(1959:387). The working fluid is initially accelerated by the rotor blades, and then decelerated in the stator blade passages wherein the kinetic energy transferred in the rotor is converted to static pressure. The process is repeated in as many stages as are necessary to yield the required overall pressure ratio.

One other aspect of an axial flow compressor is that of the blade profile types used in the industrial and aerospace industry. The most common blade profiles are the American NACA 65-series, the circular arc British C-series (C.4),(C.1) and the double (DCA) and multiple (MCA) circular arc profiles. According to Cumpsty (1989:144) and Cetin *et al.* (1987:6), the NACA 65-series and C-series profiles are used for inlet relative Mach numbers smaller that 0.75, while DCA or MCA profiles are used for transonic inlet relative Mach numbers. Cumpsty (1989:483) also suggested that the camber line shape for the C-series profiles can be classified as 'C' or 'P' respectively implying a circular arc or parabolic arc camber. Figure 1.4 illustrates various thickness distributions for different blade profiles.

Similarities arise when comparing the NACA 65-series with the C-series blade profiles using the same thickness to chord ratio. Felix and Emery (1953:1) tested C.4 and NACA 65 blades of the same thickness to chord ratio and camber at low Mach numbers. As a result, they found that the C.4 and NACA 65 blades behave very similarly with virtually identical losses, but with a slightly wider operating range for the C.4 profile. The operating range is graphically described in Figure 4.3 and the blade terminology is presented in Figure 2.6.

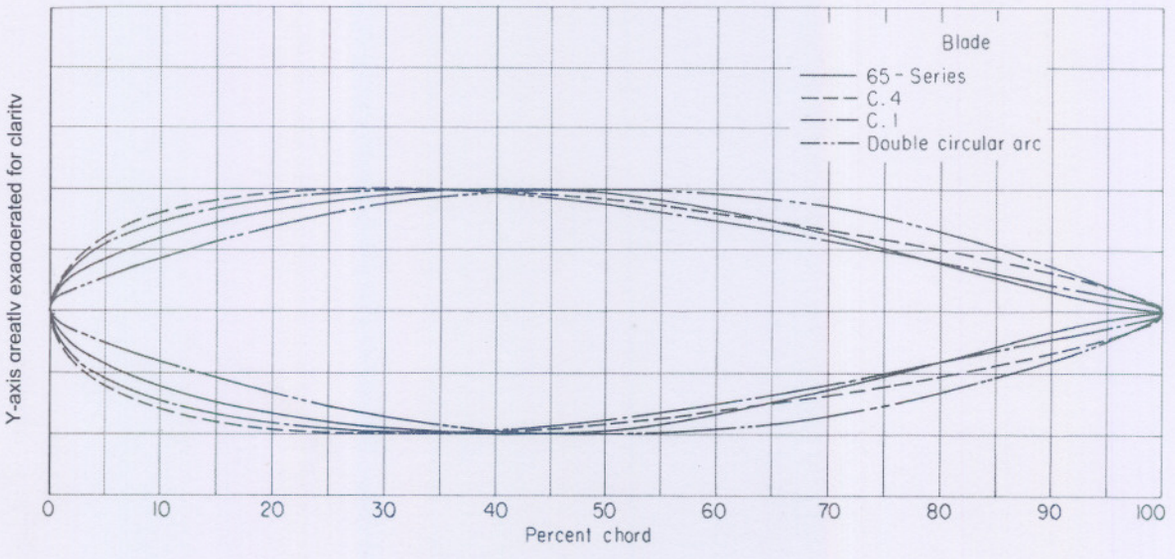

Figure 1.4 Comparisons of various thickness distributions for different blade profiles

1.4 COMPRESSOR PROCESS AND EFFICIENCY

The flow process in a turbomachine can be represented on an *h-s* (Mollier) diagram and compared with an idealized process to define efficiency. The compression process occurring in a single-stage compressor (rotor-stator) is shown in Figure 1.5.

The rotor compresses the fluid from p_1 (or p_{01}) to p_2 (or p_{02}). The static pressure would increase from p_2 to p_3 along the line 2-3, and the stagnation pressure would decrease from p_{02} to p_{03} due to viscous losses as described by Lakshminarayana (1996:52).

The purpose of the stator is that it remove swirl, thereby converting (decrease) kinetic energy from $C_2^2/2$ to $C_3^2/2$ and to further increase the static pressure. A large increase in velocity at the exit of the stage is thus avoided. The stator also serves the purpose of guiding the flow smoothly into the next rotor blade.

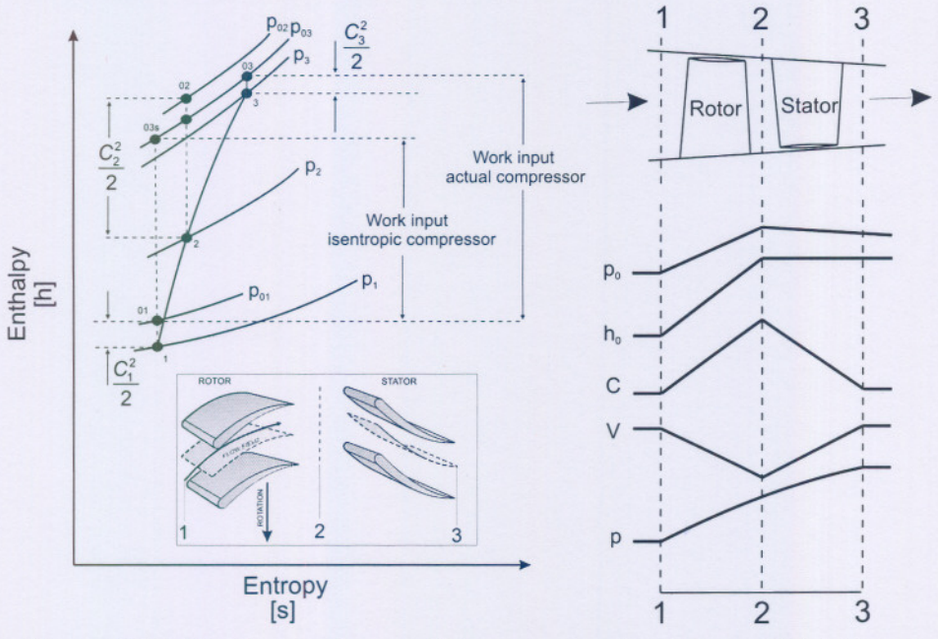

Figure 1.5 Mollier diagram for an axial compressor stage (Dixon 1998:141) and change in fluid properties and velocities (Japikse, D. & Baines, N.C. 1994)

Isentropic efficiency is based on a comparison of the actual compressor to an ideal one that is operating with the same mass flow and pressure rise as shown in Figure 1.5:

$$\eta_c = \frac{\textit{Work input to an isentropic compressor}}{\textit{Work input to an actual compressor}} = \frac{h_{03s} - h_{01}}{h_{03} - h_{01}} \qquad (1.1)$$

With today's technology axial flow compressors can reach isentropic efficiencies up to 80% and higher (Cohen *et al.*, 2001:256).

1.5 QUADRANT CLASSIFICATION

A generic compressor model consists fundamentally of a series of non-dimensional compressor performance charts. Non-dimensional performance charts are generated at a range of operating conditions. These operating conditions include rotational speed of the compressor, the inlet and outlet stagnation pressure and inlet stagnation temperature. Such a non-dimensional performance chart is shown in Figure 1.6.

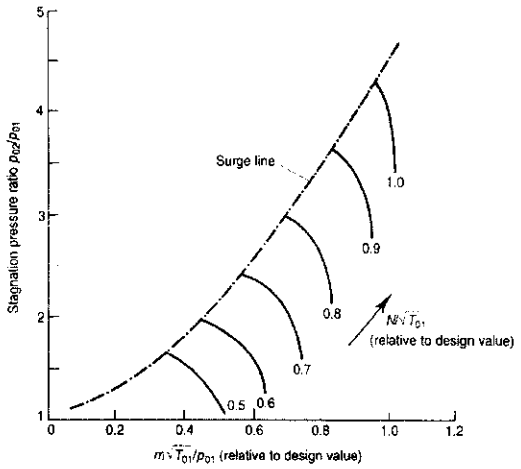

Figure 1.6 Non-dimensional axial flow compressor performance chart (Cohen *et al.*, 2001:256) [pressure ratio versus corrected mass flow]

Different types of compressor performance charts exist, such as pressure difference (p_{03}-p_{01}) (Figure 1.7 (a)) or pressure ratio (p_{03}/p_{01}) (Figure 1.7 (b)) on the y-axis versus mass flow or corrected mass flow rate on the x-axis for different sets of constant rotational speed.

Compressor performance charts are highly dependent on physical geometry of different machine types and blade geometrical changes in a single machine. Thus a variation in performance charts would be obtained for each geometrical setting.

A four quadrant performance chart consists of compressor rotation in both the positive and negative direction. Axial flow compressor rotation is defined as positive when operating under normal designed rotation and negative in opposite rotation. However, negative rotation can only be effectively described using a four quadrant performance chart displayed in Figure 1.7 (a).

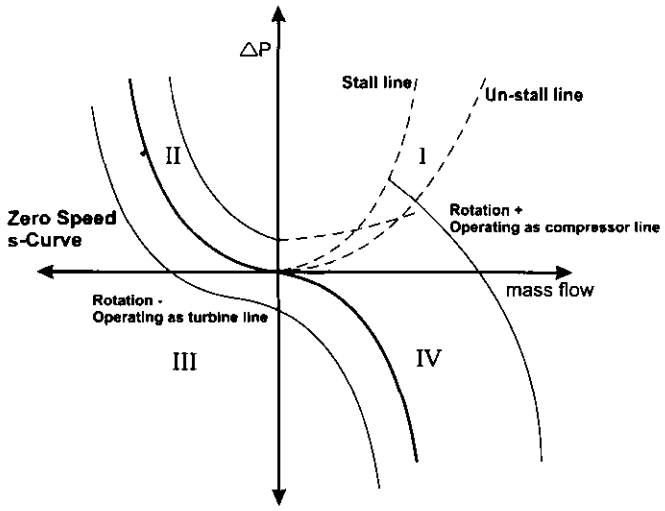

Figure 1.7 (a) Four quadrant compressor performance chart
[pressure difference $(p_e - p_i)$ versus mass flow rate]

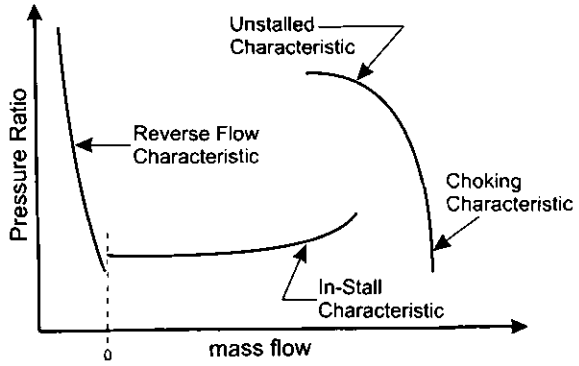

Figure 1.7 (b) Mode of operation performance chart (Bloch & O'Brien, 1992:2)
[pressure ratio $\left(\frac{p_e}{p_i}\right)$ versus mass flow rate]

When the compressor rotational speed is zero, the compressor will do no work on the fluid. A positive mass flow rate will result in a pressure drop, Δp through the axial flow compressor. Since the exit pressure would be lower than the inlet pressure, an increasing mass flow rate through the compressor will result in fourth quadrant operation. It is evident that a non-rotating axial flow compressor can operate only in the second and fourth quadrants along an S-shape curve passing through the origin of the coordinate system as shown in Figure 1.7 (a).

The region to the right of the zero rotational speed S-curve can in general be classified as the operation of an axial flow compressor with positive rotation and to the left with negative rotation (Figure 1.8).

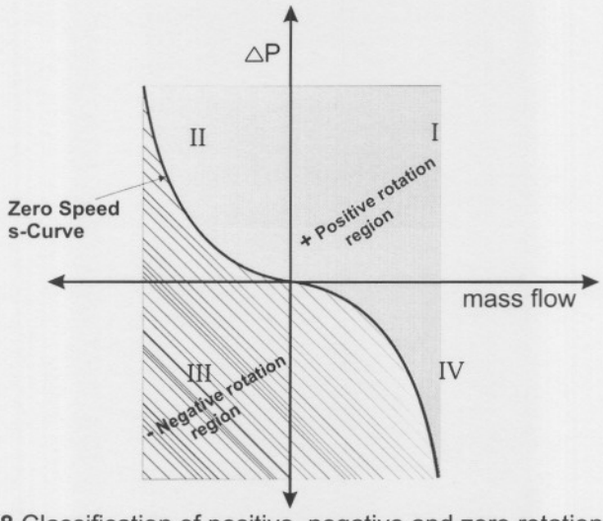

Figure 1.8 Classification of positive, negative and zero rotational regions

Thus it can be argued that:

- Zero rotational speed in an axial flow compressor results in operation in either the second or fourth quadrant. This is represented along an S-curve line passing through the origin of the coordinate system (Figure 1.8).
- Positive rotational speed in an axial flow compressor can result in an operation located in the first, second or fourth quadrant in a region right of the zero speed S-curve (Figure 1.8).
- Negative rotational speed in an axial flow compressor can result in an operation located in the second, third or fourth quadrant in a region left of the zero speed S-curve (Figure 1.8).

1.6 COMPRESSOR MODE OF OPERATION

The purpose of this section is to introduce the reader to some fundamentals on compressor mode prediction, with mode meaning the running state of an axial flow compressor. The four quadrant performance prediction chart can accommodate six operational modes for axial flow compressors. Therefore Von Backström (2005:P2,3) developed the following scheme.

Letters F, P, R, T and W will indicate flow, pressure rise, rotation, torque and power. Where each letter may be followed by a plus (+) or a minus (-) indicating whether the particular running condition of the compressor is positive or negative. For example F+P+R+T+W+ denote the normal compressor mode of operation where flow, pressure rise, rotation, torque and power are positive. This convention was chosen to agree with normal compressor practice, even though it

disagrees with normal thermodynamic practice where the positive sign is reserved for work output.

QUADRANT	RUNNING CONDITION	DESCRIPTION
1st Quadrant	$F+P+R+T+W+$	Normal operation (beyond stall included).
2nd Quadrant (Right of S-curve)	$F-P+R+T+W+$	Compressor pushing against auxiliary fans, but backflow occurs.
2nd Quadrant (Left of S-curve)	$F-P+R-T+W-$	Compressor running backwards as turbine, under backflow conditions.
3rd Quadrant	$F-P-R-T-W+$	Compressor running backwards as compressor, under backflow conditions.
4th Quadrant (Left of S-curve)	$F+P-R-T-W+$	Compressor running backwards, sucking against auxiliary fans under positive flow.
4th Quadrant (Right of S-curve)	$F+P-R+T-W-$	Compressor running forward as turbine.

Table 1.1 Compressor mode of operation indicators

The sign of the power output running condition is the product of the signs R and T. It must be emphasised that unlike power, torque values exist at zero rotational speed. A graphical presentation of axial flow compressor modes is given in Figure 1.9.

Von Backström (2005:P2,3) pointed out that third quadrant operation at positive rotational speed and first quadrant operation at negative rotational speed are two operational modes that cannot take place in an axial flow compressor.

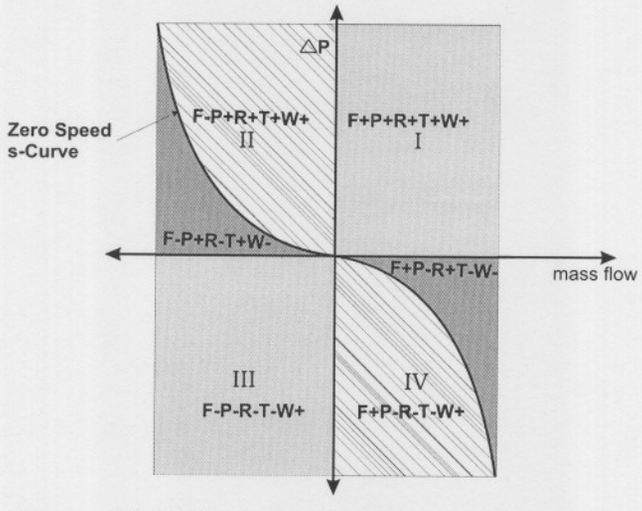

Figure 1.9 Mode of operation indicators and regions

Positive rotation in an axial flow compressor can be broken down into the following sections (Figure 1.7 (b)):

- Designed operation (design point, maximum efficiency, unstalled, off-design not far removed from design point)
- Surge and stall
- Choking
- Reverse flow

1.6.1 DESIGNED OPERATION

Under designed conditions fluid flows from the inlet to the outlet of the compressor while a pressure rise is obtained through change in angular momentum as represented by changes in tangential velocities. This means first quadrant operation without being stalled or choked (Figure 1.7 (a)). In operation the designed point is referred to as the on-design condition. However, operation is rarely constant at the design point. An axial flow compressor operating away from on-design conditions is referred to as operating at off-design conditions.

1.6.2 SURGE AND STALL

Stall is briefly mentioned in this section, because of its relevance in the broader research arena and not being a focus area of this study. The many aspects of stall, such as rotating stall and surge are abundantly discussed in open literature. Surge is not a compressor characteristic as such, but a system characteristic. According to Von Backström (2005:P1,5), the normal steady axisymmetric approximation for flow through an axial flow compressor breaks down under stall conditions. In rotating stall it is difficult to determine the number of stalled flow regions that may extend over part of, or the entire blade span, rotating at some fraction of the rotor speed. These conditions may incite blade vibration of such magnitude that blade failure may occur.

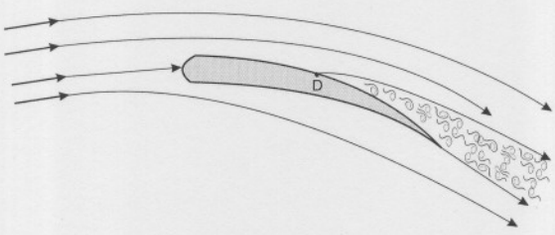

Figure 1.10 Separation of flow over an airfoil (Shames, 1992:667)

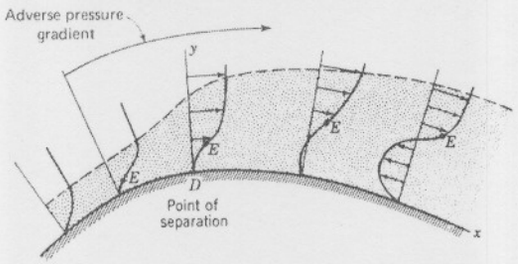

Figure 1.11 Onset of separation (Shames, 1992:668)

Many early attempts to understand or predict stall in axial flow machines made use of an aircraft-wing analogy (Figure 1.10). A more detailed presentation of Figure 1.10 is presented in Figure 1.11. These early attempts were not particularly accurate in their prediction of stall-inception, and therefore of limited use.

Researchers such as Koff and Greitzer (1986:216) described an axisymmetrically stalled flow performance model to predict rotating stall behaviour. Furthermore, Moses *et al.* (1982) also described a numerical profile pressure loss model for stall and later introduced a mean-line profile pressure loss model approximation for fully stalled cascades.

Casey (1987:227) assumed stall to occur due to leading edge incidence effects at the root mean square radius when:

$$\left(i - i_{\min}\right) \geq 0.8\left(\frac{\partial\beta}{2}\right) \tag{1.2}$$

where $\partial\beta$ is defined as the operating range which is later explained in Chapter 4. This criterion provides a crude prediction when a blade row is stalled.

1.6.3 CHOKING

According to Schwenk *et al.*(1957:1), rotor choking would occur when the over-all performance characteristics exhibit a vertical total-pressure-ratio line at the maximum mass flow for a given rotational speed (Figure 1.12). They also stated that choking in an axial flow compressor rotor, turbine rotor or any annular cascade is three-dimensional, because the flow is directed towards the hub when nearing choke conditions. This phenomenon makes the mean-line theory more difficult to apply in this operating condition.

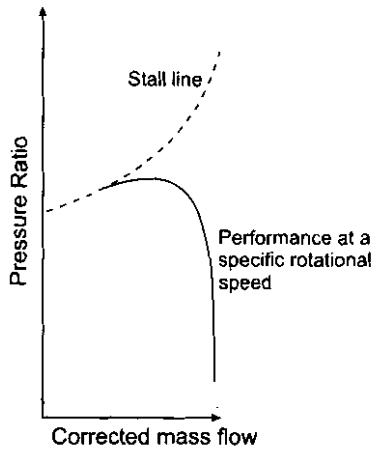

Figure 1.12 Compressor choking (Lewis and Lieblein, 1957:1)

Dixon (1998:20) also explained that choked regions in both compressor and turbine characteristics may be recognized by vertical portions of the constant speed lines. No further increase in $\dot{m}(\sqrt{T_{01}})/p_{01}$ is possible since the Mach number across some section of the machine has reached unity and the flow is said to be choked. The overall characteristic of a turbine is presented in Figure 1.13.

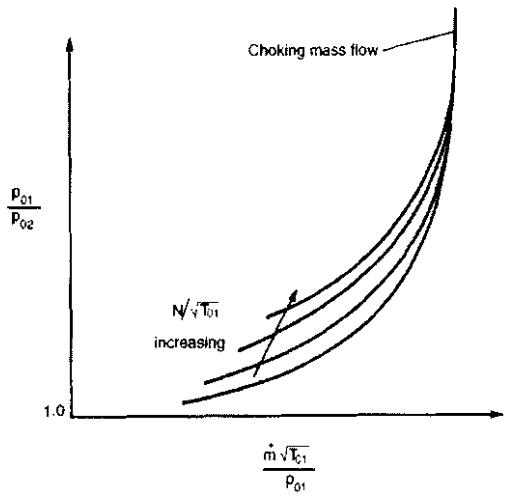

Figure 1.13 Overall characteristic of a turbine (Dixon, 1998:19)

Casey (1987:227) roughly assumed that an axial flow compressor starts to choke when operating in the fourth quadrant (no pressure rise is being produced). However, this is not the case in subsonic axial flow compressors as depicted in experimental results by Von Backström (2005:P2,5). Von Backström (2005:P2,5) clearly demonstrated that an axial flow compressor can successfully operate in the fourth quadrant without being choked.

1.6.4 REVERSE FLOW

Reverse flow in an axial flow compressor is briefly mentioned in this section, as the focus thereof falls outside this study's research scope. However a short discussion is given to increase the reference value of this study.

One of the major researchers in the field of reverse flow through an axial flow compressor was Gamache (1985:44). He stated that reverse flow with positive rotor rotation is not a common mode of operation in industrial processes. However, safety analyses must consider the effects and consequences associated with possible operating conditions which could cause a reverse flow situation to develop in extremely large industrial axial flow compressors[1].

The latest research in this field was done by Carneal (1990) and another article was published by Gamache and Greitzer (1990:4). Carneal (1990) showed that losses in the reverse-flow mode, when non-dimensionalized by wheel speed, collapsed onto a single speed parabola. Bloch and O'Brien (1992:1) used the work of Gamache and Carneal to publish an article called "A wide-range axial-flow compressor stage performance model". A typical compressor stage and the flow angles associated with reversed flow are shown in Figure A.1.

1.7 PRIMARY ASSUMPTIONS

For this study it is assumed that conditions throughout the compressor are fully subsonic. The reason for this is that the study is based on large industrial axial flow compressors operating at low blade Mach number.

When necessary, the prediction of mechanical or external losses in this study is treated as a constant input. Bearing and seal manufactures usually provide values for these losses.

This study assumes that the total pressure loss calculations are based on a superposition of theoretically separable loss components that include the following: blade profile losses, secondary losses and annulus losses. Losses due to inlet ducting, inlet guide vanes or discharge diffusers are also excluded from the investigation, because these components are not necessarily a part of all functional compressors. Von Backström (2005:P1,10) described that the experimental setup had none of such components.

[1] The power requirements of these compressors can be immense. For example, it was reported that the U.S. and Japan have plans to build liquid natural gas plants which will have compression cycles that will consume 1,500,000 kw of insulated refrigeration compressor shaft power (Gamache, 1985:44).

Von Backström (2005:P1,5) stated that stall is a whole research area on its own. For the sake of completeness only a brief overview of stall is given and no models were implemented.

Von Backström (2005:P1,5) also stated that surge is not a compressor characteristic as such, but a system characteristic. Surge mainly depends on the properties of the compressor and the volumes of pipes and pressure vessels connected to it. Therefore no models where implemented predicting surge in this study.

1.8 CONTRIBUTIONS OF THIS STUDY

The study aims to comprehensively understand positive rotational multi-stage axial flow compressor performance in the first and fourth quadrant of the performance charts. Experimental work done by Von Backström (2005:P2,1) was used to verify simulation results in the first and fourth quadrant. Evaluation of different incidence, deviation and loss models were investigated to ensure accurate power and pressure calculations. An optimized deviation model valid in first and fourth quadrant is also presented.

Choking does not occur in the first quadrant of operation when using subsonic compressors. Therefore, thorough research for when an axial flow compressor is choked under subsonic conditions was done. A term calculating the choking incidence was formulated using correlations obtained from various authors.

A term called the correctional slope factor was formulated to change the gradient of the off-design correctional parabola in pressure loss calculations. The correctional slope factor is used with axial flow compressor operation in the choke side of the loss bucket chart (Figure 4.3). This subsequently corrected the pressure loss in the fourth quadrant.

A non-dimensional power term was formulated to overcome the problem of isentropic efficiency breaking down or being invalid in the regions on the boundaries of the quadrants. This also specified a generically applicable representation when the work transfer rate is delivered or extracted from the fluid in the turbomachine.

A contribution is also made with the evaluation of the accuracy of the mean-line approach.

CHAPTER 2

SIMULATING AN AXIAL FLOW COMPRESSOR

"The important thing in science is not so much to obtain new facts as to discover new ways of thinking about them. "

(William Bragg)

2.1 INTRODUCTION

Boyer (2001:18) pointed out that CFD in turbomachinery, while tremendously successful, is not without its limitations. The choice of whether or not to use a 3-D CFD approximation (instead of other representations) essentially comes down to a trade-off between increased flow resolution and computer resources (CPU time, memory size, and cost).

The performance prediction work carried out in this thesis is, however, not aimed at calculating the fine details of the flow pattern expected from modern 3D computational methods, but rather at producing a broadly accurate method of estimating the stage performance from a rudimentary knowledge of the stage geometry and short calculation time. The thesis also aims at using incidence, deviation and loss models with a lower level of complexity to increase the solution time. These were the main reasons on choosing the mean-line prediction method. The main applications of using such a method are described by Casey (1987:273) as follows:

- Analysis of the influence of the main aerodynamic geometry parameters in the preliminary design of new compressor stages, before proceeding to the detailed design of the blade profiles and their variation with radius.
- Assessment of the effect on performance of changes in Reynolds number, aspect ratio, clearances, solidity etc.
- Testing of correlations for losses, flow deviation angles, operating range and stall, before these correlations are incorporated into more sophisticated calculation methods.

Another advantage is the fundamental simplicity and calculation speed when used in the simulation of power plants, where the accuracy of the axial flow compressor unit is not of that great importance. This chapter describes performance calculations based on 1D mean-line analysis.

2.2 MEAN-LINE DESIGN

Moustapha *et al.*(2003:66) described that mean-line design and analysis rest on an assumption that there is a mean streamline running through the machine. The fluid flow states and velocities on this streamline at any point are representative of the mean of the whole cross-section. Radial and circumferential variations of all the flow parameters are neglected. Such an analysis is inevitably a considerable simplification of the true flow field. The objective of a mean-line analysis

is not to reveal the full details of the flow state and velocities, but rather to determine the overall performance of the machine or the combination of overall geometric parameters which provide the maximum efficiency.

The 1D mean-line method is obviously not adequate for compressor stages having a high tip-to-hub diameter ratio (Y>1.5, $Y=(D_t/D_h)$), an uneven distribution of blade loading with radius, a supercritical inlet Mach number or any number of poor design features leading to a large variation in incidence with radius (Casey, 1987:273). Roos (2007), however, suggested a high tip-to-hub ratio of Y=1.667, which should not to be exceeded.

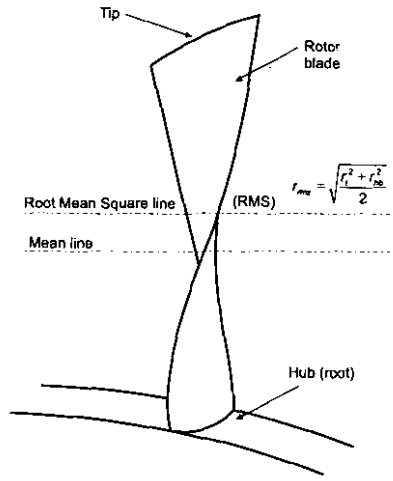

Figure 2.1 Blade root mean square radius

The given parameters for a mean-line design will vary from one application to another, but will normally comprise of some or all of the following elements:

- inlet total pressure and temperature
- mass flow rate
- pressure ratio
- rotational speed
- power or enthalpy drop for turbine but rise for compressor
- target efficiency

Examination of the pressure loss models requires some additional geometrical information in order to provide the estimates for stage efficiency. Important among these parameters are such as inner and outer radii, axial chord length, blade spacing or blade number. The root mean square radius is to be used with the mean-line design and is defined as:

$$r_{rms} = \sqrt{\frac{r_t^2 + r_{hb}^2}{2}} \tag{2.1}$$

The root mean square (rms) radius divides the annulus into two equal annular areas and is the mean radius for a uniform flow (constant axial velocity with radius). This radius is also more or less independent of the axial velocity profile for stages with non-zero gradients.

2.3 CONSERVATION EQUATIONS

One of the most useful concepts in the performance evaluation of turbo machinery is the control volume approach as applied to the basic laws of conservation of mass, momentum and energy. The simulation of flow between turbine or compressor blades is an important part of thermal-fluid system simulation and design. The conservation equations presented in this study forms the fundamental building block on which the simulation code is built, also known as the "rotating pipe" model (Rousseau, 2005).

2.3.1 CONSERVATION OF MASS

The integral form of the mass conservation equation for a finite control volume is given by:

$$\frac{\partial}{\partial t}\left(\iiint \rho \, d\forall\right) + \oiint \rho \bar{V} \cdot \overline{dA} = 0 \tag{2.2}$$

with $\forall$ the volume and V the velocity relative to the control volume. This is then applied to an infinitely small one dimensional control volume, where the full derivation of (2.2) is presented in Rousseau (2005). Eq.(2.2) is reduced to the following:

$$\forall \frac{\partial \rho}{\partial t} + m_e - m_i = 0 \tag{2.3}$$

where symbols without subscripts refer to values averaged over the control volume while the subscripts 'e' and 'i' refer to the outlet and inlet respectively.

2.3.2 CONSERVATION OF LINEAR MOMENTUM

One of the most fundamental and valuable principles in mechanics is Newton's second law of

motion. The momentum equation relates the sum of the external forces acting on a fluid element to its acceleration, or to the rate of change of momentum in the direction of the resultant external force. In the study of turbomachines many applications of the momentum equation can be found, e.g. the force exerted upon a blade in a compressor or a turbine cascade caused by the deflection or acceleration of fluid passing the blades.

When one considers the linear momentum conservation equation it is important to realize that we are now dealing with a non-inertial control volume, simply due to the fact that it is rotating. This is also true even when the rotational speed is constant. The integral form of the linear momentum conservation equation is now given by:

$$\begin{aligned}&\oiint \tau \overline{dA} + \iiint \bar{B}\rho d\forall \\ &\quad - \iiint \left[(2\omega \times V) + (\dot{\omega} \times r) + \left(\omega \times (\omega \times r)\right) \right] \rho d\forall \\ &\quad = \frac{\partial}{\partial t}\left(\iiint \bar{V}\rho d\forall \right) + \oiint \bar{V}\left(\rho \bar{V} \bullet \overline{dA}\right)\end{aligned} \tag{2.4}$$

By applying (2.4) to an infinitely small control volume and defining flow in its respected condition, (2.4) leads to the following equations for a control volume with finite length L and average cross-section A, described in detail by Rousseau (2005).

Incompressible flow transient:

$$\begin{aligned}&\rho L \frac{\partial V}{\partial t} + (p_{0e} - p_{0i}) + \rho g (z_e - z_i) + \Delta p_{0L} \\ &= \rho \omega X - \rho L Sin\alpha Sin\beta \dot{\omega} r\end{aligned} \tag{2.5}$$

Incompressible flow steady-state:

$$(p_{0e} - p_{0i}) + \rho g (z_e - z_i) + \Delta p_{0L} = \rho \omega X \tag{2.6}$$

Compressible flow transient:

$$\begin{aligned}&\rho L \frac{\partial V}{\partial t} + \frac{p}{p_0}(p_{0e} - p_{0i}) + \tfrac{1}{2}\rho C^2 \frac{1}{T_0}(T_{0e} - T_{0i}) \\ &\quad + \rho g (z_e - z_i) + \Delta p_{0L} = \rho \omega X - \rho L Sin\alpha Sin\beta \dot{\omega} r\end{aligned} \tag{2.7}$$

Where $\rho, p, p_0, C, T_0, \alpha, \beta$ is the average values, defined by the sum of the inlet and outlet conditions divided by two. Defining C as the absolute velocity in the velocity triangle, (z_e-z_i) as the height increase from inlet to the outlet and Δp_{0L} as the stagnation pressure loss coefficient. This is applicable for compressible flow as well.

Compressible flow steady-state:

$$\frac{p}{p_0}(p_{0e} - p_{0i}) + \tfrac{1}{2}\rho C^2 \frac{1}{T_0}(T_{0e} - T_{0i}) + \rho g(z_e - z_i) + \Delta p_{0L} = \rho \omega X \tag{2.8}$$

where X is defined by:

$$X = \omega(r_e^2 - r_i^2) + (Sin\alpha_e Sin\beta_e V_e r_e - Sin\alpha_i Sin\beta_i V_i r_i) \tag{2.9}$$

and β_e, β_i is -90° for forward flow in an axial flow compressor, while α_e, α_i is described in detail in Figure 2.2.

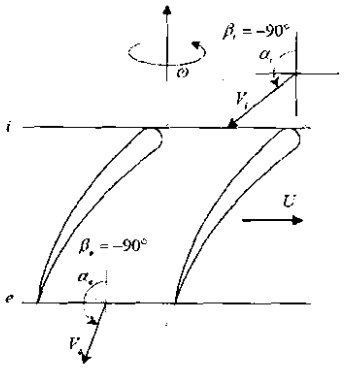

Figure 2.2 Angles used in Eq. (2.9) with permission of Rousseau (2005)

2.3.3 CONSERVATION OF ENERGY

The integral form of the energy conservation equation for a finite control volume is given by:

$$\dot{Q} + \dot{W} = \frac{\partial}{\partial t}\left(\iiint (u + \tfrac{1}{2}V^2 + gz)\rho d\forall\right) + \oiint (h + \tfrac{1}{2}V^2 + gz)\rho \bar{V} \cdot \overline{dA} \tag{2.10}$$

By applying (2.10) to an infinitely small control volume, (2.10) leads to the following equations for a control volume with finite length L and average cross-section A, described in detail by Rousseau (2005).

Conservation of energy transient:

$$\dot{Q} + \omega \dot{m} X + \rho \omega \cancel{V} \left(rSin\alpha Sin\beta \frac{\partial V}{\partial t} + \dot{\omega} r^2 \right)$$

$$= \cancel{V} \frac{\partial}{\partial t}(\rho h_0 - p) + \dot{m}_e h_{0e} - \dot{m}_i h_{0i} + \dot{m}_e g z_e - \dot{m}_i g z_i \tag{2.11}$$

Conservation of energy steady-state:

$$\dot{Q} + \omega \dot{m} X = \dot{m}_e h_{0e} - \dot{m}_i h_{0i} + \dot{m}_e g z_e - \dot{m}_i g z_i \tag{2.12}$$

$\dot{Q}$ is the total rate of heat transfer to the fluid and W the total rate of work done on the fluid[2].

2.3.4 SUMMARY

For steady-state flow through a rotating channel or each blade row we therefore have (Rousseau, 2005):

Conservation of mass:

$$\cancel{V} \frac{\partial \rho}{\partial t} + m_e - m_i = 0$$

Conservation of momentum (incompressible):

$$(p_{0e} - p_{0i}) + \rho g (z_e - z_i) + \Delta p_{0L} = \rho \omega X$$

Conservation of momentum (compressible):

$$\frac{p}{p_0}(p_{0e} - p_{0i}) + \tfrac{1}{2}\rho C^2 \frac{1}{T_0}(T_{0e} - T_{0i}) + \rho g (z_e - z_i) + \Delta p_{0L} = \rho \omega X$$

with

$$X = \omega(r_e^2 - r_i^2) + (Sin\alpha_e Sin\beta_e V_e r_e - Sin\alpha_i Sin\beta_i V_i r_i)$$

Conservation of energy:

$$\dot{Q} + \omega \dot{m} X = \dot{m}_e h_{0e} - \dot{m}_i h_{0i} + \dot{m}_e g z_e - \dot{m}_i g z_i$$

[2] Note that in most texts on classical thermodynamics the rate of work done by the fluid on the surroundings is defined as positive. However, the definition used here is consistent with most texts on fluid mechanics.

2.4 COMPONENTS OF CONSERVATION EQUATIONS

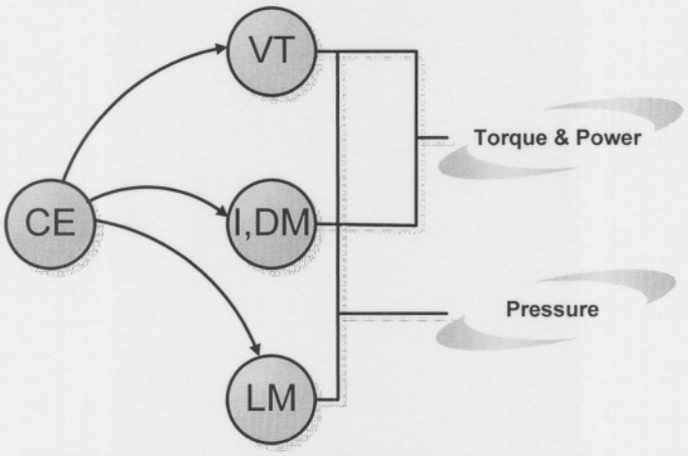

Figure 2.3 Break down of conservation equations

Conservation equations can be broken down into three components when using the "rotating pipe" model (Section 2.3) to calculate axial flow compressor performance. An accurate prediction for torque and power in an axial flow compressor can be made by using velocity magnitudes, flow angles and part of the fundamental conservation equation for linear momentum (2.9). It is clearly shown in Figure 2.3 that no pressure loss models are required to calculate compressor torque and power, only compressor blockage plays a big role. Torque is defined as $Z_i = \dot{m} X_i$ for the i_{th} blade row where X_i is defined in (2.9). The power is then defined as $\dot{\mathbb{Q}}_c = \omega \sum Z_i$ with ω the rotational speed in radians per second.

Furthermore, pressure calculations can be made by using all three components, thus calculating overall axial flow compressor performance.

2.5 VELOCITY COMPONENT CHARACTERISTICS

In an axial flow compressor rotor, the flow may be viewed from two frames of reference. One is the absolute or stationary frame fixed to the ground, and the second one is the rotating or relative frame fixed to the rotor. The relative velocities, measured with respect to the rotating frame of reference, are denoted by V and the absolute velocities, measured with respect to a fixed frame of reference by C. The blade speed is represented by U and the tangential component of the absolute or relative velocities is indicated by the subscript w. The absolute axial velocity is

indicated by the subscript a. The velocity triangle can be presented by the following vector relation:

$$\mathbf{V}+\mathbf{U}=\mathbf{C} \tag{2.13}$$

The rotating blade row (rotor) in an axial flow compressor turns the fluid towards the meridional (axial) plane in the relative frame of reference. This results in an exit relative velocity vector situated more parallel to the meridional plane than the inlet relative velocity vector shown in Figure 2.4. (The meridional plane is a plane through the compressor axis). Note that under the assumption of equal inlet and outlet axial velocity components, the magnitude of the blade row relative exit velocity vector will be less than that of the relative inlet velocity component. In general power is transferred to the fluid and implies a pressure rise in the blade row.

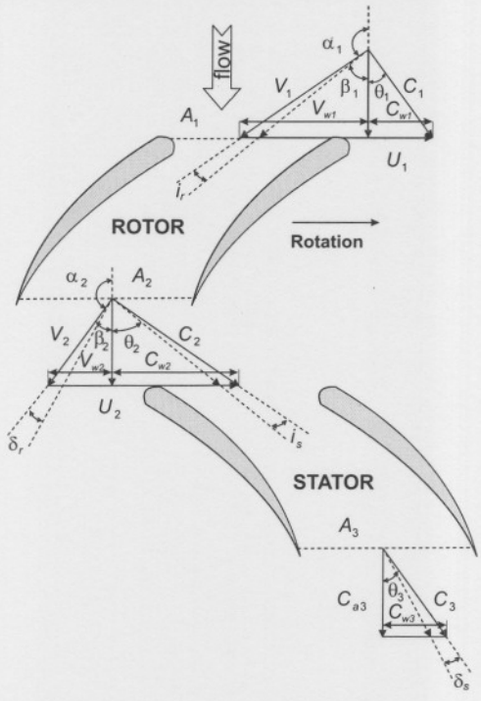

Figure 2.4 Axial compressor stage velocity triangles

The relative flow angles are denoted by β and the absolute flow angles by θ as shown in Figure 2.4. Both are measured with respect to the meridional (axial) direction. The α flow angle is to be used in conjunction with the conservation equations presented in Section 1.4. It must be emphasized that the conservation equation β angles in (2.9) and the relative flow β angles in Figure 2.6 are not the same. Flow angles are positive in the clockwise direction with the blade angle as reference and negative in the opposite direction. Blade angles are indicated by the subscript B in Figure 2.6.

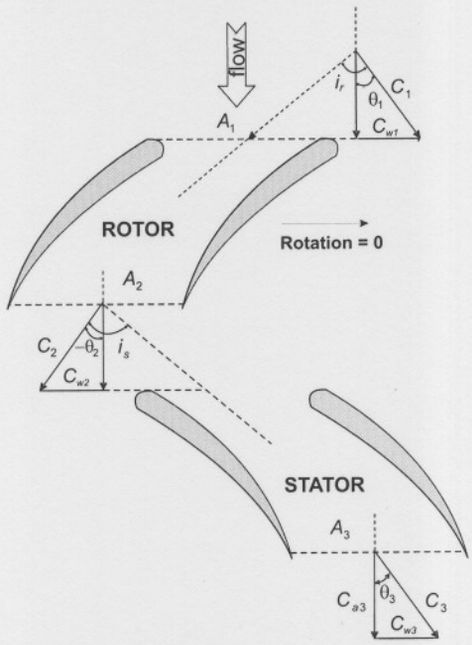

Figure 2.5 A compressor stage with zero rotational speed

It must be emphasized that when operating at zero speed rotation, compressor operation is far removed from the design point. The result is that abnormal inlet incidence angles at each blade row exist as shown in Figure 2.5.

The cascade nomenclature used throughout this thesis is based on Figure 2.6. The nomenclature for a stationary cascade is applicable to a rotor and stator blade, if the β angles are replaced with θ as shown in the velocity triangle presented in Figure 2.4. The α_1 parameter in Figure 2.6 is called the angle of attack which is used in some references. It should again be emphasized that the conservation equation α angles in Figure 2.4 and the angles of attack α_1 in Figure 2.6 are not the same.

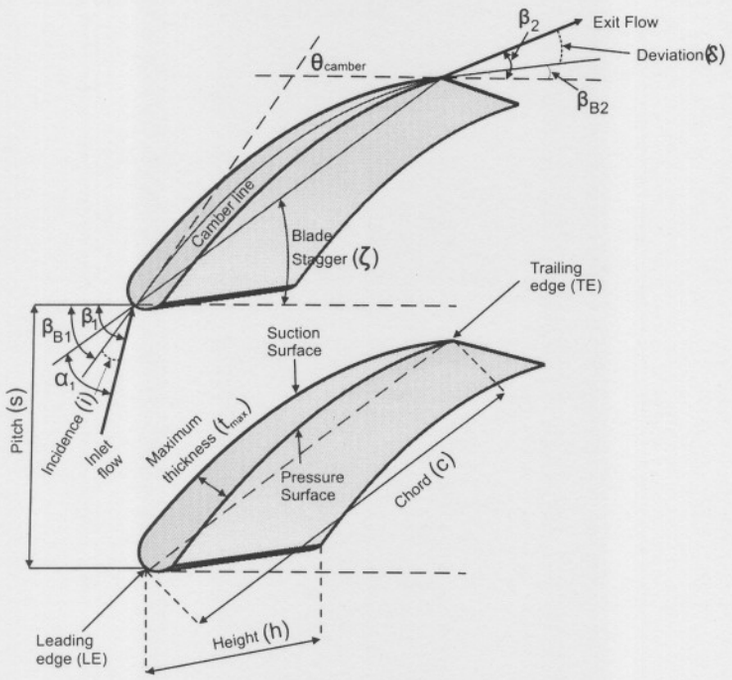

Figure 2.6 Blade terminology

Incidence is taken as the angle between the mean inlet flow angle into the blade at the leading edge and the inlet blade angle, $i = \beta_1 - \beta_{B1}$. However, deviation is the difference between the mean exit flow angle at the trailing edge and the exit blade angle, $\delta = \beta_2 - \beta_{B2}$. Some authors also use the term turning which is defined as $\varepsilon = \beta_1 - \beta_2$.

2.6 SUMMARY AND CONCLUSIONS

The objective of a mean-line analysis is not to reveal the full details of the flow state and velocities, but rather to determine the overall performance of the machine. By using the mean-line approach, relatively good accuracy can be obtained in short computing time.

A few advantages arise when using the "rotating pipe" model as the conservation equations. If compressor blockage is known, one of these advantages is that the compressor torque and power calculations can be obtained without using any pressure loss model. Another advantage is that it is valid in all four quadrants.

CHAPTER 3

INCIDENCE AND DEVIATION PREDICTION METHODS

"Everything you want is out there waiting for you to ask. Everything you want also wants you. But you have to take action to get it."

(Jules Renard)

3.1 INTRODUCTION

Chapter 3 presents different incidence and deviation models that exist in open literature. Incidence and deviation angles are of great importance when calculating axial flow compressor torque and power as previously mentioned in Chapter 2.

3.2 REFERENCE INCIDENCE

Conflicting definitions of reference (design) inlet flow angle for axial cascades exist as summarized by Cumpsty (1989:162). The two most common used definitions are:

- ***Minimum loss incidence angle.*** Defined by the inlet incidence angle where the cascade has a minimum pressure loss (Lieblein, 1960:575).
- ***Optimum incidence angle.*** Defined by the inlet incidence angle where the cascade has a maximum lift to drag ratio (Carter, 1950).

3.2.1 MINIMUM LOSS INCIDENCE

Minimum loss Model 1 (Lieblein, 1960):

Lieblein (1960:575) introduced the concept of minimum loss incidence. This is the incidence at which a cascade will experience an absolute minimum pressure loss and the incidence is not zero, as indicated by theory for infinitely thin blades (Lieblein, 1960:577). The empirical correlation is only valid for inlet flow angles between 0° and 70° as indicated by Figures 3.1 and 3.2. The minimum loss incidence angle is given by:

$$i_{min} = i_0 + n \cdot \theta_{camber} \tag{3.1}$$

where i_0 is the minimum loss incidence angle for cascade blades with zero camber and n is a slope factor for the variation of inlet air angle and solidity, presented in Figure 3.1. The i_0 parameter can in turn be calculated from:

$$i_0 = K_{sh} \cdot K_t \cdot (i_0)_{10} \tag{3.2}$$

where $(i_0)_{10}$ is the minimum loss incidence for a NACA-65 cascade blade with zero camber and a 10 percent maximum thickness to chord length ratio (Figure 3.2).

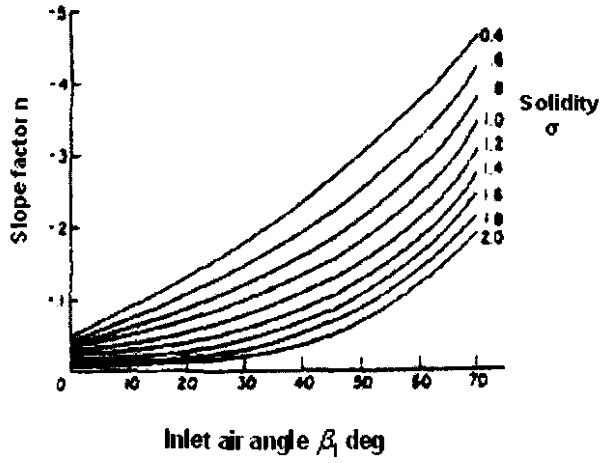

Figure 3.1 Minimum loss incidence angle slope factor

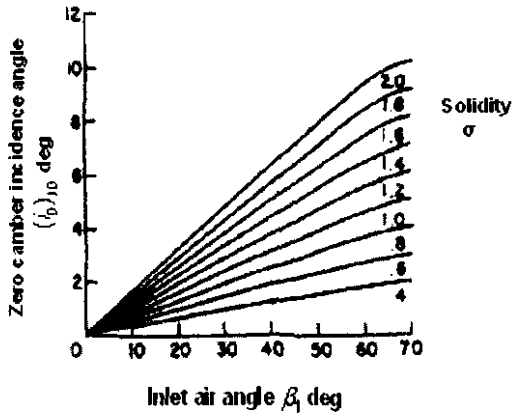

Figure 3.2 Minimum loss incidence angle for 10% thickness to chord ratio NACA 65 blades with zero camber

Further, K_{sh} and K_t are correction factors for different blade shape distributions and maximum thickness to chord length ratios. The parameter K_t can be obtained from Figure 3.3, while K_{sh} is assumed:

- 1.1 for C-series blade types,
- 0.7 for DCA blade types and
- 1.0 for NACA-65 blade types.

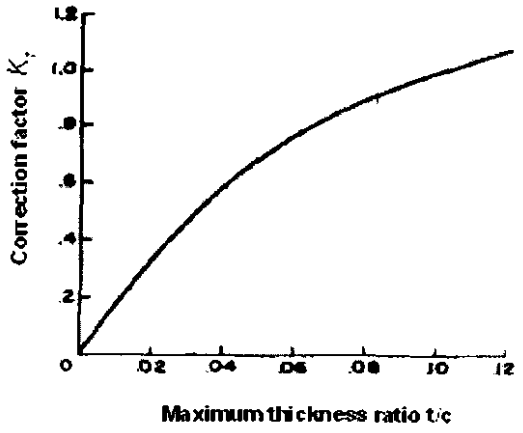

Figure 3.3 Correction factor for different thickness to chord ratios

A correction of -1 degree should be applied to the predicted minimum loss incidence according to Casey (1987:273). This correction allows for axial flow compressor operation at a constant stagger angle, whereas the measurements of Lieblein (1960:575) were carried out at a constant

air angle. Thus (3.1) becomes:

$$i_{min} = i_0 + n \cdot \theta_{camber} - 1 \tag{3.3}$$

Minimum loss Model 2 (Wright and Miller, 1991):

Wright and Miller (1991:69) use a correlation, that relates the minimum loss incidence to the relative inlet Mach number and ratio of throat width to inlet spacing. This correlation was calibrated with test data from 14 NASA single stage axial flow compressors tests. The correlation is given by:

$$\frac{o}{s\cos\beta_{1,min}} = 0.155 \cdot M_{1r} + 0.935 \tag{3.4}$$

where $i_{min} = \beta_{1,min} - \beta_{1\beta}$. The two dimensional throat width o is given by (3.7) and (3.8).

3.2.2 OPTIMUM INCIDENCE

Miller and Wasdell (1987:249) derived a correlation to calculate the optimum incidence angle for any given blade geometrical arrangement. This empirical correlation is only valid for stagger angles ζ between 0° and 60° as indicated by Figure 3.4. The optimum incidence is calculated from:

$$i_{opt} = X + Y\sigma - Z\theta_{camber} \tag{3.5}$$

where X, Y, Z are constants dependant on blade stagger angle shown in Figure 3.4 and $\sigma = c/s$.

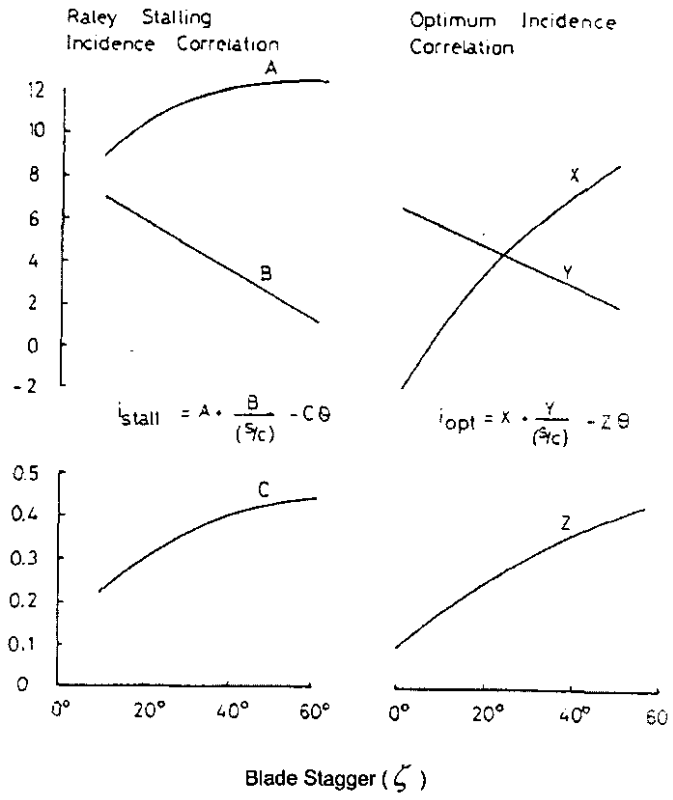

Figure 3.4 Stalling and optimum incidence correlations

3.3 *INCIDENCE ANGLES*

Two other incidence angle definitions which are referred to in this study are:

- ***Stalling incidence angle.*** Defined by the incidence where the pressure loss is assumed to be twice that of the minimum pressure loss (Miller and Wasdell, 1987:249). Flow also starts separating from the blade at the leading edge.
- ***Choking incidence angle.*** Numerous definitions for choking incidence exist. Jansen and Moffatt (1967:453) defined choking incidence for subsonic axial flow compressors as the incidence where the pressure loss would be twice that of the minimum loss value. This statement was made using NACA 65 series blades. Other definitions for choking incidence are displayed in Section 3.3.2.

3.3.1 STALLING INCIDENCE

Miller and Wasdell (1987:249) derived a correlation to calculate the stalling incidence angle for any given blade geometrical arrangement. This empirical correlation is only valid for stagger angles ζ between 0° and 60° as indicated by Figure 3.4. The stalling incidence is calculated

from:

$$i_{st} = A + B\sigma - C\theta_{camber} \tag{3.6}$$

where A, B, C are constants dependant on blade stagger angle shown in Figure 3.4. Pfitzinger and Riess (1997:120) defined a maximum incidence range $\Delta i_{max,st}$ by the difference between the stalling incidence and the minimum loss incidence which are used in off-design pressure loss calculations (Figure 4.3).

3.3.2 CHOKING INCIDENCE

Choking incidence is an important factor when an axial flow compressor tends to operate in the fourth quadrant. Authors use the choking incidence as a boundary to define when an axial flow compressor could enter choked conditions. Furthermore, choking incidence is used in conjunction with off-design pressure loss calculations when operating in the choke side of the loss bucket chart in Figure 4.3.

Different definitions of choking incidence exist:

- Jansen and Moffatt (1967:453) defined choking incidence for subsonic axial flow compressors as the incidence where the pressure loss would be twice that of the minimum loss value. This assumption was made using NACA 65 series blade sets.
- Miller and Wasdell (1987:249) assumed choking to have a greater effect than stalling and used a factor of three times that of the minimum loss value. This assumption was made using transonic DCA blade sets.
- The author defined the chocking incidence as the incidence where the relative velocity would be the highest in the passage throat area with a certain choking Mach number as inlet.

Miller and Wasdell (1987:249) also defined choking incidence as a function of the cascade throat area and the inlet Mach number. They calculated the choking incidence using an iterative method, not showed in their article. Wright and Miller (1991:69) however, presented an improved correlation for calculating the throat width in DCA blades where choking would appear and is defined as:

$$\frac{o}{c} = \frac{s}{c}\cos\zeta - l_1 - l_2\left(\frac{t_{max}}{c} - 0.1\right) \quad \text{for} \quad \frac{t_{max}}{c} > 0.1 \tag{3.7}$$

$$\frac{o}{c} = \frac{s}{c}\cos\zeta - l_1 - l_3\left(0.1 - \frac{t_{max}}{c}\right) \quad \text{for} \quad \frac{t_{max}}{c} < 0.1 \tag{3.8}$$

where o is the throat width, c the chord length, s the blade pitch, t_{max} the maximum thickness of the blade and the coefficients l_1, l_2, l_3 are functions of camber and stagger angle as shown in Figure 3.5. It was also mentioned that the two dimensional value of throat width can be corrected for reduction in annulus height and total pressure loss up to the throat position, but this method was not shown. Wright and Miller (1991:69) also stated that this throat width can be use for conventional circular arc blades as well.

An analytical model for calculating the choking incidence at specific operating conditions was developed by the author. Both the cascade throat width and the inlet Mach number were used in the derivation. This parameter was derived to obtain better off-design pressure loss calculations for when an axial flow compressor operates in the choke side of the loss bucket chart in Figure 4.3. The full derivation is presented in Appendix B.

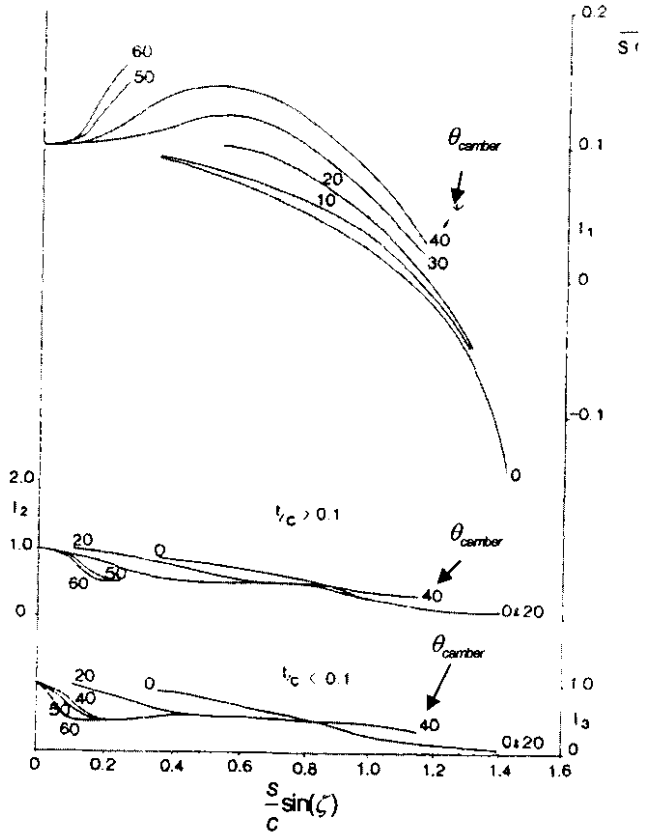

Figure 3.5 Coefficients for DCA throat area expression

Choking incidence is simply defined by:

$$i_{ch} = \beta_{ch} - \beta_B \tag{3.9}$$

where β_{ch} denotes the choking inlet flow angle and β_B the inlet blade angle.

3.4 DEVIATION ANGLES

Deviation is defined as the difference between the outlet flow and blade angle at the trailing edge. The main reason for deviation is that flow adjusts itself to a sudden removal of transverse pressure gradient near the trailing edge. Empirical correlations are used to predict the deviation for various operating conditions and geometrical changes in blade sets. Two deviation models are presented below for when an axial flow compressor operates in the turbulent flow regime $\pm$ Re_c>2x10^5.

Deviation Model 1 (Lieblein, 1960):

Lieblein (1960:575) derived an empirical deviation model using the well known Carter's correlation as basis. The empirical correlation is only valid for inlet flow angles between 0° and 70° as indicated by Figures 3.6, 3.7. etc. The deviation at minimum loss incidence is given by:

$$\delta_{\min} = \delta_0 + \left(\frac{m}{\sigma^b}\right) \cdot \theta_{camber} \tag{3.10}$$

with m the slope factor at a solidity of unity with variation of inlet air angle obtained from Figure 3.6. The variable b is the solidity exponent variable with inlet air angle which can be found in Figure 3.7 and σ the solidity.

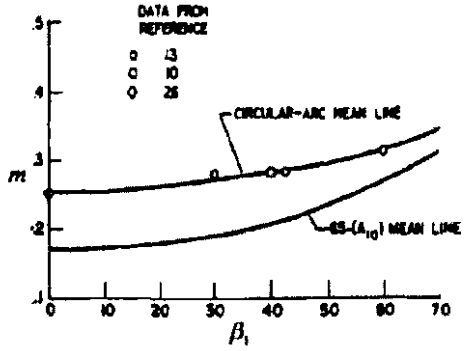

Figure 3.6 Slope factor at unity solidity

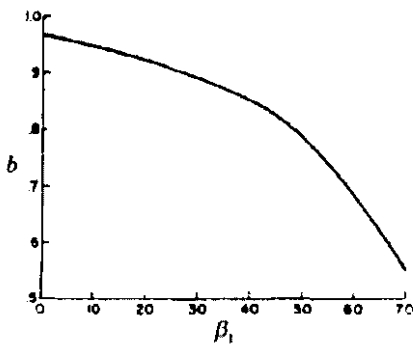

Figure 3.7 Solidity exponent variation with inlet air angle

δ_0 is the reference minimum-loss deviation angle with zero camber blades and can be represented as:

$$\delta_0 = K_{sh} \cdot K_t \cdot (\delta_0)_{10} \tag{3.11}$$

Where $(\delta_0)_{10}$ is the basic variation for the NACA-65 blade profile with a ten percent thickness distribution represented by Figure 3.9. K_{sh} is a correction for different blade types and is the same as in minimum loss incidence calculations. K_t is the correction necessary for blades with a maximum thickness other than ten percent (Figure 3.8). Off-design deviation is given by:

$$\delta = \delta_{\min} + (i - i_{\min}) \cdot \left(\frac{d\delta}{di}\right)_{\min} \tag{3.12}$$

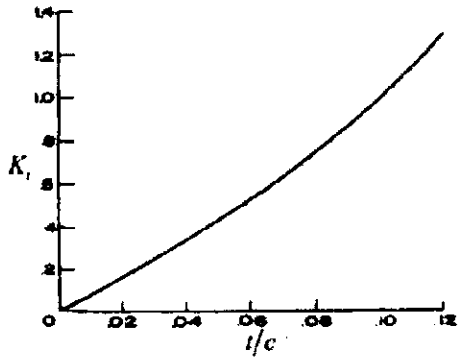

Figure 3.8 Correction necessary for blades with a maximum thickness other than 10 percent

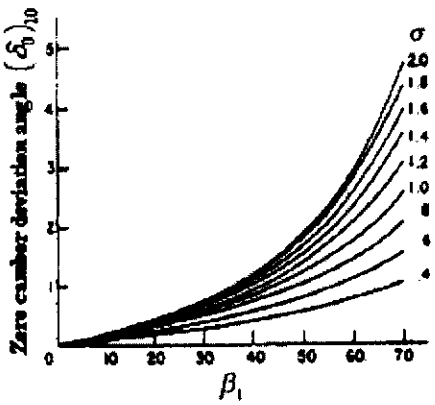

Figure 3.9 Minimum loss deviation for NACA-65 blade profile with a ten percent thickness distribution and zero camber

In Eq. (3.12), $\left(\frac{d\delta}{di}\right)_{\min}$ represents the variation of the deviation angle with a minimum loss inlet flow incidence over minimum loss incidence angle (Figure 3.10).

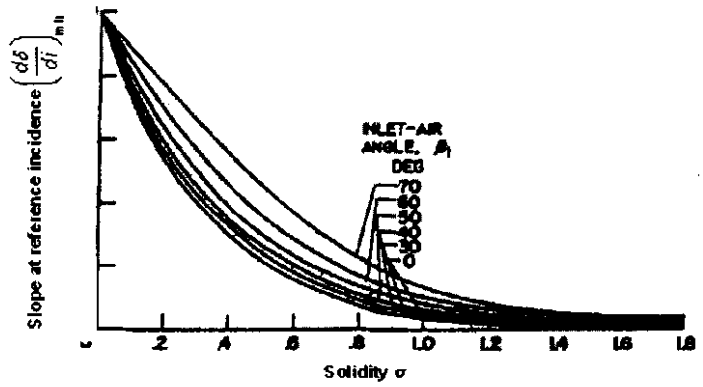

Figure 3.10 Slope of the deviation angle variation at the minimum-loss incidence angle

Deviation Model 2 (Wright and Miller, 1991):

Miller and Wasdell (1987:249) modified the corrected Carter's rule to include a term accounting for thickness to chord ratio. An axial velocity density ratio was defined by Wright and Miller (1991:69) and is given by:

$$\Omega = \frac{\rho_1 \cdot C_{a1}}{\rho_2 \cdot C_{a2}} \tag{3.13}$$

It must be emphasized that Carter's rule is based on predicting the deviation at optimum incidence (3.5) and not at minimum loss incidence.

The correlation for deviation with an optimum inlet flow incidence is given by Wright and Miller (1991:69) as:

$$\delta_{opt} = 1.13m\left(\varphi\sqrt{\frac{s}{c}} + 3\right) + m_1(\Omega - 1) + m_2\left(\frac{t_{max}}{c} - 0.05\right) + 0.8 \tag{3.14}$$

where the coefficients $m, m_1,$ and m_2 are functions of blade stagger angle (Figure 3.12). This correlation was obtained using NACA 65 series blade sets and is valid for a stagger angle ζ range between 10° and 60°.

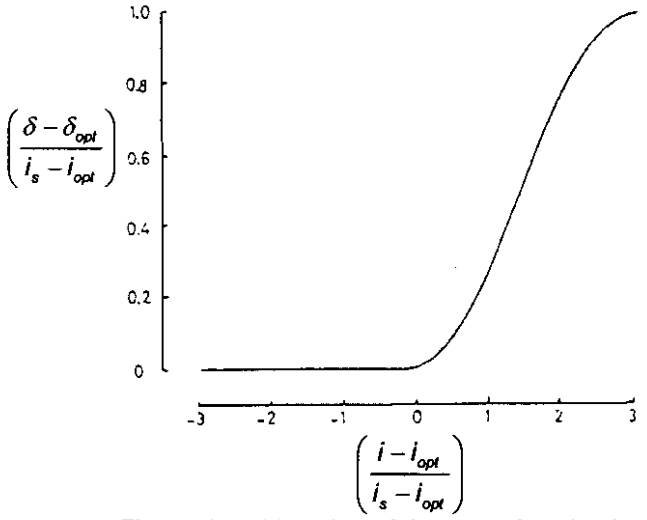

Figure 3.11 Variation of deviation function between choking and stalling incidence

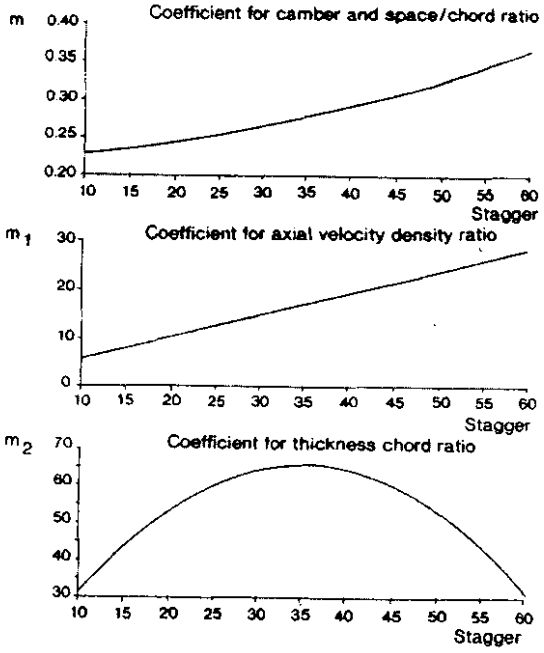

Figure 3.12 Coefficients for the deviation correlation at optimum incidence

Miller and Wasdell (1987:249) projected an empirical correlation for transonic DCA airfoils to calculate the actual deviation (Figure 3.11). The correlation has been extrapolated on the basis of a sinusoidal variation of the deviation function $\delta-\delta_{opt}$ versus the incidence function in the stall region. Miller and Wasdell (1987:249) assumed that operation in the choke region will result in constant deviation. This is however not the case for the NACA-65 series blade sets (Figure 3.13). In the analysis of White *et al.*(2002:181) they neglect the last two terms of (3.14) accounting for the effects of the thickness-chord ratio, t/c as it was found to cause excessively high values of deviation in some cases. The new optimum deviation angle derived by White *et al.*(2002:181) is given by:

$$\delta_{opt} = 1.13m\left(\varphi\sqrt{\frac{s}{c}}+3\right)+m_1(\Omega-1) \tag{3.15}$$

It was found that the deviation angle in the choked region is not constant as previously assumed by Miller and Wasdell (1987:249). A new correlation was formulated for the incidence function with increasing stagger number and is given by Figure 3.13.

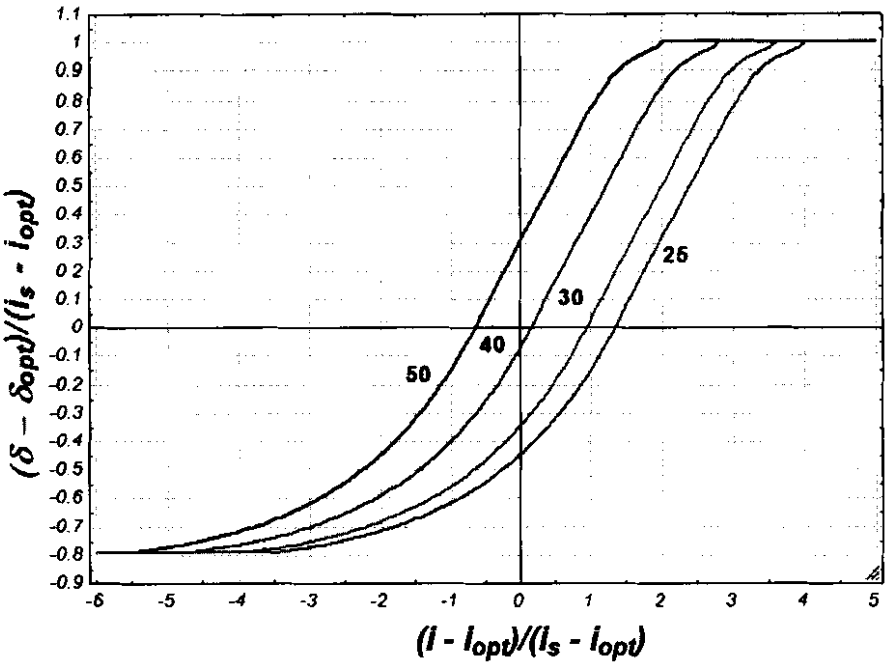

Figure 3.13 Deviation function between choking and stalling with varying stagger angle for NACA 65 blades.

3.4.1 TWO-DIMENSIONAL DEVIATION WITH BOUNDARY LAYER EFFECTS

On the surface of an airfoil there is a gradually thickening boundary layer. At the trailing edge, this causes a depression in velocity profile which gradually disappears with increasing distance as illustrated in Figure 3.14. The "equalization" of the velocity profile in the wake is one immediate cause of energy dissipation; the other is the direct heat and turbulence generation in the boundary layer as described by Csanady (1964:271). In a cascade, however, there is a loss of energy per unit mass (total head) which may be related to boundary-layer parameters. For this purpose, consider the exit section t of closely spaced cascade blades presented in Figure 3.14. Far behind the cascade (section 2) the velocity fluctuations have disappeared, with the velocity having magnitude V_2 and inclination β_2.

In the absence of boundary layers the flow V_t^* (at a given mass-flow rate) would have an axial component C_a in both sections t and 2, and the flow angle β_2 would also remain equal to β_t. However, the constriction caused by the boundary layers increases the magnitude of the axial velocity at section t. The axial component of section t is proportionately greater than C_{a1}. After section t the through-flow velocity must again reduce to C_{a2} which is equal to C_{a1}. The tangential velocity V_t changes differently, and a resultant velocity V_2 is obtained far downstream which is

different from the ideal V_t^* in both magnitude and direction.

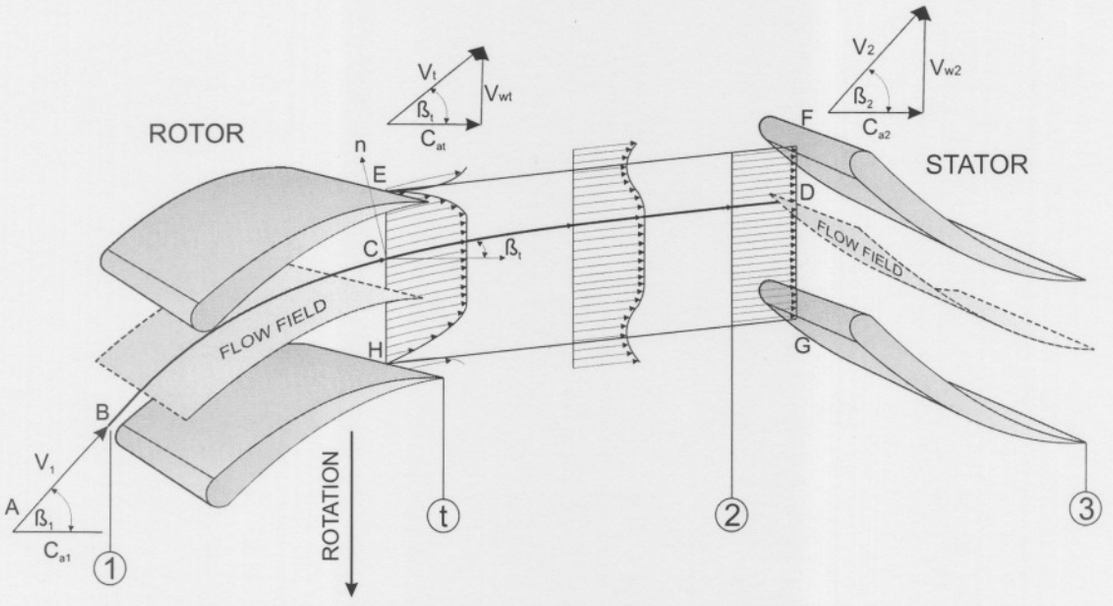

Figure 3.14 Depression of velocity profile with boundary-layer effects at the exit of a cascade

By assuming that the flow is steady and one-dimensional and applying (2.4) to a control surface EFGH, Csanady (1964:271) derived this equation:

$$V_t \cdot \cos \beta_t = \frac{C_{a2}}{1-\Delta} \tag{3.16}$$

where the blockage Δ is defined by:

$$\delta^* = \Delta\left(s \cos \beta_t\right) = \int_{-S'/2}^{+S'/2} \left(1 - \frac{\upsilon_t}{V_t}\right) \partial n \text{ with } \quad S' = s \cos \beta_t \tag{3.17}$$

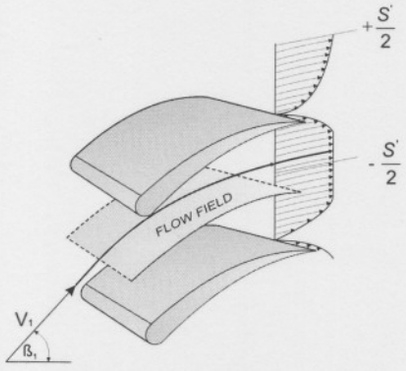

Figure 3.15 Displacement thickness at exit of a cascade

The displacement thickness is denoted by δ^* in the normal (n) direction and υ_t is the velocity inside the blade boundary layer. The momentum balance in the n direction provides the following

relationship:

$$V_t \sin\beta_t = V_{w2}\left(\frac{1-\Delta}{1-\Theta-\Delta}\right) \tag{3.18}$$

where $$\theta = \Theta(s\cos\beta_t) = \int_{-s/2}^{+s/2} \frac{v_t}{V_t}\left(1-\frac{v_t}{V_t}\right)\partial n \tag{3.19}$$

The momentum thickness is denoted by θ in the n direction in Figure 3.14. Lieblein (1959) defined a parameter called the wake form factor H_2 as a constant of 1.08. The wake form factor H_2 is a ratio between the displacement thickness and the wake momentum thickness $H_2 = \delta^* / \theta$. It will be convenient to introduce the non-dimensional parameters:

$$\Delta = \frac{\delta^*}{s\cos\beta_1} \qquad \Theta = \frac{\theta}{s\cos\beta_1} \tag{3.20}$$

The physical meaning of this result is simply that the magnitude of the ideal V_t^* has been increased by a constriction ratio $1/(1-\Delta)$. Thus boundary layer growth and the subsequent deflection of the wake cause an extra deviation in the outlet flow angle at section 2 with reference to section t. The outlet flow angle defined by Csanady (1964:271) can be described by:

$$\tan\beta_2 \approx (1-\Theta-\Delta)\tan\beta_t \tag{3.21}$$

Other authors describe this phenomenon under the heading blockage factor. The deviation caused by the boundary layer growth in control surface EFGH can now be defined by:

$$\delta_B = \beta_2 - \beta_t \tag{3.22}$$

Thus the final deviation can be presented by:

$$\delta_{tot} = \delta + \delta_B \tag{3.23}$$

where δ is assumed to be the deviation described by Lieblein (1960:575).

3.4.2 DEVIATION CAUSED BY LOW REYNOLDS NUMBERS

The blading designed for all compressors relies on there being a turbulent boundary layer on the suction surface to allow the flow to decelerate without major separation. Many blades do in fact operate with some regions of separated flow, but if this is too extensive there is a marked rise in deviation.

It is very common for the laminar boundary layer formed near the leading edge or just downstream of the region of maximum velocity to separate to form what is known as a separation bubble. In most bubbles the shear layer between the nearly stationary fluid in the bubble and the fast moving fluid outside it is very unstable, so that the separated shear layer undergoes transition and the flow reattaches as a turbulent boundary layer. There is good reason to think that the presence of a small separation bubble does no harm, at least for subsonic flows. The harm is real, however, if the flow is unstable to reattach, which may be the case at low Reynolds numbers.

The deviation measured is shown in Figure 3.16 for three values of incidence. For the case of $i = -1$ the deviation has reached its asymptotic value by $Re = 1.8 \times 10^5$. It will be noted that positive incidence leads to achievement of the asymptotic condition for deviation at lower Reynolds numbers, because the steeper velocity gradient encourages an earlier transition to turbulence (Cumpsty, 1989:176).

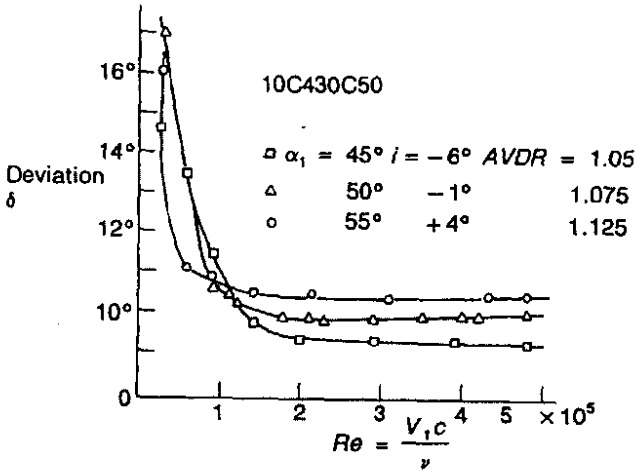

Figure 3.16 Deviation caused by low Reynolds number for C4 blade cascade (Cumsty 1989:178)

Roos (1995) developed a correlation for the effect of low Reynolds numbers on deviation from the data of Roberts (1975). Roberts (1975), however, developed a correlation for the bursting blade chord Reynolds number

$$\mathrm{Re}_{cB} = \left[\frac{(D+0.4)}{7.5\sqrt{TF}}\right] x10^5 + 10000 \tag{3.24}$$

as a function of the NACA diffusion factor

$$D = 1 - \frac{V_1}{V_2} + \frac{\Delta V_\theta}{2\sigma V_1} \tag{3.25}$$

and Taylor's turbulence factor

$$TF = Tu\left(\frac{c}{L_s}\right)^{\frac{1}{5}} \tag{3.26}$$

Incorporating turbulence intensity *Tu* and macroscale L_s:

$$Tu = \frac{\sqrt{\overline{u'^2}}}{V_1} \tag{3.27}$$

$$L_s = \int_0^{X_p} \frac{u_1' u_2'}{\sqrt{u_1'^2}\sqrt{u_2'^2}}\, d(X_p) \tag{3.28}$$

If *TF* is not available then *Tu* can be used as an approximation. No bursting takes place at values of D below 0.14. Roberts (1975) gave *TF* values of 0.0063 and 0.0074 for tests done on a chord blade length of 127mm and 60mm for different blade chord Reynolds numbers. In practice, however, none of the bursting Reynolds numbers from the correlation of Roberts (1975) reached $2x10^5$, so the *TF* value of 0.0074 was never used (Roos, 1995). According to Roos (1995), Roberts (1975) referred to the value of *TF* as 0.006 and it was decided to drop the fourth decimal place.

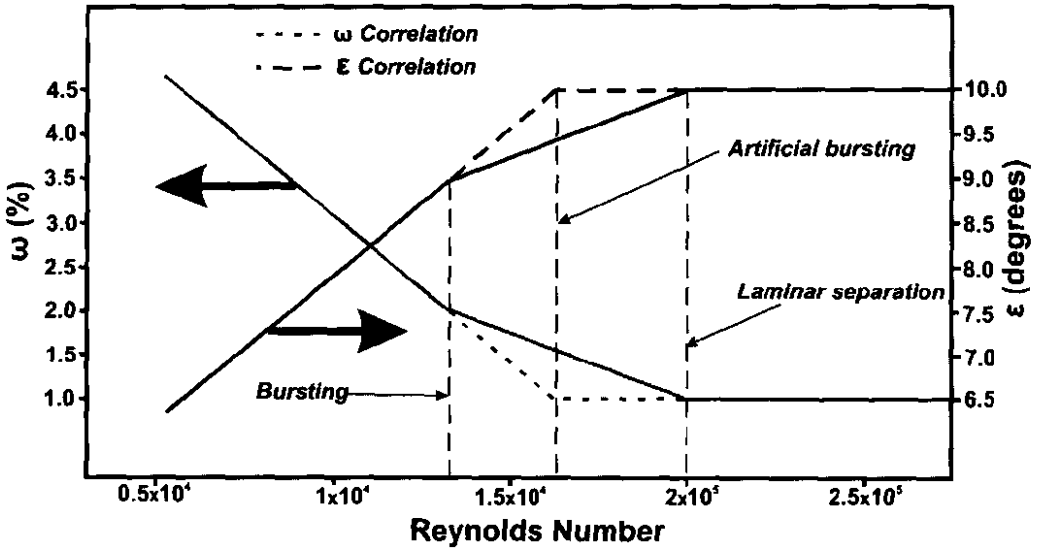

Figure 3.17 Definition of "artificial" bursting Reynolds number for turning and pressure loss coefficient (Roos, 1995)

A new Reynolds number difference was defined by Roos (1995)

$$\Delta \mathrm{Re}_c = \mathrm{Re}_{cB} - \mathrm{Re}_{cSB} \tag{3.29}$$

where B refers to bursting, i.e. $\mathrm{Re}_c = Re_{cB}$ and SB refers to sub-bursting $\mathrm{Re}_c < Re_{cB}$. The

uncertainty domain is removed to eliminate having to calculate the bursting $\overline{\omega}$ and $\overline{\varepsilon}$ values of laminar bubble Reynolds number, so separation and long laminar bubble "bursting" are assumed to take place at the same Reynolds number. This higher "artificial" bursting Reynolds number is defined such that the rate of decay of $\overline{\omega}$ and $\overline{\varepsilon}$ in the new sub-bursting regime remains the same as before, but bursting values of $\overline{\omega}$ and $\overline{\varepsilon}$ is the same as the attached flow values. The "artificial" Reynolds number is defined by Roos (1995) as:

$$\mathrm{Re}_{cB} = \left[\frac{D+0.4}{7.5\sqrt{TF}}\right] x10^5 + 10000 + 17766 \tag{3.30}$$

Furthermore, the turning in the sub-bursting regime is defined as:

$$\varepsilon_{SB} = \varepsilon_B - 1.72523x10^{-6}\theta\left(\frac{s}{c}\right)\Delta\mathrm{Re}_c \tag{3.31}$$

3.5 SUMMARY AND CONCLUSIONS

The difference between minimum loss incidence and optimum incidence as well as their respective calculation models were described. Furthermore, a stalling incidence model was presented in Section 3.3.1 to calculate when an axial flow compressor starts stalling. The author derived an approximation to estimate what the choking incidence at a given mass flow rate, rotational speed and inlet Mach number will be which is presented in Appendix B.

Two deviation models were located in open literature. One of these models used the minimum loss incidence as reference described by Lieblein (1960:575), while the other referred to the optimum incidence as reference described by Miller and Wasdell (1987:249). A deviation model due to boundary layer growth and low Reynolds numbers where also presented.

CHAPTER 4

PRESSURE LOSS PREDICTION METHODS

"I have been impressed with the urgency of doing. Knowing is not enough; we must apply. Being willing is not enough; we must do."

(Leonardo da Vinci)

4.1 INTRODUCTION

Turbomachinery are designed to meet certain system requirements. Under these designed operating conditions an axial flow compressor delivers a required pressure ratio at a specified rotational speed and mass flow rate.

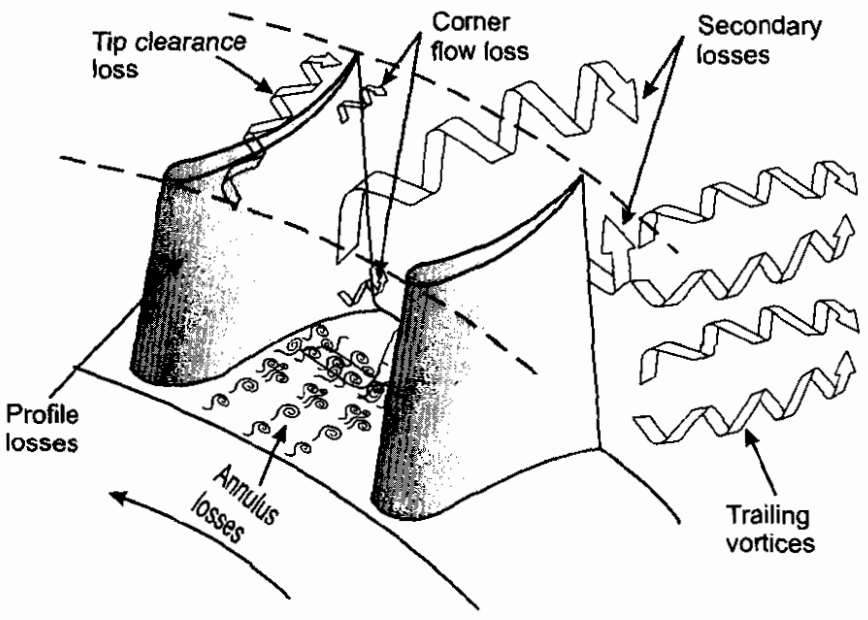

Figure 4.1 Losses obtained in an axial flow compressor

The axial velocity C_a displayed in Figure 2.4 is a function of mass flow rate $\dot{m} = \rho C_a A$. As the axial velocity varies in an axial flow compressor so does the inlet flow angle that enters a specific blade row. Decreasing axial velocity will result in an increase in the inlet flow angle. This increases the pressure ratio in the stage until stalling occurs. This continues until the flow separates from the blade profile and a sudden decrease in the pressure ratio is experienced. This separation point is known as the stall point and can be seen in Figure 1.10. Increasing axial velocity will result in a decrease in the inlet flow angle. This continues to the extent that the flow in the blade passages tends to choke, which leads to a significant increase in pressure losses.

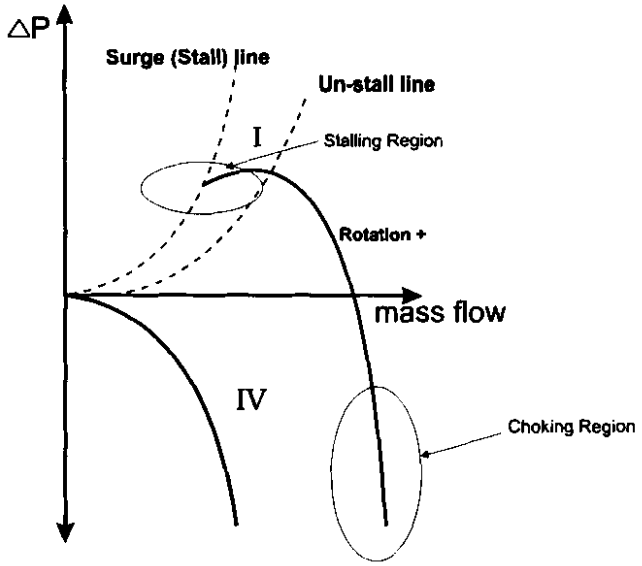

Figure 4.2 Axial flow compressor performance chart with stalling and choking regions specified at subsonic conditions

Figure 4.2 demonstrates where an axial flow compressor tends to stall and choke. The distance between the incidence where an axial flow compressor tends to choke i_{ch} and where it tends to stall i_s is called the operating range $\partial\beta$ (Casey, 1987:273). Lieblein (1959:387) was one of the first to introduce the concept of incidence angle and its variation with total pressure loss, widely referred to as the loss bucket chart presented in Figure 4.3.

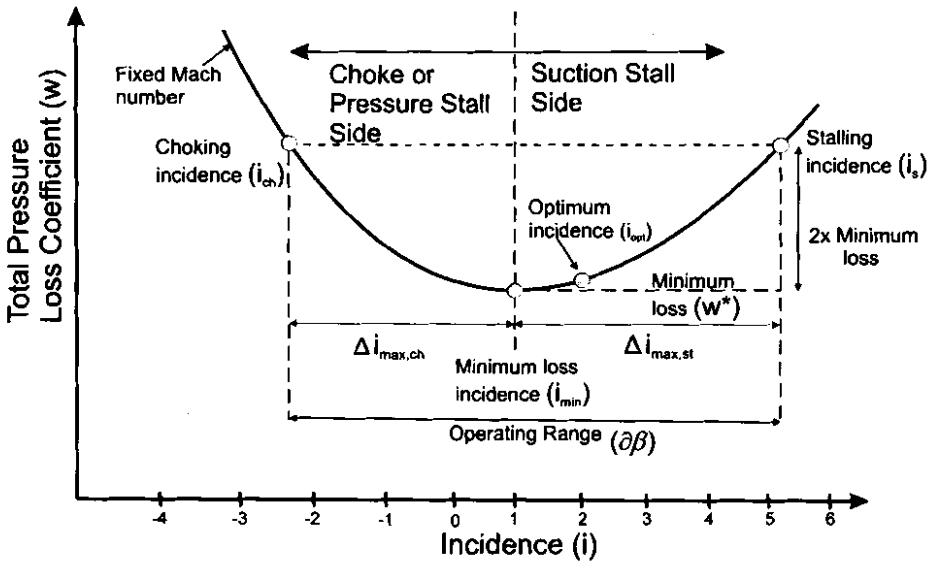

Figure 4.3 Loss bucket chart

To predict the total pressure loss in an axial flow compressor a superposition of theoretically separable loss components is used. More specifically, for this thesis the different pressure loss components will be discussed under the following headings:

- ***Blade profile losses***
- ***Secondary losses*** (sum of tip clearance, corner losses and trailing vortices described by Cohen *et al.* (2001:240)). Also referred to as endwall losses.
- ***Annulus losses***

The total pressure loss can be formulated as follows:

$$\omega = \omega_p^* \cdot \left(\frac{\omega}{\omega_i}\right)_{inc} \cdot \left(\frac{\omega}{\omega_i}\right)_{Re} \cdot \left(\frac{\omega}{\omega_i}\right)_{Ma} + \omega_s \cdot \left(\frac{\omega}{\omega_i}\right)_{Re} + \omega_a \qquad \text{for } i > i_{min} \qquad (4.1)$$

$$\omega = \omega_p^* \cdot \left(f(\frac{\omega}{\omega_i}, \Phi)\right)_{inc} \cdot \left(\frac{\omega}{\omega_i}\right)_{Re} + \omega_s \cdot \left(\frac{\omega}{\omega_i}\right)_{Re} + \omega_a \qquad \text{for } i < i_{min} \qquad (4.2)$$

Where ω_p^* is the profile pressure loss coefficient at minimum loss angle (Section 4.3). Off-design correction $(\omega/\omega_i)_{inc}$ is the correction for an axial flow compressor not operating near the design point (Section 4.4). Annulus losses ω_a and secondary losses ω_s are defined in Section 4.5. Reynolds correction factor $(\omega/\omega_i)_{Re}$ is the correction for Reynolds number effects on pressure loss (Section 4.8). The correction for Mach number effects $(\omega/\omega_i)_{Ma}$ is the correction for increasing pressure loss with increasing Mach number (Section 4.9). The correctional slope factor denoted by Φ is a correction on $(\omega/\omega_i)_{inc}$ when an axial flow compressor operates in the choke side of Figure 4.3 (Section 4.10).

4.2 LOSS COEFFICIENTS

Analysis in axial flow compressors requires that both relative and absolute frames are considered. Therefore it is necessary to define a different absolute and relative stagnation state, but with the same static state. Thus for enthalpy:

$$h_0 = h + \frac{1}{2}C^2 \tag{4.3}$$

$$h_{0r} = h + \frac{1}{2}V^2 \tag{4.4}$$

The subscript h_0 denotes the stagnation enthalpy in the absolute frame and h_{0r} the stagnation enthalpy in the relative frame called the rothalpy. Stagnation enthalpy h_0 is constant across the stator blade row, while the rothalpy h_{0r} is constant across the rotor blade row.

For incompressible flow, the total pressure losses are related to the cascade loss parameters by:

$$\omega_R = \frac{p_{01r} - p_{02r}}{\frac{1}{2}\rho V_1^2} \qquad \text{for the Rotor} \tag{4.5}$$

$$\omega_S = \frac{p_{02} - p_{03}}{\frac{1}{2}\rho C_2^{\,2}} \qquad \text{for the Stator} \tag{4.6}$$

Where the pressure loss coefficient for compressible flow is defined by:

$$\omega_R = \frac{p_{01r} - p_{02r}}{p_{01} - p_1} \qquad \text{for the Rotor} \tag{4.7}$$

$$\omega_S = \frac{p_{02} - p_{03}}{p_{02} - p_2} \qquad \text{for the Stator} \tag{4.8}$$

The stagnation pressure is related to the static pressure for compressible fluid by:

$$p_0 = p\left(1 + \frac{\gamma - 1}{2}Ma^2\right)^{\frac{\gamma}{\gamma-1}} \tag{4.9}$$

where

$$Ma = \frac{C}{\sqrt{\gamma RT}} \tag{4.10}$$

This terminology is used in conjunction with the respective conservation equations described in Chapter 2 to accurately calculate the inlet and outlet pressures, Mach numbers, temperatures, enthalpy etc. for a given blade row.

4.3 BLADE PROFILE PRESSURE LOSS AT DESIGN REFERENCE CONDITIONS

Blade profile pressure loss at reference conditions can be defined as the pressure loss over a cascade with an optimum or minimum loss inlet incidence angle (Section 3.2.1). Howell (1945) attempted to estimate blade profile loss in terms of the familiar drag and lift coefficients using optimum incidence as reference angle. However, the most popular profile loss model used today is that of Lieblein (1959:387). This two-dimensional incompressible cascade model uses the smallest number of empirical correlations and the minimum loss incidence angle as reference.

Lieblein's (1959:387) blade profile loss model served as a vantage point for many researchers.

- Bloch and O'Brien (1992:3) used Lieblein's (1959:387) blade profile loss model (4.11) in conjunction with annulus (4.42) and secondary losses (4.43) to specify total pressure loss in an axial flow compressor.
- Koch and Smith (1976:411) also used Lieblein's (1959:387) profile loss model (4.11), but defined a different momentum thickness to chord ratio and wake form factor H_2, which will be described later in this section.
- Casey (1987:273) adopted Lieblein's (1959:387) profile loss model and tied it with his own empirical correlations for the momentum thickness to chord ratio.

The blade profile pressure loss model derived by Lieblein (1959:387) is given by:

$$\omega_p^* = 2 \cdot \sigma \cdot \frac{\cos^2 \beta_1}{\cos^3 \beta_2} \cdot \left(\frac{\theta^*}{c} \right) \cdot \left\{ \frac{\frac{2H_2}{3H_2 - 1}}{\left[1 - \left(\frac{\theta^*}{c} \right) \cdot \frac{\sigma \cdot H_2}{\cos \beta_2} \right]^3} \right\} \tag{4.11}$$

where θ^* denotes the wake momentum thickness at reference conditions, σ the blade solidity and c the blade chord length. A measure of the degree to which the wake is mixed out after a given blade row is referred to as the wake form factor H_2 defined by $H_2 = \delta^* / \theta$, where δ^* is the boundary layer displacement thickness and θ the momentum thickness. These parameters are widely used today and can be located in many boundary layer theory literatures (Young, 1989).

- Lieblein (1959:387) used a constant value for the wake form factor H_2 of 1.08.
- Koch and Smith (1976:411) however, described a nominal wake form factor H_2 presented in Figure 4.4. This nominal wake form factor is then corrected for inlet Mach

numbers other than 0.05 and streamtube height variation effects obtained from Figures 4.5, 4.6. Streamtube ratio is defined as the ratio between the in and outlet blade height.

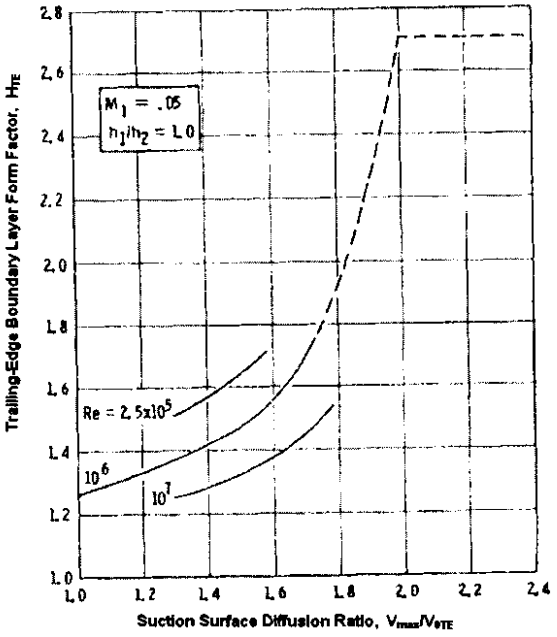

Figure 4.4 Koch and Smith correlation for H_2

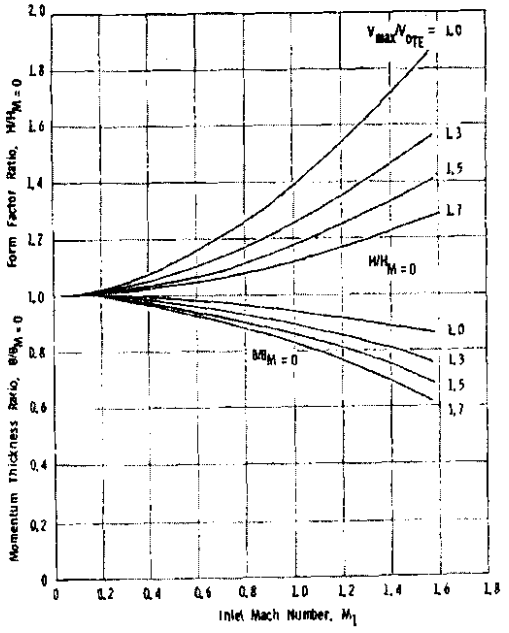

Figure 4.5 Effect of inlet Mach number on trailing edge momentum thickness and wake form factor for varying D_{eq}

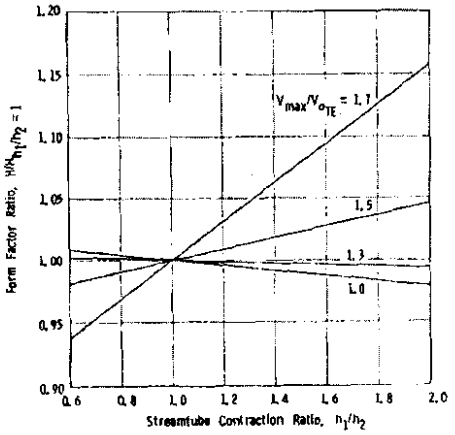

Figure 4.6 Effect of streamtube height variation on calculated trailing-edge wake form factor with varying D_{eq}

Momentum Thickness to Chord Length Ratio Model 1 (Casey, 1987):

For blades with "healthy" boundary layers, the mixing takes place rapidly after the trailing edge. The difference is usually small between measurements of the boundary layer parameters in the wake or at the trailing edge as suggested by Cumpsty (1989:172). Lieblein (1959:387) showed a

correlation between the equivalent diffusion ratio and the wake momentum thickness to chord ratio. This is valid for both NACA 65-(A_{10}) and C.4 circular arc blades. Casey (1987:273) gave the following optimized correlation of Lieblein's work:

$$\left(\frac{\theta^*}{c}\right) = \frac{0.0045}{1 - 0.95 \cdot \ln(D_{eq})} + 0.0025 \tag{4.12}$$

where D_{eq} is defined as the diffusion ratio. Koch and Smith (1976:411) suggested adding 0.0025. There seems to be no real theoretical justification for this, other than it leads to better predictions of efficiency (Casey, 1987:275).

Momentum Thickness to Chord Length Ratio Model 2 (Koch and Smith, 1976):

Koch and Smith (1976:411) presented the trailing edge momentum thickness to chord ratio correlation shown in Figure 4.7. This correlation is valid for nominal condition with a chord Reynolds number $\mathrm{Re}_c = \frac{\rho_1 V_1 c}{\mu_1}$ of 1×10^6, hydraulically smooth blades, a streamtube height ratio h_1/h_2 of 1 and a Mach number of 0.05. Corrections should be applied to conditions operating away from these nominal conditions Figure 4.7 and 4.8.

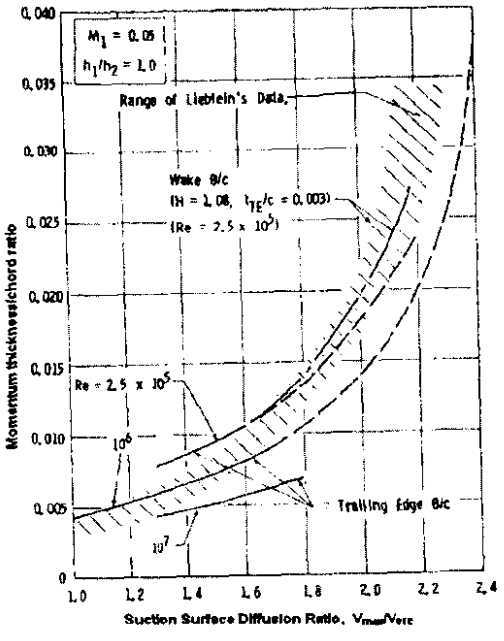

Figure 4.7 Koch and Smith correlation for θ_{te}/c

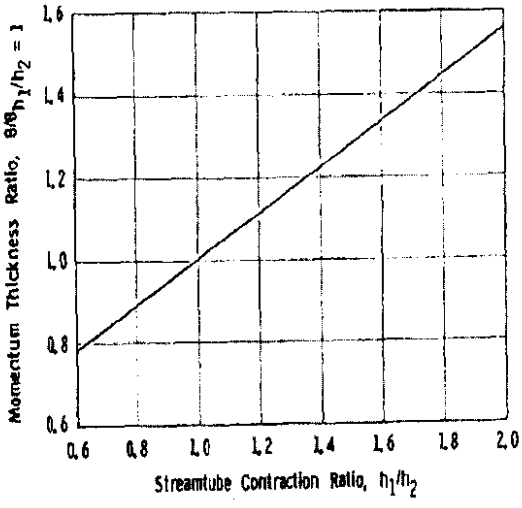

Figure 4.8 Effect of streamtube height variation on calculated trailing edge momentum thickness

Lieblein (1959:387) defined a diffusion ratio, dividing the difference of the maximum relative flow velocity in the blade passage and the relative outlet velocity, by the inlet relative velocity as given by:

$$D = \frac{V_{max} - V_2}{V_1} = 1 - \frac{1}{2}\frac{|\Delta V_w|}{\sigma V_1} - \frac{V_2}{V_1} \tag{4.13}$$

where $\Delta V_w = V_{w1} - V_{w2}$. Through the years, different authors optimized the diffusion ratio equations and expanded Lieblein's work.

Diffusion Ratio Model 1 (Lieblein, 1959):

Lieblein (1959:387) derived an equivalent diffusion ratio with minimum loss incidence as reference. The model is obtained in terms of inlet and outlet conditions and is given by:

$$D_{eq}^{*} = \frac{\cos\beta_2}{\cos\beta_1}\left[1.12 + 0.61 \cdot \frac{\cos^2\beta_1}{\sigma} \cdot \left(\tan\beta_1 - \tan\beta_2\right)\right] \tag{4.14}$$

Diffusion Ratio Model 2 (Lieblein, (1959) → Klapproth):

In discussion of Lieblein's (1959:387) paper Klapproth modified the equivalent diffusion equation D_{eq}^{*}. Klapproth modified the diffusion-parameter concept to accommodate an axial flow compressor rather than for cascade analysis. The changes are to accommodate streamline shift and change in axial velocity in stages that is given by:

$$D_{eq}^{*} = \frac{\cos\beta_2}{\cos\beta_1}\frac{C_{a1}}{C_{a2}}\left[1.12 + 0.61\frac{\cos^2\beta_1}{\sigma}K\right] \tag{4.15}$$

where

$$K = \tan\beta_1 - \frac{r_2}{r_1}\frac{C_{a2}}{C_{a1}}\tan\beta_2 - \frac{\omega r_1}{C_{a1}}\left(1 - \left(\frac{r_2}{r_1}\right)^2\right) \tag{4.16}$$

Axial velocities C_{a1} and C_{a2} are a function of mass flow rate as previously mentioned and ωr is zero for stators. Pfitzinger *et al.* (1997:120) also used this model in their simulation calculations.

Diffusion Ratio Model 3 (Koch and Smith, 1976):

Koch and Smith (1976:411) optimized Lieblein's model to account for compressibility, Reynolds number effects and streamtube contraction effects found in axial flow compressors. Koch and Smith (1976:411) defined a semi-empirical approximation for the trailing-edge diffusion ratio with minimum loss incidence as reference and is given by:

$$D_{eq}^{*} = \frac{V_1}{V_{te}} \frac{V_{max}}{V_{ps}} \frac{V_{ps}}{V_1} \tag{4.17}$$

The free stream trailing-edge velocity V_{te} is the velocity before wake mixing. This is elaborated in Section 3.4.1., where V_{te} is equal to the free stream velocity V_t in Figure 3.14. V_{max} is the maximum relative velocity occurring on the blade suction surface. V_{ps} is the mean velocity in the passage throat region. V_{ps} is composed of a tangential component that is affected by circulation, and an axial component that is affected by blade thickness blockage, streamtube contraction and compressibility. The correlations between the different velocity ratios obtained in (4.17) are given by:

$$\frac{V_{max}}{V_{ps}} = \left(1 + 0.7688 \frac{t_{max}}{c} + 0.6024\Gamma\right) \tag{4.18}$$

and

$$\frac{V_{ps}}{V_1} = \left[\left(\sin\beta_1 - 0.2445\sigma\Gamma^2\right) + \left(\frac{\cos\beta_1}{A^* \frac{\rho_{ps}}{\rho_1}}\right)^2\right]^{0.5} \tag{4.19}$$

The minimum loss area contraction ratio from blade inlet to the throat is given by:

$$A^* = \left(\frac{1 - 0.4458\sigma\left(\frac{t_{max}}{c}\right)}{\cos\left(\frac{\beta_1 + \beta_2}{2}\right)}\right)\left(1 - \frac{A_1 - A_2}{3A_1}\right) \tag{4.20}$$

The density in the passage throat to inlet density ratio is given by:

$$\frac{\rho_{ps}}{\rho_1} = 1 - \frac{M_a^2}{1 - M_a^2}\left(1 - A^* - 0.2445\frac{\tan\beta_1}{\cos\beta_1}\sigma\Gamma\right) \tag{4.21}$$

The minimum loss circulation parameter for a two-dimensional incompressible cascade is defined by:

$$\Gamma = \frac{\cos\beta_1(\tan\beta_1 - \tan\beta_2)}{\sigma} \tag{4.22}$$

The throat area can be defined as the region where the suction surface velocity V_{ps} is the highest. Further detail of the aforementioned parameters can be located in Koch and Smith (1976:411).

Diffusion Ratio Model 4 (Wright and Miller, 1991):

Wright and Miller (1991:69) modified the original diffusion ratio model to account for compressibility and thickness to chord ratio effects observed in high speed cascades and compressor tests. This correlation has been established for transonic DCA aerofoils but is used for conventional circular arc aerofoils. The equivalent diffusion ratio with reference to minimum loss incidence is given by:

$$D_{eq}^* = \left(1 - \frac{V_2}{V_1} + \left(0.1 + \frac{t_{max}}{c}\left(10.116 - 34.15\frac{t_{max}}{c}\right)\right)\frac{s}{c}\frac{(V_{w1} - V_{w2})}{V_1}\right)\frac{V_1}{V_2} + 1.0 \tag{4.23}$$

4.4 OFF-DESIGN PRESSURE LOSS PREDICTION

Axial flow compressors are designed to operate at maximum efficiencies (design point). When operating at maximum efficiency the difference between the blade angle and the inlet flow angle is called the minimum loss incidence angle (Section 3.2.1). In reality axial flow compressors seldom operate at the design point, thus off-design correction factors have to be implemented in profile pressure loss predictions. Different loss bucket charts were obtained from experimental tests on various blade types (Figure 4.9 and 4.10).

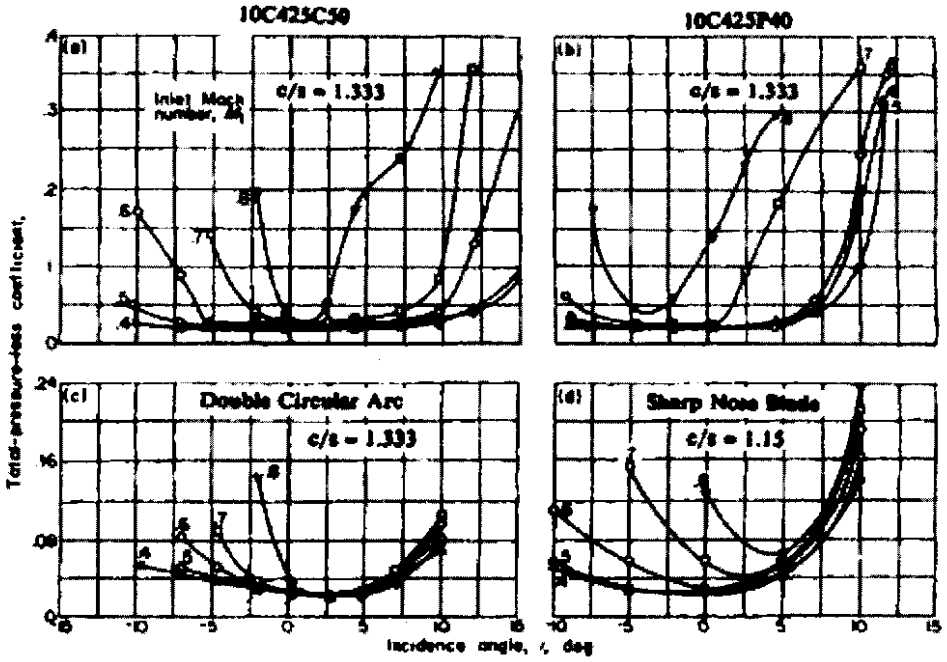

Figure 4.9 Typical loss distribution for various blade profiles (a) C4 circular arc, (b) P4 parabolic arc and (c) double circular arc with a camber angle of 25°, (d) sharp nose blade with a camber angle of 27.5°. (NASA SP-36, 1965)

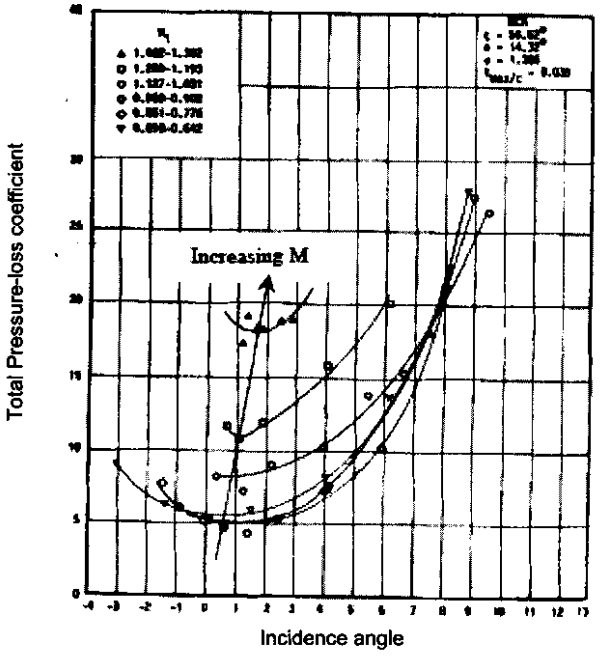

Figure 4.10 The variation of total losses with incidence at 10% span for a single stage transonic compressor with MCA blade profiles (Cetin, *et al.* 1987:12)

Subsonic axial flow compressors operate mostly in the choke side for the front stages and suction stall side at the rear stages of the loss bucket chart (Figure 4.3). This is done so that at reduced speed the efficiency is not degraded to badly in first quadrant operation. When the operating point tends to go to the fourth quadrant the incidence angle operates in the choking side of the loss bucket chart (Figure 4.3). Therefore it can be concluded that with a fixed rotational speed, a decrease in the mass flow rate will result in an incidence increase to the positive stall side of the loss bucket chart (Figure 4.3). However, an increase in mass flow rate will result in a decreasing incidence to the negative choking side of the loss bucket chart. An increasing pressure loss is the result of an axial flow compressor which operates at conditions far removed from the design point (Figure 4.9).

Off-design loss prediction methods located in open literature are:

- Lieblein (1959:387) used a method where he corrected the diffusion factor D_{eq}^* to accommodate for off-design losses.
- Cetin *et al.* (1987:6) derived correlations for transonic compressor blades.
- Jansen and Moffatt (1967:453) used an off-design correction assuming a parabolic variation of loss with incidence such that at stalling or choking incidence the pressure loss is twice that of the minimum loss value. Casey (1987:273) also used this expression to define the operating range for NACA 65-series compressor blades.
- Miller and Wasdell (1987:249) presented a model for Rolls-Royce, almost the same as Jansen and Moffatt (1967:453) but for transonic DCA aerofoils. Their description of stalling incidence is the incidence at which the blade loss is twice the minimum loss value. However, choking appears to have a greater effect on loss than stalling and a factor of three times the minimum loss value is used.
- The author presented a slope correctional factor derived in Appendix C. This slope correctional factor was derived to correct the parabolic correction of Miller and Wasdell (1987:249) when operating in the choke side of the loss bucket chart in Figure 3.3.

Off-Design Model 1 (Lieblein, 1959):

Lieblein (1959:387) corrected the D_{eq}^* (4.14) at incidence angles greater than minimum loss incidence. The following correlation was given:

$$D_{eq} = \frac{\cos\beta_2}{\cos\beta_1}\left[1.12 \cdot a \cdot (i - i_{min})^{1.43} + 0.61 \cdot \frac{\cos^2\beta_1}{\sigma} \cdot (\tan\beta_1 - \tan\beta_2)\right] \quad (4.24)$$

Where a = 0.117 for the NACA 65-(A_{10}) blades and a = 0.007 for the C.4 circular arc blades. Swan (1961:322) and Konnig *et al.* (1996, Pt. I:73) adapted this method of prediction, which is only applicable for subsonic conditions. This method was modified and extended by Swan (1961:322) to include the additional losses caused by shock waves in transonic axial flow compressors.

Off-Design Model 2 (Cetin *et al.*, 1987):

Cetin *et al.* (1987:6) presented a method to include the incidence loss for transonic DCA and MCA profiles, where changing Mach numbers do not greatly effect off-design profile losses. The profile pressure loss coefficient, including the effect of the incidence loss is given by:

$$\overline{\omega}_p = \overline{\omega_p^*} + c_m (i - i^*)^2 \quad (4.25)$$

where $\overline{\omega_p^*}$ is the total pressure loss at minimum loss incidence including the shock loss if applicable. Values of c_m are highly empirical and are presented in Table 4.1.

Profile Type	(i - i*)	Equation
MCA Ma ≥ 0.56	< 0	c_m = 0.02845 Ma – 0.01741
	> 0	c_m = 0.00363 Ma – 0.00065
DCA Ma ≥ 0.62	< 0	c_m = 0.05336 Ma – 0.02937
	> 0	c_m = 0.00500 Ma – 0.00075

Table 4.1 Variation of c_m with relative inlet Mach number

Cetin *et al.* (1987:6) derived these correlations from Koch and Smith's (1976:411) correlations for $\overline{\omega_p^*}$. They also modified Lieblein's minimum loss correlations for i^*. The choking and stalling incidences are taken as the incidences where the losses are twice their minimum value so that:

$$i_{st} \text{ or } i_{ch} = i^* + \left(\frac{\overline{\omega_p^*}}{c_m}\right)^{0.5} \quad (4.26)$$

where c_m are obtained from Table 4.1 and Ma denotes inlet Mach number. The c_m value for

predicting stall incidence was found from equations given for $(i - i^*) > 0$, whereas for the choking incidence, equations for $(i - i^*) < 0$ are used. This section is also summarized in the Flownex Theory Manual (2005:FNXTH-0035).

Off-Design Model 3 (Jansen and Moffatt, 1967):

Jansen and Moffatt (1967:453) assumed a parabolic variation of loss with incidence such that at the stall suction side and choke pressure side of Figure 4.3 the loss is twice the minimum-loss value. The loss coefficient is therefore given by the relation:

$$\overline{\omega} = \overline{\omega}_p^*(0.8333\,\overline{S}^2 + 0.1667\,\overline{S} + 1.0) \tag{4.27}$$

where $\overline{S}$ is defined as:

$$\overline{S} = \frac{\beta_1 - \beta_1^*}{\beta_{ch} - \beta_1^*} \qquad \beta_1 < \beta_1^* \quad \text{Choking pressure side} \tag{4.28}$$

and

$$\overline{S} = \frac{\beta_1 - \beta_1^*}{\beta_{st} - \beta_1^*} \qquad \beta_1 > \beta_1^* \quad \text{Stalling suction side} \tag{4.29}$$

Jansen and Moffatt (1967:453) did not specify how the stalling and choking incidence can be calculated. Casey (1987:273) further elaborated on the model of Jansen and Moffatt (1967:453). Casey (1987:273) included Mach number effects and defined an operation range in the place of using choking and stalling inlet flow angles. Casey (1987:273) defined an operating range in a compressor cascade as the range of inlet angle $\partial\beta$ within which the loss coefficient is less than twice the minimum loss value. For simplicity the operating range is defined as $i_{ch} - i_s$ where the loss is less than twice the minimum loss value. This is calculated as follows:

$$\partial\beta = \partial\beta_i\,(\partial\beta / \partial\beta_i)_{Ma} \tag{4.30}$$

where $\partial\beta_i$ is the operating range of the NACA 65-series cascades at low Mach numbers and $(\partial\beta / \partial\beta_i)_{Ma}$ is a multiplication correction for the effect of Mach number on the operating range. Choking incidence is highly dependant on inlet Mach number and throat width as described by Miller and Wasdell (1987:249). That's why choking incidence increases to the positive side with higher inlet Mach numbers, making $i_{max,ch}$ smaller (Figure 4.3).

Note that this correction factor $(\partial\beta/\partial\beta_i)_{Ma}$ does not hold any connection to the Mach correction factor as described in Section 4.7. It merely narrows the operating range from Figure 4.3 due to the fact that i_{ch} is highly dependant on inlet Mach number. Analysis of the NACA data by Hugentobler (1986) (represented by Casey, 1987:273) has led to the following correlation for the operating range at low Mach numbers:

$$\partial\beta_i = 21 + K(1+\sqrt{\sigma})/\sigma\theta_{camber} \tag{4.31}$$

and

$$K = 0.001(-40 - 7(\beta_{1B} - 45) + 0.25(\beta_{1B} - 45)^2 - 0.02(\beta_{1B} - 45)^3 \tag{4.32}$$

within the range of the NACA data $30^\circ \le \beta_{1B} \le 70^\circ$. The correction for the effect of Mach number on operating range of NACA 65-series blading is taken into account as proposed by Hoheisel (1969), as:

$$Ma < 0.2 \qquad (\partial\beta/\partial\beta_i)_{Ma} = 1 \tag{4.33}$$

$$Ma > 0.2 \qquad (\partial\beta/\partial\beta_i)_{Ma} = 10^A \tag{4.34}$$

where

$$A = -2.5(Ma - 0.2)^{4.4} \tag{4.35}$$

Casey(1987:273) defined an off-design factor related to the flow incidence angle and operating range χ, as follows:

$$\chi = \frac{|i - i^*|}{\partial\beta/2} \tag{4.36}$$

The correction for incidence losses on the rotor and stator is similar to the method proposed by Jansen and Moffatt (1967:453) and is given by:

$$(\omega/\omega_i)_{inc} = 1.0 + 0.1667\,\chi + 0.8333\,\chi^2 \tag{4.37}$$

The operating range defined by Casey (1987:273) is highly empirical and is only valid for NACA 65-series blades. Secondly $i_{max,ch}$ and $i_{max,st}$ were calculated by dividing the operating range in two (4.36). The parameter $i_{max,ch}$ may be questionable when a compressor operates in the fourth quadrant. An accurate i_{max} value has to be obtained to calculate the correct χ parameter.

$$\chi = \frac{|i - i^*|}{i_{max,ch\,or\,st}} \tag{4.38}$$

Off-Design Model 4 (Miller and Wasdell, 1987):

Miller and Wasdell (1987:249) developed an off-design correction factor on the same basis as Jansen and Mofatt (1967:453).

Miller and Wasdell (1987:249) defined stalling incidence as the incidence at which the blade loss is twice the minimum loss and introduced a method to calculate stalling incidence. Hence, the determination of choking incidence required a knowledge of the inlet Mach number and throat width. The loss at the choking incidence was taken as three times the minimum loss. This assumption was made by Miller and Wasdell (1987:249) using transonic DCA aerofoils. Miller and Wasdell (1987:249) used an iterative process to calculate the choking incidence. Unfortunately, no details regarding their method exist. Wright and Miller (1991:69) adapted the off-design prediction method and used the same principles as Miller and Wasdell (1987:249). The off-design prediction is given as:

$$(\omega/\omega_i)_{inc} = \left(\frac{i-i^*}{i_{st}-i^*}\right)^2 + 1 \qquad \text{for } i > i^* \tag{4.39}$$

$$(\omega/\omega_i)_{inc} = 2.25\left(\frac{i-i^*}{i^*-i_{ch}}\right)^2 + 1 \qquad \text{for } i < i^* \tag{4.40}$$

A comparison between Jansen and Mofatt (1967:453) and Wright and Miller (1991:69) is given in Figure 4.11.

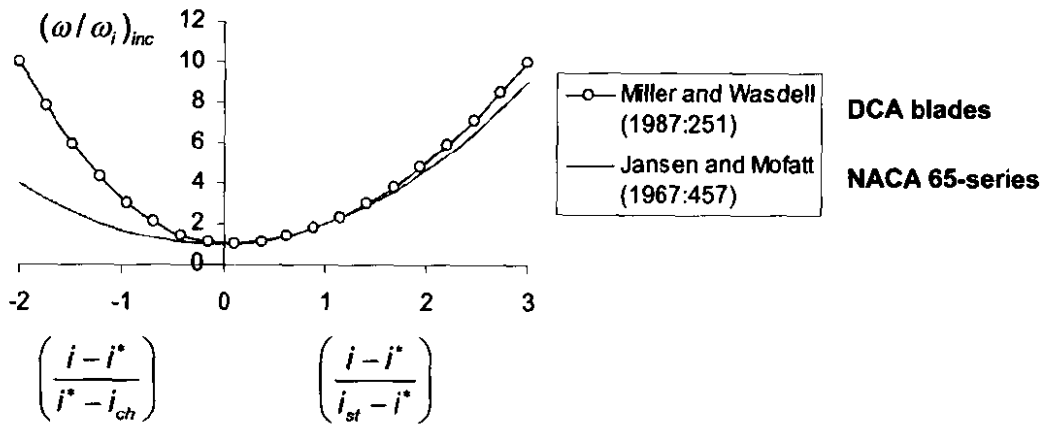

Figure 4.11 Comparison between two different off-design calculations

Off-Design Model 5 (Current study):

Von Backström (2005:P2) tested an axial flow compressor at two operating rotational speed lines, namely 0 r.p.m and 2000 r.p.m. It was found that in the fourth quadrant the off-design correlations given by Jansen and Moffatt (1967:453) and Wright and Miller (1991:72) resulted in pressure losses that are over-estimated.

A correctional slope factor was derived by the author to accurately predict the shape of the off-design parabolic curve in Figure 4.11 when operating in the choke side of Figure 4.3. The standard parabolic term from Miller and Wasdell (1987:249) was used to define the off-design pressure loss (4.40). The slope of the parabola is then corrected with the slope correctional factor Φ. The following assumption was made:

$$\left(\frac{\omega}{\omega_i}\right)_{inc} = \Phi\left(\frac{i-i^*}{i^*-i_{ch}}\right)^2 + 1 \qquad \text{for } i < i^* \qquad (4.41)$$

After using an optimization program created in EES the following empirical correlation was derived:

$$\Phi = \frac{0.65 \cdot Ma + 0.01}{489.8 \cdot \mathrm{Re}^{-0.5}} \qquad \text{for } 10^4 < \mathrm{Re}_{chord} < 10^5 \text{ and } Ma < 0.2 \qquad (4.42)$$

The full derivation of the slope correctional factor can be located in Appendix C, while the core of the optimization program is displayed in Appendix F.6.

4.5 SECONDARY AND ANNULUS LOSSES

The two additional losses (annulus and secondary) described by Dixon (1998:74) and Cohen *et al.* (2001:241) must be taken into account when calculating the overall pressure loss in an axial flow compressor.

- Annulus loss refers to the additional drag effects caused by the walls of an axial flow compressor.
- Secondary losses arise from a complex three-dimensional flow set-up as a result of the end wall boundary layers passing through the cascade Dixon (1998:84).

The assumption was made that annulus and secondary losses are applicable in the first and fourth quadrant. The annulus losses are represented in Bloch and O'Brien (1992:3) who

originated from Dixon (1998) as:

$$\varpi_a = 0.02 \cdot \sigma \cdot \left(\frac{c}{H}\right) \cdot \frac{\cos^2 \beta_1}{\cos^3 \beta_m} \tag{4.43}$$

Analysis of compressor performance charts by Bloch and O'Brien (1992:3) proved that the secondary loss is of major importance. It was also found that the magnitude of the secondary losses is of the same order as the losses caused by profile drag in a given blade set. Tip clearance is one of the greatest influences in secondary loss. The secondary loss is represented in Bloch and O'Brien (1992:3) who also originated from Dixon (1998) by:

$$\varpi_S = \frac{0.072}{\sigma} \cdot \frac{\cos^2 \beta_1}{\cos \beta_m} \cdot \left(\tan \beta_1 - \tan \beta_2\right)^2 \tag{4.44}$$

where

$$\tan \beta_m = \frac{\left(\tan \beta_1 + \tan \beta_2\right)}{2} \tag{4.45}$$

4.6 REYNOLDS CORRECTION FACTOR

The loss correction due to Reynolds number is assumed to be valid in the first and fourth quadrants. This is because pressure loss due to Reynolds number increase, depends mainly on blade surface roughness.

Reynolds Correction Model 1 (Koch and Smith & Mills and Xu Hang 1976):

A Reynolds correction factor was defined by Koch and Smith (1976:411) because of surface finishes, laminar and turbulent flows, affecting compressor performance.

1. Koch and Smith (1976:411) used a different chord Reynolds number exponent n for laminar and turbulent flows which is presented in Figure 4.12:

$$\left(\frac{C_D}{C_{Dcr}}\right)_{Re} = \left(\frac{Re}{Re_{cr}}\right)^n \tag{4.46}$$

The critical Reynolds number is taken as $Re_{cr} = 2 \times 10^5$.

For laminar flow: $Re \leq Re_{cr}$, n = -0.5

For turbulent flow: $\mathrm{Re} \geq \mathrm{Re}_{cr}$, n = -0.166

2. The correction for the roughness effects are done using an equation from Mills and Xu Hang (1983) for the skin-friction coefficient of a fully rough flat plate.

$$\left(\frac{C_D}{C_{Dref}}\right)_{ro} = \left(\frac{\left(2.635 - 0.618 \cdot \ln\left(\frac{k_s}{c}\right)\right)^{-2.57}}{C_{Dref}}\right) \tag{4.47}$$

$$k_s = 6.2 \cdot k_{CLA}$$

Where k_{CLA} is the centreline average deviation of roughness particles and C_{Dref} is the reference friction factor taken as 0.006 for laminar flow and 0.0028 for turbulent flow. For the purpose of this study k_{CLA} is taken to be $67x10^{-6}$.

The two corrections are combined such that correction of Reynolds number $(\omega/\omega_i)_{Re}$ is given by the largest value of $(C_D/C_{Dref})_{Re}$ and $(C_D/C_{Dref})_{ro}$.

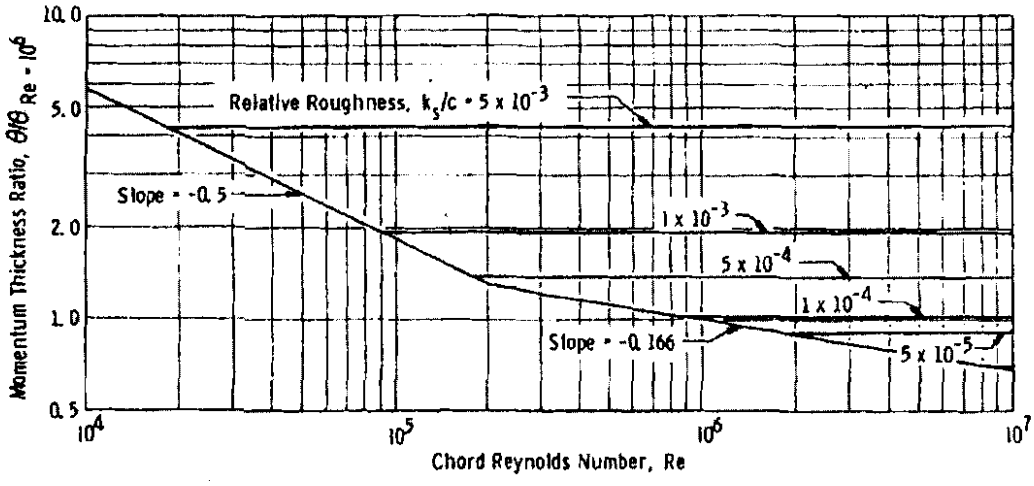

Figure 4.12 Effect of Reynolds numbers and surface finish on calculated trailing edge momentum thickness (Koch and Smith, 1976:415)

Reynolds Correction Model 2 (Wright and Miller 1991):

The Reynolds number correction from Wright and Miller (1991:69) is based on the Koch and Smith (1976:411) correlation. The correction for the influence of Reynolds number assumes that

the flow is hydraulically smooth up to a Reynolds number of 10^6. The same Koch and Smith (1976:411) Reynolds number exponent is used for laminar and turbulent flows.

$$\left(\frac{\omega}{\omega_i}\right)_{Re} \rightarrow \begin{cases} = 489.8 \cdot Re^{-0.5} & Re < 10^5 \\ = 13.8 \cdot Re^{-0.19} & 10^5 < Re < 10^6 \\ = 1.0 & Re > 10^6 \end{cases} \quad (4.48)$$

The exponent -0.5 is also used by Koch and Smith (1976:411) for change in loss due to Reynolds number in the laminar flow region $Re < 10^5$.

For $10^5 < Re < 10^6$ the change in loss with Reynolds number is similar to the Prandtl equation for the skin friction of a flat plate in a hydraulically smooth turbulent flow.

For $Re > 10^6$ the flow is assumed to be hydraulically rough and the losses constant irrespective of increases of Reynolds number.

Reynolds Correction Model 3 (Roos 1995):

In addition of the deviation caused by low Reynolds number, Roos (1995) also presented a pressure loss model for operation in that regime. This correlation is graphically presented in Figure 3.17. The correlation is defined as:

$$\overline{\omega_{SB}} = \bar{\omega}_B + 2.458x10^{-7}\left(\hat{\theta}\hat{t}\hat{s}\right)\Delta Re_c \quad (4.49)$$

where

$$\hat{\theta} = \frac{\theta}{\theta_{ref}}, \; \hat{t} = \frac{t/c}{(t/c)_{ref}}, \; \hat{s} = \frac{s/c}{(s/c)_{ref}}$$

$$\hat{\theta} = 10^{\circ}, \; (t/c)_{ref} = 0.1, \; (s/c)_{ref} = 1.0 \quad (4.50)$$

where θ is the blade camber angle, t is the maximum blade thickness, s is the blade pitch length and ΔRe_c is defined in Section 3.4.2.

4.7 MACH NUMBER CORRECTION FACTOR

This section presents a Mach correction factor valid only for the first quadrant of operation and a compressor operating with an incidence angle in the suction stall side of Figure 4.3.

Mach Correction Model 1 (Jansen and Moffatt 1967):

The Mach correction factor is based on compressibility of the fluid that enters the axial compressor. The correction for the effect of inlet Mach number is presented by Jansen and Moffatt (1967:453). The loss coefficient is corrected for Mach number effects only when the inlet Mach number exceeds the critical Mach number Ma_{1cr}. The correction is of the form:

$$\left(\frac{\omega}{\omega_i}\right)_{Ma} = 1 + 2 \cdot (Ma_1 - Ma_{1cr}) \tag{4.51}$$

where the critical Mach number is given by an analytical solution from a set of equations (4.53). For inlet Mach numbers less than Ma_{1cr} it is assumed that the flow is incompressible. Jansen and Moffatt (1967:453) derived a pressure coefficient for incompressible flow that is given by:

$$\left(\frac{\Delta P}{q_1}\right)_{inc} \equiv \frac{P_{01} - P}{q_1} = \left(\frac{V_{max}}{V_1}\right)^2 - 1 \tag{4.52}$$

However, a correction was derived that included Mach number to account the pressure loss due to compressibility effects that may occur.

$$\left(\frac{\Delta P}{q_1}\right)_{inc} = \frac{1 - \left(\frac{2}{\gamma+1} + \frac{\gamma-1}{\gamma+1} \cdot Ma_{1cr}^{\,2}\right)^{\frac{\gamma}{\gamma-1}}}{\left(1 + \frac{\gamma-1}{2} \cdot Ma_{1cr}^{\,2}\right)^{\frac{\gamma}{\gamma-1}} - 1} \tag{4.53}$$

Jansen and Moffatt (1967:453) indicated that the maximum velocity for NACA-65 series blades can be represented by an expression of the form:

$$\frac{V_{max}}{V_1} = 1 + E\left(\frac{\Delta V_w}{\sigma V_1}\right) + F \tag{4.54}$$

where ΔV_W is the change in whirl velocity, and E and F are thickness dependant empirical variables. Expressions for E and F of the following form have been developed:

$$E = 0.4 + \frac{t}{c} \text{ and } F = 0.03 + 0.7\left(\frac{t}{c}\right) \tag{4.55}$$

Mach correction Model 2 (Wright and Miller 1991):

This correlation relates blade profile loss at reference conditions to the equivalent diffusion ratio (4.23) and inlet Mach number (Figure 4.13). The empirical correlation is valid for transonic DCA blade sets. Wright and Miller (1991:69) defined the Lieblein loss parameter as follows:

$$\omega_{Ma} = \frac{\omega_{par}}{0.5\cos\beta_2\left(\frac{V_1}{V_2}\right)^2} \tag{4.56}$$

where ω_{par} can be located in Figure 4.13. The final profile loss at reference conditions can be defined as:

$$\omega_p^* = \omega_{Ma} \cdot \left(\frac{\omega}{\omega_i}\right)_{Re} \tag{4.57}$$

where $\left(\frac{\omega}{\omega_i}\right)_{Re}$ can be located in (4.48).

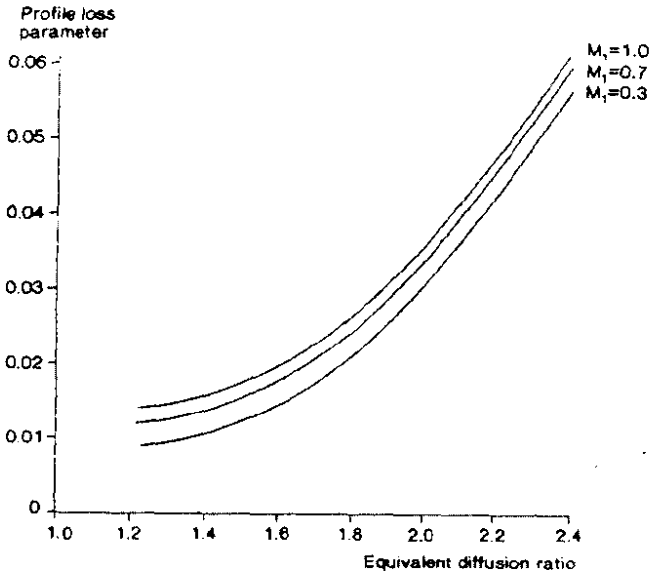

Figure 4.13 Correlation for profile loss coefficient

4.8 ANNULUS BLOCKAGE PREDICTION

Low momentum fluid in the endwall regions due to viscous effects and form boundary layers, leads to blockage causing a reduction in the effective flow area which in turn leads to an increase in the freestream axial velocity. The effect of blockage is included in the calculation of the freestream axial velocity through the use of a blockage factor according to:

$$\dot{m} = \rho C_a A_{eff} \tag{4.58}$$

where

$$A_{eff} = A_{geo} BF \tag{4.59}$$

A_{eff} denotes the effective flow area including the effect of blockage, A_{geo} is the geometrical flow area calculated from $\pi\left(\bar{r}_t^{-2} - \bar{r}_{hb}^{-2}\right)$ and BF is the blockage factor calculated by different methods.

The method by Koch and Smith (1976:411) calculates an average blockage factor over the whole stage, while the model given by Wright and Miller (1991:69) calculates an average blockage factor for the specific bladerow. Koch and Smith (1976:411) realized that their model is of limited scope and questionable general applicability. They suggest that the model should not be used for aspect ratios, $\frac{h}{c}$, less than unity. Therefore only the model of Wright and Miller (1991:69) is presented. It must be emphasized that no blockage calculation was found to be valid when the inlet flow angles become negative usually in the fourth quadrant of operation.

The model owes much to the boundary layer model from De Ruyck and Hirsch (1980) and has its basis in a two-dimensional incompressible semi-empirical model for calculating the growth of endwall boundary layer momentum thickness across a bladerow (Wright and Miller,1991:73)

$$\theta_2 - \theta_1 = \frac{cC_f}{2\cos\beta_m} - \bar{\theta}\left(2+\bar{H}\right)\frac{C_{a2}-C_{a1}}{\bar{C}_a} + \frac{F_{xs}}{\rho\bar{C}_a^2} + \frac{F_{xt}}{\rho\bar{C}_a^2} \tag{4.60}$$

where c, is the blade axial chord and β_m is calculated by Eq. (4.45).

The first two terms on the right hand side of (4.60) are the terms accounting for skin friction and axial velocity ratio, while the second two terms are empirical expressions for the axial component of the blade force through the endwall boundary layer due to dissipation forces along the

streamlines and lift forces at right angles to the streamlines. This is given by:

$$\frac{F_{xs}}{\overline{\rho C_a^2}} = (C_{Dt} + C_{Ds})\frac{h}{2}\sigma\cos^2\beta_m \tag{4.61}$$

$$\frac{F_{xt}}{\overline{\rho C_a^2}} = \frac{0.9\tau}{2\cos^2\beta_m}\sigma^2 C_L^{3.1} - \frac{1.7\bar{\theta}\sin(2\beta_m)}{2}\left(1-e^{-\sigma}\right)\frac{\bar{U}}{\overline{C_a}} \tag{4.62}$$

In (4.61), C_{Dt} is the drag coefficient due to blade tip clearance and C_{Ds} is the drag coefficient due to the secondary flows. These coefficients are given by:

$$C_{Dt} = 0.97\frac{\tau}{h}\sigma C_L^{3.1} \tag{4.63}$$

$$C_{Ds} = \frac{0.04}{2}\frac{c}{h}C_L^{4.66} \tag{4.64}$$

The lift coefficient, C_L, is given by (Cohen *et al.*, 2001,239) as:

$$C_L = \frac{2}{\sigma}(\tan\beta_1 - \tan\beta_2)\cos\beta_m \tag{4.65}$$

The skin friction coefficient in (4.60) is calculated using the semi-empirical formula (Wright and Miller,1991:73):

$$C_f = \frac{0.246\,\mathrm{Re}_\theta^{-0.268}\,e^{-1.56\bar{H}}}{1+0.6408\dfrac{(\bar{\gamma}-1)}{2}M_1^2} \tag{4.66}$$

where Re_θ is the Reynolds number based on the boundary layer *momentum* thickness, i.e. $\dfrac{\overline{\rho C_a \theta}}{\mu}$. By assuming a simple power law for the axial velocity profile through the boundary layer the form factor can be calculated from the Heads shape factor by:

$$H = \frac{H^*}{H^* - 2} \tag{4.67}$$

and the Heads shape factor can in turn be calculated from the Greens entrainment equation:

$$\frac{1}{c}\left(C_{a2}\theta_2 H_2^* - C_{a1}\theta_1 H_1^*\right) = 0.0306\bar{C}_a\left(\overline{H^*} - 3\right)^{-0.653} \tag{4.68}$$

It must be noted that the Heads shape factor H^* and the form factor H differs. Eq. (4.60) to (4.68) constitutes a coupled system of equations. These equations can be solved iteratively to calculate boundary layer momentum thickness and displacement thickness at the bladerow exit from the known values of θ_1, δ_1^* at the bladerow inlet for the hub and tip. The boundary layer displacement thickness is calculated as:

$$\delta^* = \theta H \tag{4.69}$$

The blockage factor is then calculated as:

$$BF = 1 - \frac{2\pi\left(\bar{r}_{hb}\delta_{hb}^* - \bar{r}_t\delta_t^*\right)}{A_{geo}} \tag{4.70}$$

If it is assumed that the blades are not twisted in the radial direction, the necessary hub and tip parameters can be assumed form knowledge of the parameters at the mean radius and the annulus dimensions.

4.9 SUMMARY AND CONCLUSIONS

A detailed description of pressure loss models, as described in open literature was presented in Chapter 4. Pressure loss in an axial flow compressor was presented as three separable loss components, namely blade profile loss, secondary loss and annulus loss. The operation of an axial flow compressor in the first and fourth quadrant was classified by using the loss bucket chart located in Figure 4.3.

Different types of diffusion ratio models were presented, using the Lieblein blade profile loss model at minimum loss incidence. A detailed description was given for the case where a compressor operates at conditions far removed from the design point. The author derived a correctional slope factor to vary the off-design correctional parabola with varying inlet Mach and Reynolds number. Different models describing loss due to varying Reynolds number were also presented in Section 4.6. Correctional models due to varying Mach number and blockage in an axial flow compressor were presented in Section 4.7 and 4.8 and are only valid in the first quadrant of operation.

CHAPTER 5

UNCERTAINTY ANALYSIS ON EXPERIMENTAL RESULTS

"It's not that I'm so smart, it's just that I stay with problems longer. "

(Albert Einstein)

5.1 INTRODUCTION

Characteristics for pressure rise, torque, power and efficiency were successfully measured in all four quadrants by Von Backström (2005), using a small three stage laboratory compressor. A summarised experimental report is presented in Appendix D. However, no uncertainty analysis was done on the experimental measurements. An uncertainty analysis was therefore done by the author on the experimental results in the first and fourth quadrant with positive rotation.

5.2 METHODOLOGY

Uncertainty of data can be calculated in one of two ways. Firstly the uncertainty interval of the equipment can be used to calculate the uncertainty in experimental readings also called the *standard error in a single observation*. Secondly uncertainty can be determined by the *standard error in the mean,* meaning *a set of data readings* were obtained for a *single experimental measurement.* The uncertainty is then calculated using the set of data readings. Uncertainty in the experimental measurements was taken as the largest uncertainty in both methods.

In the experimental setup a set of data readings were obtained and the mean of those data readings were to be transformed with calibration curves to a single pressure or torque measurement (Figure 5.1). Thus, a set of data readings provided one pressure or torque result. Using this set of data readings one can calculate an uncertainty in each experimental measurement using the *standard error in the mean* method.

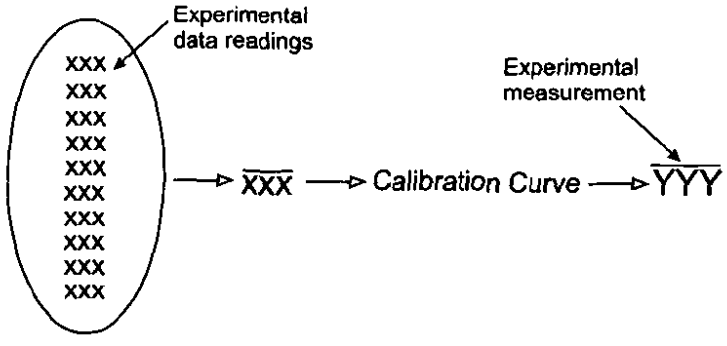

Figure 5.1 Calculation and terminology used to obtain experimental measurements in the experimental setup

The residual of i_{th} measurement is given by Squires (2001:16) as follows:

$$d_i = x_i - \bar{x} \tag{5.1}$$

where d_i is the residual with x_i one reading of the data reading set and $\bar{x}$ the mean of the data reading set. Then a *standard deviation of the sample* can defined as **s**:

$$s^2 = \frac{1}{n}\sum d_i^2 \tag{5.2}$$

This is for a data set of n measurements. The *standard deviation of the distribution* denoted by σ is given by (Squires, 2001:12):

$$\sigma \approx \left[\frac{n}{n-1}\right]^{\frac{1}{2}} s \tag{5.3}$$

The *standard error in the mean* denoted σ_m is described by this relation:

$$\sigma_m = \frac{\sigma}{\sqrt{n}} \tag{5.4}$$

The result of a set of readings is quoted as $\bar{x} \pm \sigma_m$. The *standard error in the mean* σ_m can be called the uncertainty interval in this analysis.

The uncertainty interval for a set of readings can easily be calculated, but it should be kept in mind that the measurements from the equipment were scaled to 2000 r.p.m. in the experimental setup. Thus, other uncertainties should also be taken into account.

When a final quantity Z is related to two directly measured quantities by a function of the form:

$$Z = AB \quad or \quad A/B$$

then an error of x% in A and B gives rise to an error of X% in Z. If we now take the function

$$Z = A/B$$

and made a set of readings and founded an error in the mean of:

$$A = 1000 \pm 20$$
$$B = 10 \pm 1$$

Now, when the percentage error in the mean value is calculated, the following is known:

$$\frac{\Delta A}{A} = 2\% \quad and \quad \frac{\Delta B}{B} = 10\%$$

A final percentage error can then be obtained in the final quantity Z.

$$\frac{\Delta Z}{Z} = \sqrt{\left(2^2 + 10^2\right)} = 10.2\% \tag{5.5}$$

However, for a function in this form:

$$Z = A + B \quad or \quad A - B$$

the situation changes and the error in the final quantity can be obtained from:

$$\frac{\Delta Z}{Z}\% = \left(\frac{\Delta A}{A}\%\right) \cdot \left(\frac{\Delta B}{B}\%\right) \tag{5.6}$$

A complete uncertainty analysis was derived with methods described above.

5.3 UNCERTAINTY ANALYSIS

An uncertainty analysis was done on the first and fourth quadrant (positive rotation) to identify data measurements with the most uncertainty.

As mentioned in Appendix D the measurements obtained in the experimental setup were:

- Inlet stagnation pressure [P_{01}]
- Inlet static pressure [P_1]
- Outlet stagnation pressure [P_{03}]
- Outlet static pressure [P_3]
- Rotational speed [r.p.m]
- Torque [N.m.]
- Inlet temperature [°C]
- Volume flow rate [m^3/s]

An uncertainty analysis was done on pressure and torque measurements. Power uncertainty was calculated using uncertainty derived from the torque measurements. As previously mentioned, experimental measurements were scaled to 2000 r.p.m. Therefore methods in (5.5) and (5.6) were used to calculate the uncertainty in the final quantity for pressure, torque and power measurements. An example how the uncertainty for torque measurements were derived in the experimental analysis is presented below.

The formula used to scale the data measurements is presented as follows:

$$\overset{\oplus}{Scaled}\ Torque = \overset{\oplus}{Torque}\ coef \times \overset{\odot}{Scaled}\ Blade\ speed \times \overset{\odot}{Scaled}\ \rho_{in}$$

where $\oplus$ denotes an uncertainty in the parameter below and $\odot$ denoting a very small or no uncertainty. The torque coefficient is described by:

$$\overset{\oplus}{Torque}\ coef = \overset{\oplus}{Measured}\ Torque \times \overset{\oplus}{Measured}\ \rho_{in} \times \overset{\odot}{Measured}\ Blade\ speed$$

where the measured ρ_{in} can be defined as:

$$\overset{\oplus}{\rho_{in}} = \overset{\otimes}{\rho_{atm}} \left(\frac{\overset{\oplus}{p_1}}{\overset{\otimes}{p_{atm}}} \right)$$

Using this approach, methods presented in equations (5.5) and (5.6) were easily implemented in the uncertainty analysis. Uncertainty analysis for pressure and power were done on the same principles as presented above and is summarized in Table E.2. Charts presenting torque and power uncertainties in error bar format are presented in Figure E.6 and E.7. Furthermore, pressure uncertainties are very small and are only presented in Table E.2.

It was found that the uncertainty of the transducers is 0.75% of every pressure measurement and was taken as the biggest uncertainty of both methods explained in Section5.2. However, no uncertainty was found on the equipment measuring torque etc.

5.4 SUMMARY AND CONCLUSIONS

Experimental work was done by Von Backström (2005) with no uncertainty analysis. An uncertainty analysis was done to verify the accuracy of the experimental results. A distinction

was made between a set of data readings and a single experimental measurement.

Very small uncertainties were found in the pressure measurements. However, larger uncertainties were found in the torque and power measurements using the *standard error in the mean* approach. It can thus be concluded that the uncertainty of the pressure transducers is bigger than the *standard error in the mean* calculation for pressure measurements. However, this is not the case for torque and power measurements.

Von Backström (2005) recommended that the rig needs to be modified with a damping system incorporated into the torque measurement system. This motivates the larger uncertainties in the torque measurements. A conclusion can be made that simulation results can be assumed to be accurate if the results are within the uncertainty range.

CHAPTER 6

IMPLEMENTATION OF THE SIMULATION CODE

"Everyone is a genius at least once a year. The real geniuses simply have their bright ideas closer together. "

(George C. Lichtenberg)

6.1 INTRODUCTION

This chapter will focus on the methodology employed to generate a performance analysis code from literature described in Chapters 2 - 4. The main requirement of the code is that it should be capable of performing parametrical studies, reflecting the use of various variable input parameters on compressor performance. Compressor performance charts can then be obtained by using various mass flow rates as an input variable in parametrical studies.

6.2 METHODOLOGY

A software package called Engineering Equation Solver (EES) Professional Version 7.450-3D (F-Chart Software, 2005) was used to simulate the Rofanco axial flow compressor used by Von Backström (2005). The advantage of EES is that a set of equations can be solved simultaneously by automatically identifying and grouping equations.

The EES code can consist of multiple equation groups called modules, procedures and functions. The advantage of the grouping approach is its ability to easily switch between incidence, deviation and loss models. Modules are stand-alone EES programs that can be called from the main EES program or from other modules lower in the equation window. A further advantage of using the EES code is that a single set of equations can be placed in an array solving the same set of equations simultaneously for different input parameters. Thus a multi-stage axial flow compressor can be solved showing results of different variables for any blade row.

An algorithm to generate the simulation code was developed in such a way that easy implementation in other analysis codes would be possible for future studies. The analysis code uses different compressor and blade geometrical parameters obtained from Von Backström (2005) and is presented in Appendix F.2. Furthermore, attention was given to the EES simulation code to ensure that the algorithm is user-friendly with inlet and operating conditions easily changeable. Parametrical studies on the axial flow compressor can be calculated and verified with experimental data.

In Chapter 3, different incidence and deviation models were described. These models which were implemented into the EES algorithm are summarized in Table 6.1:

Reference Incidence		
Minimum loss incidence		
Lieblein (1960)	Wright and Miller (1991)	
Optimum loss Incidence		
Miller and Wasdell (1987)		
Incidence		
Stalling incidence		
Miller and Wasdell (1987)		
Choking incidence		
Current Study		
Deviation		
Lieblein (1960)	Wright and Miller (1991)	White *et al.*(2002)
Deviation with boundary layer effects		
Csanady (1964)		
Deviation caused by low Reynolds numbers		
Roos (1995)		

Table 6.1 Incidence and deviation models implemented into EES

Each incidence and deviation model was implemented in its own sub-section program containing the set of equations which describe the model. It was also provided with the necessary input variables from the main program.

In Chapter 4, different pressure loss models were described. The models which were implemented into EES are summarized in Table 6.2. Loss models are evaluated and compared with each other to obtain the best suitable loss model for simulating the Rofanco axial flow compressor.

On-Design Blade Profile Loss		
Lieblien (1959)		
On-Design Diffusion Ratio		
Lieblein (1959)	Lieblein→ Klapproth (1959)	Wright and Miller (1991)
Secondary Losses (Endwall Losses)		
Bloch and O'Brien (1992)		
Annulus Losses		
Bloch and O'Brien (1992)		
Off-Design Blade Profile Loss Correlations		
Lieblein (1959)	Jansen and Moffatt (1967) - Casey (1987)	Miller and Wasdell (1987) – Author
Reynolds Number Correction		
Koch and Smith (1976)		
Mach Number Correction		
Jansen and Moffatt (1967)		
Annulus Blockage Factor		
Wright and Miller (1991)		

Table 6.2 Pressure loss models implemented into EES

Each loss model was implemented in its own sub-section program containing all the necessary equations describing the model. Models are then recalled from the main program containing the input variables for each rotor and stator blade row.

6.3 SIMULATION SETUP

Simulating compressor performance using the mean-line approach is based on fluid conditions at the leading and trailing edge of each blade row. The calculation of these fluid conditions can be broken down into conservation equations with various incidence, deviation and loss models. The main program consisting of conservation equations, velocity triangles and basic thermodynamics is the core structure of the simulation code (Appendix F.3). Calling of sub-section programs containing incidence, deviation and loss models is done from the main program. A breakdown of the program algorithm is given in Appendix F.1.

6.3.1 INPUT VARIABLES

Input variables for the axial flow compressor are provided in the main program (Figure F.2.1). However, geometrical variables for each blade row are called from the main program, located in an EES lookup table (Figure F.2.2).

6.3.2 ROW BY ROW ANALYSIS

Each blade row is calculated separately. The inlet conditions at the leading edge for a given blade row is coupled with the outlet conditions of the previous blade row at the trailing-edge. This coupling of blade row conditions is done by using the array function in EES. Results for velocity in their respected frames, pressures, temperatures, density, viscosity, enthalpy, entropy, incidence at the leading edge, deviation at the trailing edge and so forth are calculated for each blade row. The overall performance of the compressor is calculated by means of using the inlet conditions of the first blade row and the outlet conditions of the last blade row. Using this approach a multi-stage axial flow compressor can easily be simulated for a desired number of stages.

6.4 SIMULATION OF INCIDENCE AND DEVIATION MODELS

6.4.1 INCIDENCE

The minimum loss incidence is calculated in a sub-section called $Minimum_{incidence}$. For the Lieblein (1960:575) model polynomial curve fits for the lines σ = 0.4 and 2 where obtained in Figure 3.1 and 3.2. Values in-between are obtained using linear interpolation. This method was also used by Swift (2003:57). As previously mentioned, the Lieblein (1960:575) minimum loss model is only valid for operation with an inlet flow angle between 0° and 70°. However, when operating at zero speed, inlet flow angles in an axial flow compressor become negative (Figure 2.5). The reason being that the blade speed U is zero and no relative velocity component exists. This results in an invalid Lieblein (1960:575) minimum loss model in the fourth quadrant of operation.

The model presented by Wright and Miller (1991:72) does not have the restriction of inlet flow angles. It mainly depends on single blade and blade row geometry. It also gives a simple

relation between minimum loss incidence and inlet Mach number (3.4). Furthermore, the throat width o is calculated in a sub-section called choking. Formatted equations for the two minimum loss incidence models can be located in Appendix F.4.2. The desired minimum loss incidence model is activated by using the comment function of EES. This function makes a certain line that was programmed active or inactive.

The optimum and stalling incidences of Miller and Wasdell (1987:249) are calculated in a sub-section called *StalledDeviation,* for which the formatted equations are presented in Appendix F.4.3. The choking incidence derived by the author is calculated in a sub-section called *Choking* with the formatted equations presented in Appendix F.4.4.

6.4.2 DEVIATION

The sub-section programs containing the equations for predicting the deviation of each blade row is presented in Appendix F.4.3, F.4.6 and F.4.7.

The Wright and Miller (1991:69) deviation model can be located in the *StalledDeviation* sub-section (Appendix F.4.3). The advantage of this model is that it is not restricted to inlet flow angles between 0° and 70°. This model uses the blade stagger angle ζ to calculate the optimum and stalling incidences as well as the optimum deviation angle. The optimum deviation angle is then translated to the actual deviation angle using an incidence function presented in Figure 3.11. White *et al.*(2002:181) suggested neglecting the last term of (3.14) as it was found to cause excessively high values of deviation in some cases. So equation (3.15) was implemented into the *StalledDeviation* sub-section. However, it was found that the deviation is not constant in the choked region as displayed by Figure 3.11 and Figure 3.13 was derived.

The sub-section *Deviation* was created using the Lieblein deviation model (Appendix F.4.6). Figure 3.9 was implemented by obtaining polynomial curve fits for the lines σ = 0.4, 1.2 and 2 and performing linear interpolation for the values in-between. Curve fits were also obtained for Figures 3.6, 3.7 and 3.8. In Figure 3.10, the graph is evenly distributed for the lines β_1 = 0, 30, 40 and 50. Polynomial curve fits were obtained for β_1 = 0, 50, 60, 70 and linear interpolation was used to find the values in-between. The main weakness of this model is that it is only valid for inlet flow angles between 0° and 70° and highly empirical.

The sub-section *BoundryDev* was created to calculate the deviation caused by boundary layers after each blade row. The wake form factor $H_2 = \delta^* / \theta$ is taken as a constant value of 1.08,

when calculating the deviation caused by boundary layers (Lieblein, 1959:387). The wake momentum thickness θ can be calculated by using (4.12). Subsequently the displacement thickness δ^* can be calculated by using the constant wake form factor. The final outlet flow angle of the fluid and the final deviation can be determined from (3.22) and (3.23). Note that the *BoundryDev* deviation value is added to the value obtained by the *Deviation* sub-section. Different combinations of these incidence and deviation models were simulated and the results are shown in Chapter 6.

The sub-section *ReynoldsDeviation* was created to calculate the deviation caused by low Reynolds numbers in each blade row. The model presented by Roos (1995) was implemented and added to the deviation value calculated in the *StalledDeviation* sub-section.

6.4.3 STALL AND CHOKE

The $Blade_{Stall}$ subsection was created to test if a blade row is stalled (Appendix F.4.9). Casey (1987:277) assumed that stall will occur in terms of incidence using the mean line approach when:

$$|i - i_{min}| \geq 0.8\left(\frac{\partial\beta}{2}\right) \tag{6.1}$$

The operating range $\partial\beta$ is calculated in a sub-section called Opp_{range} (Appendix F.4.8). Stalling of a blade row can also be seen when the incidence angle of the fluid is more than that of the stalling incidence ($i \geq i_{st}$) described in (3.6).

The $Blade_{Choke}$ subsection is created to test if a blade row is nearing the choked region (Appendix F.4.5). This is done by assuming that a blade row will be near the choked region when $i \leq i_{ch}$. The choking incidence i_{ch} is derived in Appendix B and the formatted equations are presented in a sub-section called *Choking* (Appendix F.4.4).

6.4.4 NON-DIMENSIONAL POWER

Problems with using isentropic efficiency arise when calculating the work transfer rate of compressors at operation far removed from the design point, i.e. during start-up transients and operation in other relevant quadrants. The definition of power in a compressor (6.2) fails when isentropic efficiency ≤ 0. Using the isentropic efficiency to define and calculate work transfer rate (power), the following challenges emerged:

- The isentropic efficiency fails to incorporate for the possibility of a zero work transfer rate to the compressor.
- When the compressor pressure difference drops below zero, implying operation in the fourth quadrant, whilst the direction of work transfer remains unchanged (torque +, first quadrant), isentropic efficiency becomes negative.
- When the compressor pressure difference drops below zero, implying operation in the fourth quadrant, and the direction of work transfer rate changes (operating as a highly inefficient turbine). This implies that equation (6.2) is no longer valid.

$$\dot{\mathbb{Q}}_c = \frac{\dot{m} C_p T_{0i}}{\eta_c}\left[\left(\frac{p_{0e}}{p_{0i}}\right)^{(\gamma-1)/\gamma} - 1\right] \tag{6.2}$$

A new and more generically applicable representation of the work transfer rate to the compressor element was developed, called non-dimensional power. Non-dimensional power allows for calculation of the compressor power in all of the relevant quadrants. The full derivation can be found in Appendix G. The non-dimensional power term is given by:

$$\dot{\mathbb{Q}} = \frac{\dot{\mathbb{Q}}_c}{p_{0i}\sqrt{T_{0i}}} \tag{6.3}$$

where $\dot{\mathbb{Q}}$ is called non-dimensional power, $\dot{\mathbb{Q}}_c = \dot{m} C_p \Delta T_{0,c}$ and inlet pressure and temperature p_{0i}, T_{0i} with units of [bar,K]. This non-dimensional term can also be found in the book of Lakshminarayana (1996:63). Non-dimensional power was calculated in the EES code under the heading "Overall Machine Parameters" (Appendix F.3).

6.5 SIMULATION OF LOSS MODELS

6.5.1 IMPLEMENTATION OF PROFILE LOSS MODELS AT REFERENCE CONDITIONS

The Lieblein blade profile loss model (4.11) and different diffusion equation models are integrated into a sub-section in EES called $\text{Total}_{\text{Loss}}$. Different diffusion ratio models can be activated by means of using the comment function of EES. The formatted equations are shown in Appendix F.5.1.

The momentum thickness to chord ratio (4.12) defined by Casey (1987:277) were also integrated into the $Total_{Loss}$ sub-section. The added 0.0025 suggested by Koch and Smith (1976:411) was also taken into account. Furthermore, the wake form factor H_2 is taken as a constant 1.08.

6.5.2 IMPLEMENTATION OF THE OFF-DESIGN LOSS MODELS

Section 4.4 presented the reader with five off-design pressure loss models. However, only the off-design pressure loss models displayed in Table 6.2 were implemented. The off-design pressure loss models are integrated into the $Total_{Loss}$ sub-section and activated by means of using the comment function of EES.

The Lieblein (1959:387) off-design pressure loss correlation in (4.24) was implemented for a compressor with NACA 65(A_{10}) blade sets where a = 0.117. This off-design diffusion equation is directly implemented into the profile loss equation presented in (4.11).

The Casey (1987:273) off-design pressure loss correlation in (4.37) was also implemented into the $Total_{Loss}$ sub-section. The operating range $\partial\beta$ was obtained from the calculation done in the Opp_{range} sub-section.

The slope correction factor described in (4.41) and Appendix C was also integrated into the $Total_{Loss}$ sub-section. The slope correction factor varies the slope of the parabola with changes in inlet Mach and Reynolds numbers. The inlet Mach number to a given blade row would begin to rise when nearing choked conditions. An increasing inlet Mach number will directly result in an increasing slope correction factor, subsequently changing the off-design pressure loss parabola and resulting in a higher pressure loss. This slope correction factor is only valid for $i<i_{min}$ and NACA 65(A_{10}) blade sets. Further restrictions are given in Appendix C.

6.5.3 IMPLEMENTATION OF SECONDARY AND ANNULUS LOSS MODELS

The secondary and annulus losses given by (4.43) and (4.44) were implemented as suggested by (4.1) and (4.2) into the $Total_{Loss}$ sub-section. The formatted equations can be found in Appendix F.5.1.

6.5.4 IMPLEMENTATION OF REYNOLDS CORRECTION FACTOR

Surface finish and laminar and turbulent flows, all affect the compressor performance. This phenomenon is described in a correction referred to as the Reynolds correction factor.

The Reynolds correction factor described by Koch & Smith and Mills & Xu Hang was implemented into a sub-section called $\text{Reynolds}_{\text{Correct}}$. The formatted equations for this sub-section can be found in Appendix F.5.2. The centerline average deviation of roughness particles k_{CLA} was taken to be $67x10^{-6}$ and the critical Reynolds number as $\text{Re}_{cr} = 2 \times 10^5$.

6.5.5 IMPLEMENTATION OF MACH NUMBER CORRECTION FACTOR

The Mach number correction factor of Jansen and Moffatt (1967:453) was implemented for compressibility of fluid that enters the axial flow compressor. This correction factor is only activated when the Mach number exceeded the critical Mach number described in Section 4.7. Inlet Mach numbers did not exceed the critical Mach number due to subsonic analysis. However, this correction factor was implemented to calculate the critical Mach number and is integrated into sub-sections called $\text{Mach}_{\text{Critic}}$ and $\text{Mach}_{\text{Correct}}$. The formatted equations are shown in Appendix F.5.3.

6.5.6 IMPLEMENTATION OF ANNULUS BLOCKAGE FACTOR

The annulus blockage factor of Wright and Miller (1991:69) was implemented, calculating the blockage factor over each blade row. A boundary value for the first bladerow was given for boundary momentum and displacement thickness. This boundary value was calculated by using a constant wake form factor for the inlet of the first blade row H = 1.08 suggested by Lieblein (1959:387). The displacement thickness is then calculated using the momentum thickness of (4.12) for the first bladerow. The consecutive bladerows used the exit values of the previous bladerow.

6.6 SUMMARY AND CONCLUSIONS

This Chapter reviewed the methodology used for implementing axial flow compressor performance models into a software package called EES. The code was made more user friendly by implementing sub-sections containing different incidence, deviation and pressure loss models.

A row by row analysis was implemented using the array function of EES, connecting each blade row's inlet conditions to the previous blade row's outlet conditions. The inlet conditions of the first blade row set were taken as atmospheric conditions. Deviation was calculated using models of Lieblein, Csanady, Wright and Miller and Roos while correlations given in graphical format were obtained using curve fits containing the specific variables.

A new application was created called non-dimensional power due to the fact that problems occur when using isentropic efficiency for compressor operation far removed from the design point. This application accurately defines work transfer rate to or from a turbo machine in all four quadrants.

On and off-design profile pressure loss correlations of all the relevant authors were implemented into a sub-section called $Total_{Loss}$. The secondary and annulus losses were also implemented into the $Total_{Loss}$ sub-section.

A Reynolds correction factor was implemented to correct the blade profile and secondary losses due to surface finish, laminar and turbulent flows affecting the compressor performance. However, a Mach correction factor was implemented to correct the loss models for compressibility. The annulus blockage factor of Wright and Miller were also implemented.

CHAPTER 7

VALIDATION & VERIFICATION

"The conclusion of design flow naturally from the data; we should not shrink from it; we should embrace it and built on it. "

(Michael Behe)

7.1 INTRODUCTION

Chapter 6 presented the reader with the different sub-sections implemented into the EES code. Each sub-section contained a set of equations simulating a certain incidence, deviation and loss model.

In this chapter, the validity and accuracy of the EES code will be presented. Validation will be done by comparing the simulation results with blade row level data. Further verification is achieved by comparing simulation results with machine level data in the first and fourth quadrant.

7.2 METHODOLOGY

Validation of incidence, deviation and loss models are only achieved when compared to blade row level data. In reality, only machine level data exist for the first and fourth quadrant generated by Von Backström (2005:P2,1).

Therefore the incidence and deviation model combination sets displayed in Table 7.1 were validated with the Mellor and Wood plots. These plots were developed for NACA 65 profile cascades from the US cascade data of Emery *et al.* (1957). An example of these plots is sketched in Figure 7.1, with choke and stall line specified at 1.5 times the minimum loss. Verification was further done by comparing the incidence and deviation models against the Von Backström torque data set for the first and fourth quadrant.

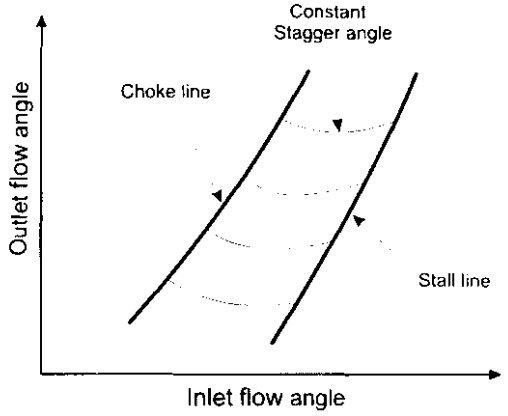

Figure 7.1 Mellor and Wood plots for NACA 65 series cascade blades (Horlock, 1978)

Pressure loss model verification was achieved by comparing results with the Von Backström data set in the first and fourth quadrant. Further validation for the loss models were achieved by comparing the selected combination set displayed in Table 7.2 with experimental blade row measurements at stall, choke and near the design point from the Roos data set.

7.3 VALIDATION AND VERIFICATION OF INCIDENCE AND DEVIATION MODELS

Table 6.1 presented different incidence and deviation models that have been implemented into the EES code. Different combination sets were tested to obtain the best results (Table 7.1).

Set	Minimum Loss Incidence $[i_{min}]$	Optimum Incidence $[i_{opt}]$	Stalling Incidence $[i_{st}]$	Deviation $[\delta]$	Deviation with Boundary Layers
1	Lieblein	-	-	Lieblein	Csanady
2	-	Miller & Wasdell	Miller & Wasdell	Wright & Miller	-
3	-	Miller & Wasdell	Miller & Wasdell	White et.al – Figure 3.11	-
4	-	Miller & Wasdell	Miller & Wasdell	White et.al – Figure 3.13	-

Table 7.1 Incidence and deviation model combinations

Figure 7.2 compares these combination sets with the Mellor and Wood plots for different solidities, stagger and camber angles.

It must be emphasized that the deviation model presented by Lieblein (1960:575) is only valid with inlet flow angles between 0° and 70°. In fourth quadrant operation it was found that the inlet flow angle to a given blade row is negative. Therefore it can be concluded that the Lieblein (1960:575) deviation model is invalid in fourth quadrant operation.

White *et al.*(2002:181) made an observation that the term accounting for thickness-chord ratio in equation (3.14) cause excessively high values of deviation in some cases. The model presented by White et al.(2002:181) with the new derived incidence function presented in Figure 3.13, showed very good comparison with experimental data. Thus a final conclusion can be made that the deviation model of White *et al.*(2002:181) in conjunction with Figure 3.13 (Combination Set 4) is sufficient for cascades with higher Reynolds numbers. Further deviation caused by low Reynolds numbers identified in Cumsty (1987:177) is added to the deviation of combination set 4 to verify simulation results with machine level data. The model of Roos (1995) presented in equation (3.31) was used for this purpose.

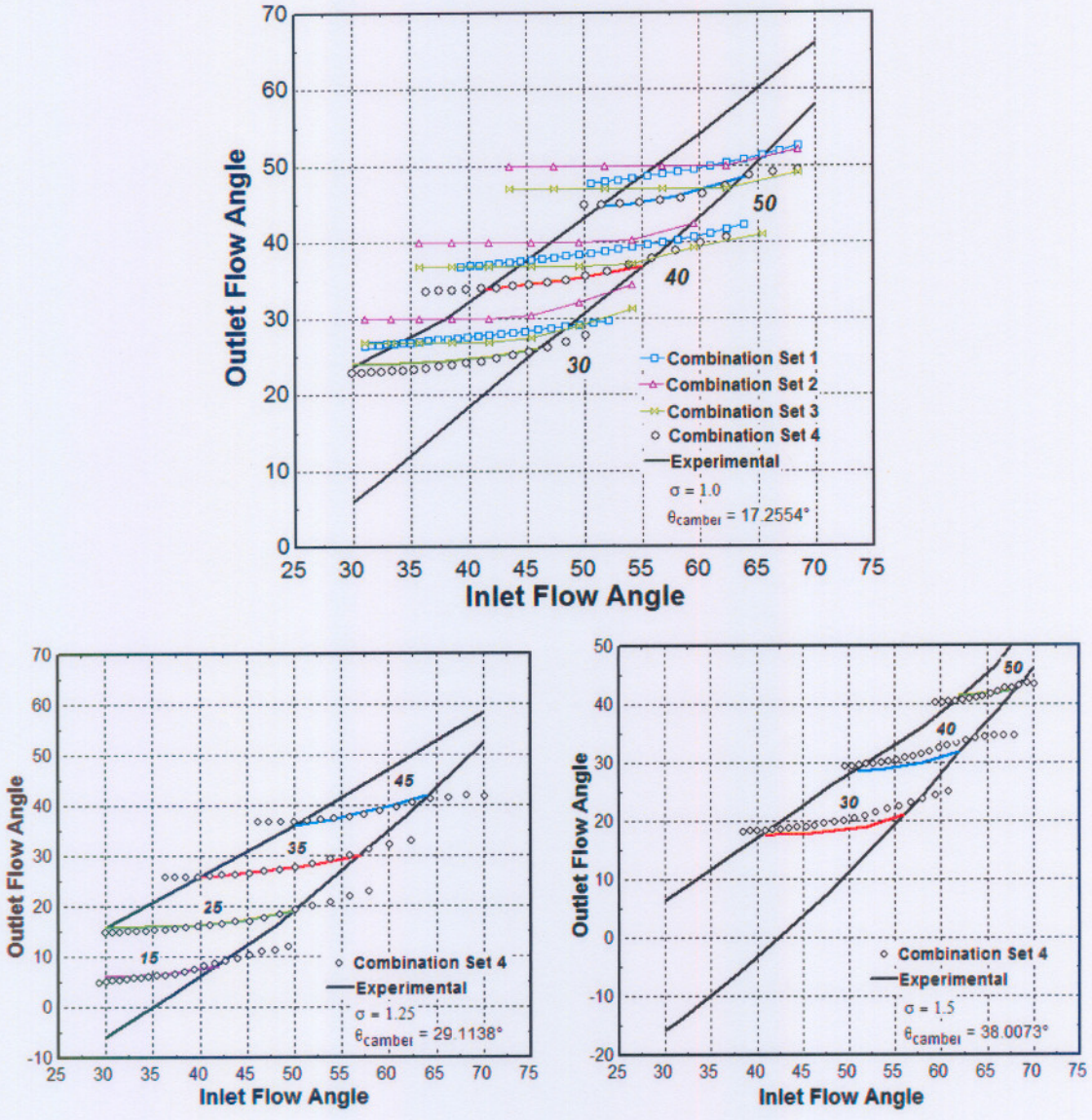

Figure 7.2 Simulation results verified against different solidities, stagger and camber angles for the first rotor stage (Mellor and Wood)

Compressor torque in the EES code is defined as $Z = \dot{m} X_{total}$ and simulation results are compared with experimental data in Figure 7.3. As previously mentioned, no blockage factor calculation model could be found to be valid for first and fourth quadrant of operation. So the blockage factor was calculated at near design conditions with the model presented by Wright and Miller. Those blockage values calculated for each blade row were then used as constants for the first and fourth quadrant. For zero rotation no blockage was assumed.

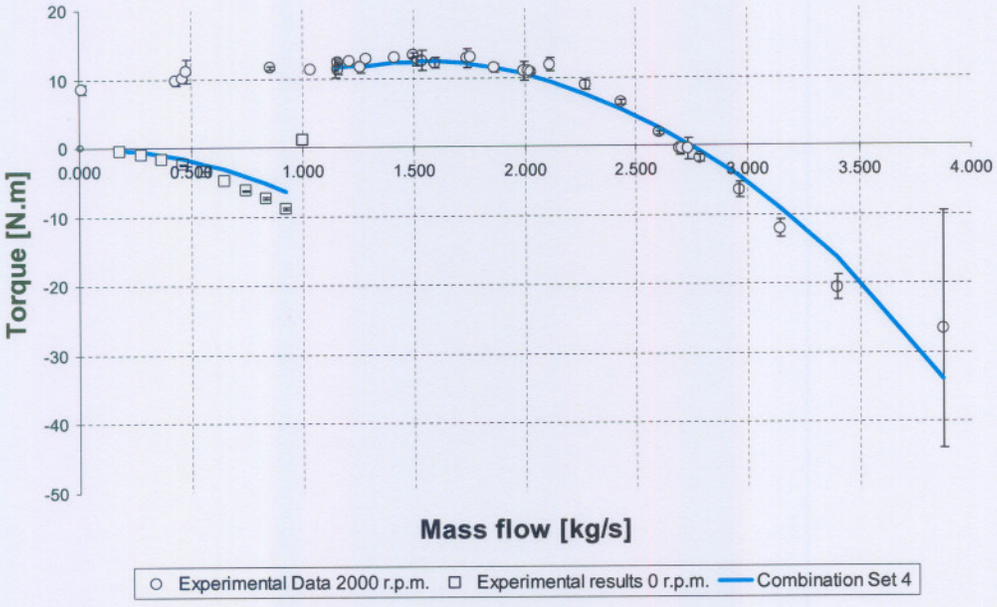

Figure 7.3 Performance prediction for torque versus mass flow rate

Compressor power in the EES code is defined as $\dot{\mathbb{Q}}_c = \omega Z$ and the results are presented in Figure 7.4.

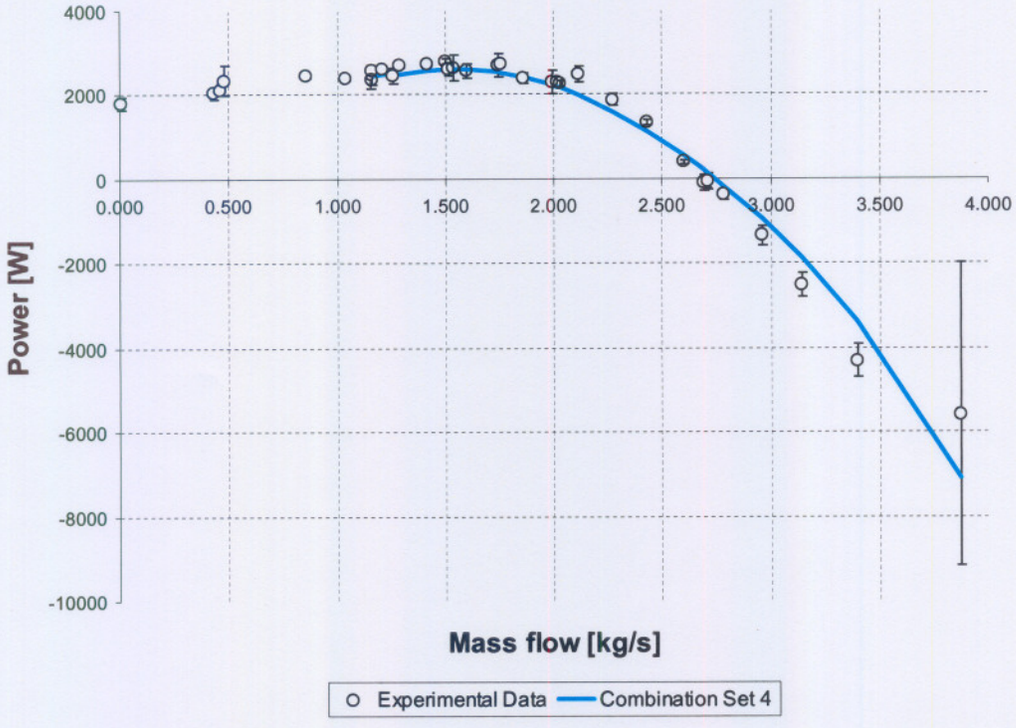

Figure 7.4 Performance prediction for power versus mass flow rate

7.4 VERIFICATION OF LOSS MODELS

Table 6.2 presented different loss models that were implemented into the EES code. Different combinations were tested to verify the best results with experimental data (Table 6.2). It must be emphasised that no loss model was found in open literature testing validity for compressor operation in the fourth quadrant. The minimum loss incidence was calculated using the Wright and Miller (1991:69) model. Furthermore, combination set 4 was used in Table 7.1 to calculate the deviation of the fluid after each blade row with the added deviation for low Reynolds number by Roos (1995).

Set	On-Design Blade Profile Loss $\left[\omega_p^*\right]$	On-Design Diffusion Ratio $\left[D_{eq}^*\right]$	Secondary & Annulus Losses $\left[\omega_s\right]\&\left[\omega_a\right]$	Off-Design Blade profile Loss $\left[\left(\frac{\omega}{\omega_i}\right)_{inc}\right]$	Reynolds Number Correction $\left[\left(\frac{\omega}{\omega_i}\right)_{Re}\right]$	Mach Number Correction $\left[\left(\frac{\omega}{\omega_i}\right)_{Ma}\right]$
2000 r.p.m.						
1	Lieblein	-	Bloch and O'Brien	Lieblein *(Corrected diffusion ratio D_{eq})*	Koch & Smith	Jansen & Moffatt
2	Lieblein	Lieblein→ Klapproth	Bloch and O'Brien	Casey	Koch & Smith	Jansen & Moffatt
3	Lieblein	Wright & Miller	Bloch and O'Brien	Miller & Wasdell	Koch & Smith	Jansen & Moffatt
4	Lieblein	Lieblein→ Klapproth	Bloch and O'Brien	Wright & Miller + Φ	Koch & Smith	Jansen & Moffatt
0 r.p.m.						
5	Lieblein	Lieblein→ Klapproth	Bloch and O'Brien	Casey	Koch & Smith	Jansen & Moffatt

Table 7.2 Pressure loss model combinations

The different loss model combination results for 2000 r.p.m and 0 r.p.m. are presented in Figure 7.5. Different sub-sections were called from the main program to formulate the different combination sets shown in Table 7.2. Further it was found that the maximum uncertainty of the pressure readings is 0.75%.

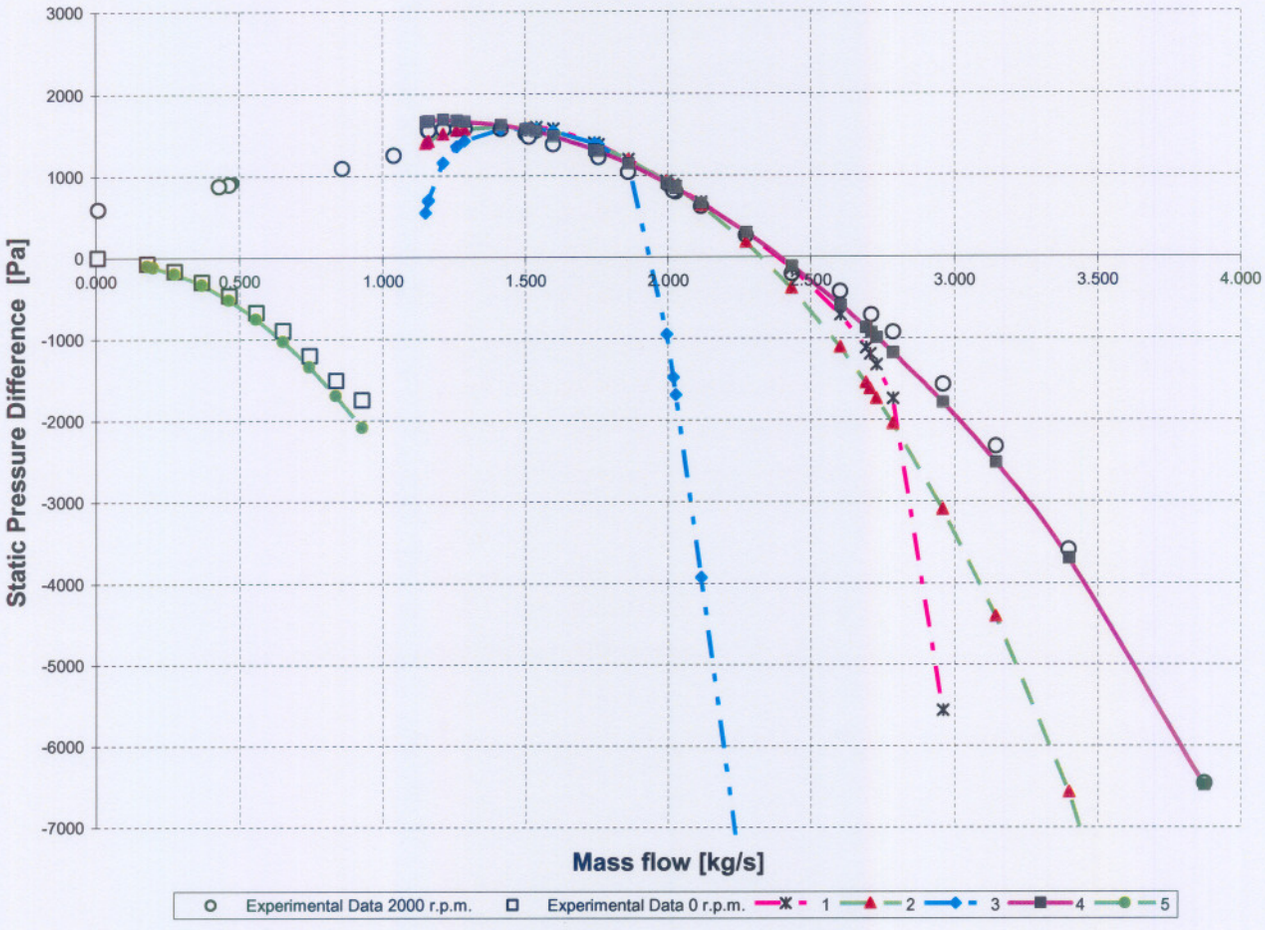

Figure 7.5 Pressure loss model combinations for static pressure difference versus mass flow rate

Pressure loss calculations at 2000 r.p.m deviated from experimental results, especially in the fourth quadrant. This confirms the observation that no pressure loss model within the fourth quadrant of operation is valid. A short discussion on each combination set operating at 2000 r.p.m. follows:

Combination set 1 showed good agreement exists in the first quadrant of operation, but deviates heavily in the fourth quadrant.

Combination set 2 shows better agreement to experimental data, it still deviates in the fourth quadrant.

Combination set 3 deviated at the stalling region in the first quadrant as well as in the fourth quadrant.

Combination set 4 shows good results in the first as well as in the fourth quadrant of operation. The correlation derived by the author in Appendix C should undergo further verification with experimental results for different rotational speeds in the spectrum of $10^4 < \mathrm{Re} < 10^5$ and $Ma < 0.3$ to verify the validity of the slope factor Φ. Further investigation should also be done on the annulus blockage that occurs in the fourth quadrant. This could have an impact on the slope factor Φ.

Only one combination set was implemented for zero rotational speed, due to the fact that all the other combination sets used for 2000 r.p.m. greatly deviated from experimental results. Combination set 4 could not be implemented for zero rotation due to the slope factor Φ falling outside the validity boundaries.

Combination set 5 used the same principles described in combination set 2. This combination shows a relatively good agreement to experimental data.

7.5 APPLICABILITY OF THE MEAN-LINE METHOD

Dixon and Angier argue against using the mean-line approach unless used in certain bounds. One of these bounds is that of an axial flow compressor operates near design conditions. The mean-line approach was used away from design conditions with calculations done in the fourth quadrant. Roos (1995) developed experimental results for near surge, near design and near choke conditions for each rotor and stator for the Rofanco axial flow compressor. So some means of validity could be tested. Figures I.8 to I.16 shows the comparison between the experimental and mean-line simulation results for each rotor stage. The mean-line analysis showed relative good accuracy for this compressor.

7.6 VALIDATION AND VERIFICATION OF CHOKING AND STALLING INCIDENCE

Validation of choking and stalling incidence was done comparing the simulation results with the Mellor and Wood plots. The simulation results show relatively good answers. It must however be noted that the Mellor and Wood plots were generated with the assumption that the stalling and choking incidence is 1.5 times that of the minimum loss value. Results are presented in Figure 7.6.

Further improvement to the choking incidence can be made by multiplying a correction factor to the two dimensional throat width (area). This correction factor is dependent on total pressure loss up to the throat width and a reduction in annulus height (Wright and Miller, 1991:69). It can be advised that the two factors for calculating the correction factor in Figure 7.6 should be solidity multiplied by stagger angle. The reason for that is, with a decrease in stagger angle the throat width (area) moves to the back (Figure B.1). Thus a correction of more than one should be applied. The need for the correction can be seen in Figure 7.6 with a solidity of one.

Furthermore, with a higher solidity the length of the blade pitch reduces if the chord length stays constant, causing the throat width to decrease and ultimately moving the two dimensional throat width (area) with chord length. Thus with higher solidities a correction factor less than one should be applied.

However to validate this correction multiplied with the two dimensional throat width (area), experimental data should be generated demonstrating the choke line with pressure loss two times that of the minimum loss value.

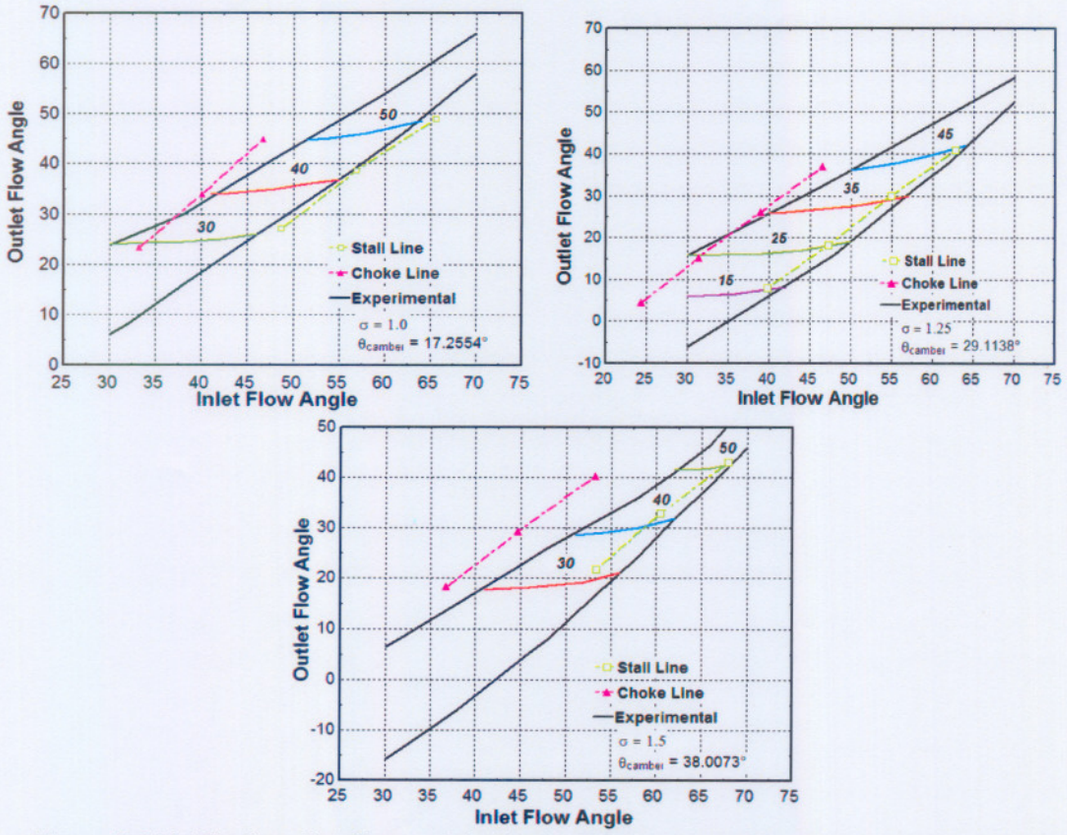

Figure 7.6 Verification of stalling and choking incidences against the Mellor and Wood plots.

Howell *et al.* (1978:699) demonstrated the experimental relation of rotor choke incidences versus relative inlet Mach number for the first stage of a transonic axial flow compressor in Figure 7.7. Simulation results for the Rofanco subsonic axial flow compressor was plotted in Figure 7.8. Comparison between Figure 7.7 and 7.8 shows the same trends, but it must be noted that results presented in Figure 7.7 is for much lower inlet Mach numbers. It is of interest to note that the choking incidences for transonic blades are mainly positive, while negative for subsonic NACA 65(A_{10}) blades. The spectrum of the loss bucket chart shifts with different blade types (Figure 7.9).

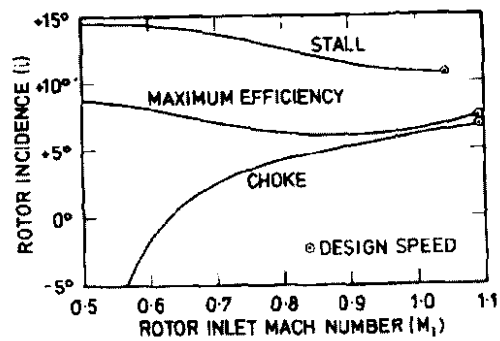

Figure 7.7 Maximum efficiency, stall and choke incidences versus rotor inlet Mach numbers at mean radius for first stage of the C135 transonic axial flow compressor (Howell *et al.*,1978:699)

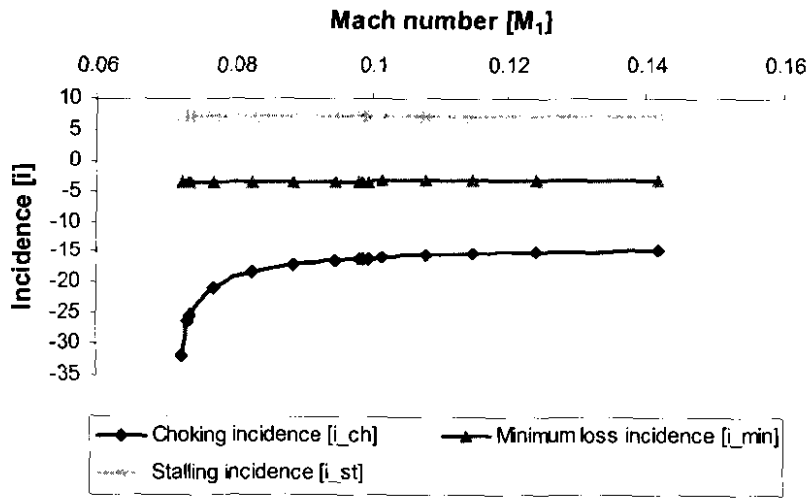

Figure 7.8 Simulation results for minimum loss, stall and choke incidences versus rotor inlet Mach number at r.m.s radius for the first stage of the Rofanco subsonic axial flow compressor when $i<i_{min}$

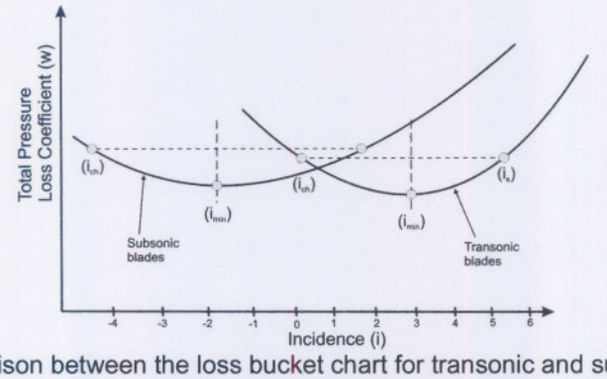

Figure 7.9 Comparison between the loss bucket chart for transonic and subsonic blade types

7.7 NON-DIMENSIONAL POWER

As previously mentioned in Section 6.4.4, non-dimensional power allows for calculation of the compressor power in all of the relevant quadrants. If a four quadrant non-dimensional power performance chart for any given axial flow compressor exists, the actual power for any quadrant can be calculated without using conservation equations. The non-dimensional power for the first and fourth quadrant is presented below:

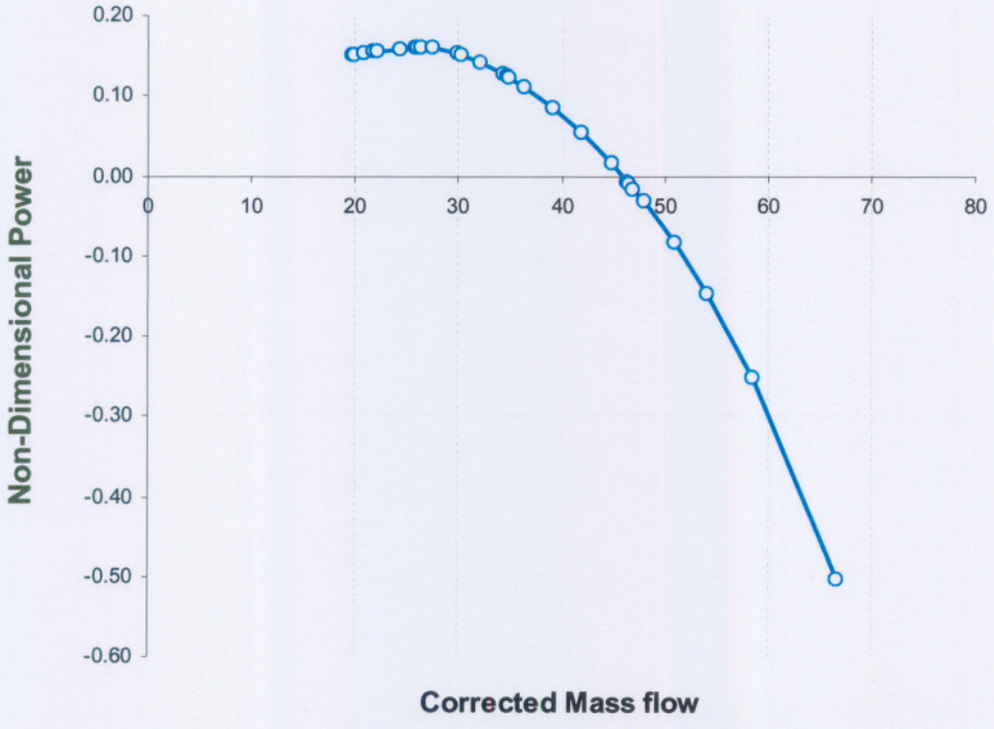

Figure 7.10 Non-dimensional power for the Rofanco axial flow compressor at 2000 r.p.m.

In Figure 7.7 the axial flow compressor starts extracting work from the fluid when the corrected mass flow $\frac{\dot{m}\sqrt{T_{0i}}}{p_{0i}}$ is in the region of 47, thus operating as a turbine. The units used to define corrected mass flow and non-dimensional power is [kg/s],[K],[bar]. Non-dimensional power provides a straight forward way to define operating modes in a turbomachine.

7.8 SUMMARY AND CONCLUSIONS

In this chapter, the accuracy of the performance prediction code was verified against experimental work done by Von Backström (2005). Different deviation and loss models were interchanged and evaluated with the aid of experimental measurements. Conclusions on deviation and loss models were made, specifically with regards to the deviation from the experimental measurements.

For the deviation models, it was concluded that combination set 4 should be used. The deviation model with the new incidence function presented in Figure 3.13 showed good comparison at both 0 and 2000 r.p.m. The main advantage of using the Wright and Miller deviation model is that it is valid in the first and fourth quadrant.

For the pressure loss models, it was concluded that combination set 4 should be used for 2000 r.p.m. and combination set 5 for 0 r.p.m. It is further advised that verification with experimental results be performed for different rotational speeds in the spectrum of $10^4 < \mathrm{Re} < 10^5$ and $Ma < 0.3$ to verify the validity of the author's off-design correlation called the slope correctional factor Φ. The non-dimensional power was also calculated and presented in Figure 7.7.

It can also now be concluded that the mean-line analysis is a valid method of simulation for the Rofanco axial flow compressor by comparison to the Roos (1995) data set.

CHAPTER 8

CONCLUSION

"Every idea which is backed by a plan and followed with massive action leaves a trail that *is recorded as history* "

(Glen McQuirk)

8.1 SUMMARY

In ***Chapter 1***, Brayton cycle power plants such as the PBMR identified the need to simulate start-up transients and operation in other relevant quadrants. Outcomes of this study were identified such as generating a preliminary analytical performance prediction code in a software package called EES, simulating performance in the first and fourth quadrant. A quick overview was given about multi-stage axial flow compressors and the compression process. Furthermore, different quadrants in a performance prediction chart were categorised and a short discussion followed explaining each mode of operation.

Chapter 2 introduced the reader with different methods of simulating an axial flow compressor. The mean-line theory in conjunction with the fundamental conservation equations for mass, momentum and energy for compressible "rotating pipe" flow were implemented into the performance prediction code. The conservation equations were broken down into three components namely velocity triangles, incidence and deviation models and loss models. By using the "rotating pipe" model only incidence and deviation models are necessary to calculate compressor torque and power. However, to calculate the pressure difference in an axial flow compressor, all three components are necessary. Furthermore, different velocity triangles and the blade nomenclature were also presented.

Chapter 3 showed distinctions that were made between various incidence and deviation angle models used in different flow angle calculations.

Chapter 4 classified total pressure loss in an axial flow compressor as a superposition of theoretical separable loss components that includes the following: blade profile losses, secondary losses and annulus losses. The left and right hand side of the loss bucket chart were classified as the choke and suction stall side. Different loss models for various conditions were presented in detail. Furthermore, since pressure calculations in the fourth quadrant deviated from experimental results, a new correctional slope factor Φ was presented correcting the off-design parabola when operating at $i < i_{min}$.

Chapter 5 presented the reader with uncertainty calculations on experimental results obtained from Von Backström. Both uncertainty methods explained in Section 5.2 were calculated and the biggest uncertainty was taken. Uncertainty analysis was done on the experimental results to accurately compare simulation results with experimental measurements.

Chapter 6 showed how different incidence, deviation and loss models were implemented into the analytical performance prediction code called EES. Sub-sections containing different equation sets from various models made it possible for the user to interchange between different deviation and loss models. This made it possible to test the validity of different loss and deviation models in the first and fourth quadrant of operation. The non-dimensional power term was also implemented and presented in this chapter.

Chapter 7 presented the various deviation and loss model combination sets tested in the performance prediction code. It was found that the power performance prediction of an axial flow compressor, can be best simulated using the Wright and Miller minimum loss incidence model. However, the Wright and Miller deviation model showed too high deviation calculations, also noted by White *et al.*(2002:185). The suggestions made by White *et al.*(2002:185) were implemented and a new incidence function chart Figure 3.13 was developed to accommodate fourth quadrant operation. Incidence and deviation combination set 4 showed relatively good results at both the rotational speed lines.

Pressure loss combination set 5 showed very good agreement with experimental results in the fourth quadrant of operation with zero rotational speed. However, with an increase in rotational speed to 2000 r.p.m. a deviation was found from experimental results. An off-design correctional slope factor was derived using an optimization program developed in EES. This correctional slope factor Φ varied the gradient of the off-design correction parabola when operating at $i < i_{min}$. Both the choking incidence and the new correctional slope factor were implemented in the off-design correction parabola. Good agreement was shown with experimental results using pressure loss combination set 4 in the first and fourth quadrant when operating at 2000 r.p.m. Choking incidence was compared with that of a transonic axial flow compressor. The result was that the derived choking incidence represented the same trend as that of the transonic axial flow compressor. The non-dimensional power chart was presented in Figure 7.7 for the first and fourth quadrant of operation.

8.2 CONCLUSION

It can thus be concluded that all the outcomes defined in Section 1.2 were met. Comprehensive research was done understanding and implementing the different incidence, deviation and pressure loss models. A new definition and method for calculating the choking incidence was presented. The non-dimensional power term was implemented and accurately indicated when

the axial flow compressor is functioning as a compressor and when it is functioning as an inefficient turbine. The simulation results from the analytical performance prediction model showed good agreement with experimental data.

8.3 RECOMMENDATIONS FOR FURTHER RESEARCH

Recommendations can be made regarding further work with the idea of improving the analytical performance prediction code for subsonic multi-stage axial flow compressors:

- Inlet guide vane losses should be implemented into the analytical performance prediction code if desired.
- Stall loss models in an axial flow compressor should be researched in more detail.
- The correctional slope factor should be verified at different rational speeds while staying within the boundaries of validity.
- A better incidence and deviation model when predicting torque at zero rotational speed should be investigated.
- The more complex Koch and Smith pressure loss model can be implemented into the analytical performance prediction code should one desire more accurate pressure simulation results in the first quadrant.
- The code can be improved by implementing transonic and supersonic correlations.
- Incidence, deviation and loss models such as Carneal's (1990) work should be investigated to accurately simulate performance in the second quadrant with positive rotational axial flow compressors.
- Analytical performance prediction results should be compared with different compressor builds and blade types.

REFERENCES

AUNGIER, R.H., 2003. Axial-Flow Compressors: A Strategy for Aerodynamic Design and Analysis. ASME Press.

AINLEY, D.G., MATHIESON, G.C.R., 1957. A Method of Performance Estimation for Axial-Flow Turbines. R.& M. No. 2974

BAMMERT, K., ZEHNER,P., 1980. Measurements of the Four-Quadrant Characteristic on a Multi-Stage Turbine. Journal of Engineering for Power, 102.

BLOCH, G.S., COPENHAVER, W.W., O'BREIN, W.F., 1999. A Shock Loss Model for Supersonic Compressor Cascades. Journal of Turbomachinery ; VOL. 121 ; ISSUE: 1 ; 42. international gas turbine and aeroengine congress and exhibition, Orlando, FL (United States), 2-5 Jun 1997 ; PBD: Jan 1999, ISSN 0889-504X

BLOCH, G.S., O'BREIN, W.F., 1992. A Wide-Range Axial-Flow Compressor Stage Performance Model. ASME International Gas Turbine and Aeroengine Congress and Exposition Cologne, Germany June 1-4, 1992

BOYER, K.M., 2001. An Improved Curvature Approach for Off-Design Analysis of Transonic Compression Systems. Dissertation submitted to the faculty of the Virginia Polytechnic Institute and State University, PHD

CARNEAL, J.P., 1990. Experimental Investigation of Reversed Flow in a Compressor Cascade. *M.S. Thesis*, V.P.I.&S.U.,Blacksburg, VA.

CASEY, M.V., 1987. A Mean Line Prediction Method for Estimating the Performance Characteristic of an Axial Compressor Stage. MA, DPhil, Ceng MIMechE, Silzer Escher Wyss Limited, Zurich, Switzerland

CETIN, M., ÜCER, A.S., HIRSCH, Ch., SEROVY, G.K., 1987. Application of Modified Loss and Deviation Correlations to Transonic Axial Compressors. AGARD-R-745. ISBN 92-835-0346-4

COHEN, H., ROGERS, G.F.C., SARAVANAMUTTOO, H.I.H., 2001. Gas Turbine Theory. Fifth Edition, Prentice Hall

CSANADY, G.T., 1964. Theory of Turbomachines. McGraw-Hill, New York.

CUMPSTY, N.A., 1989. Compressor Aerodynamics. 1st ed, Longman Scientific & Technical, ISBN 0-582-01364-X

DIXON, S.L., 1998. Fluid Mechanics and Thermodynamics of Turbomachinery. Pergammom Press. Fourth Edition. ISBN 0750670592

DUNAVANT, J.C, EMERY J.C., 1958. Two-Dimensional Cascade Investigation at Mach Numbers up to 1.0 of NACA 65-Series Blade Sections at Conditions Typical of Compressor Tips. NACA RM L58A02, 17 March 1958.

EMERY, J.C., HERRIG, L.J., ERWIN, J.R., FELIX, A.R., 1957. Systematic Two-Dimensional Cascade Tests of NACA 65-Series Compressor Blades at Low Speeds. NACA TN 3916.

FELIX, A.R., EMERY, J.C., 1953. A Comparison of Typical National Gas Turbine Establishment and NACA Axial-Flow Compressor Blade Sections in Cascade at Low Speed. NACA TN 3937, 14 March 1953.

FLOWNEX THEORY MANUAL – COMPRESSOR ELEMENT, 2006. M-Tech industrial. Document nr. FNXTH-0010, www.mtechindustrial.com

FLOWNEX THEORY MANUAL – MODELLING OF LOSS AND DEVIATION IN AXIAL COMPRESSORS, 2005. M-Tech industrial. Document nr. FNXTH-0035, www.mtechindustrial.com

GALLIMORE, S.J., 1999. Axial Flow Compressor Design. Rolls-Royce, Proc Instn Mech Engrs Vol 213 Part C.

GAMACHE, R.N., 1985. Axial Compressor Reversed Flow Performance. *Ph.D Dissertation*, M.I.T., Cambridge, MA.

GAMACHE, R.N., GREITZER, E.M., 1990. Reverse Flow in Multistage Axial Compressors. Journal of Propulsion, Vol 6, pp.4

HIRSCH, C.H., *et al.*, 1981. Propulsion and Energetics Panel Working Group 12 on Through Flow Calculations in Axial Turbomachines. AGARD-AR-175.

HORLOCK, J.H., 1978. Actuator Disk Theory Discontinuities in Thermo-Fluid Dynamics. McGraw-Hill. ISBN 0070303606

HOWELL, A.R., 1945. Fluid Dynamics of Axial Compressors, Proc. Instn. Mech Engrs.,153

HOWELL, A.R., CALVERT, W.J., 1978. A New Stage Stacking Technique for Axial-Flow Compressor Performance Prediction. ASME Journal of Engineering for Power, October, pp.698-703

JANSEN, W., MOFFATT, W.C., 1967. The Off-Design Analysis of Axial-Flow Compressors. ASME Journal of Engineering for Power, October, pp.453-462

JAPIKSE, D., BAINES, N.C., 1994. Introduction to Turbomachinery. Concepts ETI, Inc. and Oxford University Press.

JOHNSEN, I.A., NASA SP-36, 1965. Aerodynamic Design of Axial-Flow Compressors.

KUGELER, K., ALKAN, Z., PÖPPE, N., 2006. High Temperature Reactor Technology. *Course notes*, North-West University.

KIRKUP, L., 1994. Experimental Methods. John Wiley & Sons Australia, Ltd. ISBN 0471335797

KOCH, C.C., 1981. Stalling Pressure Rise Capability of Axial Flow Compressor Stages. ASME Journal of Engineering for Power, Vol.103, Oct.1981, pp.645-656

KOCH, C.C., SMITH Jr., L.H., 1976. Loss Sources and Magnitudes in Axial-Flow Compressors. ASME Jnl. Of Eng. For Power. Vol.98, No.3, pp.411-424

KOFF, S.G., GREITZER, E.M., 1986. Axisymmetrically Stalled Flow Performance for Multistage Axial Compressors. ASME Journal of Turbomachinery, Vol.108, Oct.1986, pp.216-223

KONNIG, W.M., HENECKE, D.K., FOTTNER, L., 1996. Improved blade profile loss and deviation angle models for advance transonic compressor bladings: Part 1 – A model for subsonic flow. ASME Journal of Turbomachinery, Vol 118, pp.73-80

KUHNEL, J., GYARMATHY, G., ORTMANN, P., Estimation of the Compressor Map for Incompletely Specified Axial Compressors. Institute of Energy Technology, Turbomachinery Laboratory, Zurich, Switzerland.

LAKSHMINARAYANA, B,, 1996. Fluid Dynamics and Heat Transfer of Turbomachinery. Department of Aerospace Engineering. The Pennsylvania State University. John Wiley and Sons,Inc. ISBN 0-471-85546-4

LIEBLEIN, S., 1959. Loss and Stall Analysis of Compressor Cascades. ASME, Journal of Basic Engineering, pp.387-400.

LIEBLEIN, S., 1960. Incidence and Deviation Angle Correlations for Compressor Cascades. Trans.

ASME, Jnl. Basic Engineering. September 1960, pp.575-587

MILLER, D.C., WASDELL, D.L., 1987. Off-Design Prediction of Compressor Blade Losses. Rolls-Royce, Bristol, C279/87 Imech, pp.249-260

MILLS, A.F., Xu HANG, 1983. On the Skin Friction Coefficient for a Fully Rough Flat Plate. ASME Journal of Fluids Engineering, Vol.105, September, pp.364-365

MOSES, H.L., HILL, J.M., THOMASON, S.B., 1982. Calculation of the Flow Over a Stalled Airfoil. AIAA/SAE/ASME 18th joint propultion conference, June 21-23, 1982. Cleveland, Ohio.

MOSES, H.L., THOMASON, S.B., 1986. An Approximation for Fully Stalled Cascades. ASME Journal of Propulsion, pp.188-189.

MOUSTAPHA, H., ZELESKY, M.F., BAINES, N.C., JAPIKSE, D., 2003. Axial and radial turbines. Published by Concepts NREC. ISBN 0933283121

PFITZINGER, E.W., RIESS, W., 1997. A New Concept for Loss and Deviation Prediction in Throughflow Calculations of Axial Flow Compressors. Proceedings of the 1997 2nd European Conference on Turbomachinery - Fluid Dynamics and Thermodynamics, Antwerpen, Belgium, 5-7 March 1997, pp.117-126

ROOS, T., 1995. A prediction method for flow in axial flow compressors. Masters project University of Stellenbosch, Faculty of Engineering.

ROOS, T., 2007. Private Communication.

ROBERTS, W.B., 1975. Calculation of laminar separation bubbles and their effect on airfoil performance. AIAA Journal 18, pp.25-31.

ROUSSEAU, P.G., 2005. Advanced Thermal-Fluid Systems. *Course notes*, North-West University, Potchefstroom Campus.

SCHWENK, F.C., LEWIS Jr. G.W.L., LIEBLEIN, S., 1957. Experimental Investigation of an Axial-Flow Compressor Inlet Stage Operating at Transonic Relative Inlet Mach Numbers V-rotor Blade Element Performance at Reduced Blade Angle. NACA RME56J17, January 24, 1957

SHAMES, I.H., 1992. Mechanics of Fluids. Third edition, McGraw Hill, ISBN 0-07-056387-X

SQUIRES, G.L., 2001. Practical Physics. Cambridge Publishing. ISBN 0521779405

SWAN, W.C., 1961. A Practical Method of Predicting Transonic Compressor Performance. Trans. of the ASME Journal of Eng. for Power, pp.322-330

SWIFT, W.J., 2003. Modeling of Losses in Multi-Stage Axial Compressors with Subsonic Conditions. *M.S. Thesis*, North-West University,Potchefstroom Campus.

VON BACKSTRÖM, T.W., 2005. Four Quadrant Axial Flow Compressor Maps: Part 1 – Literature Review and Experimental Layout. Private experimental report.

VON BACKSTRÖM, T.W., 2005. Four Quadrant Axial Flow Compressor Maps: Part 2 – Experimental Results. Private experimental report.

WHITE, N.M., TOURLIDAKIS, A., ELDER, R.L., 2002. Axial Compressor Performance Modelling with a Quasi-One-Dimensional Approach. Proc Instn Mech Engrs Vol 216 Part A: Journal of Power and Engery.

WRIGHT, P.I., MILLER, D.C., 1991. An Improved Compressor Performance Prediction Model. Rolls-Royce, Bristol, C423/028.

YOCUM, A.M., II, 1988. An Experimental and Numerical Investigation of the Performance of

Compressor Cascades With Stalled Flow. Ph.D. Dissertation, V.P.I.&S.U., Blacksburg,VA.

YOUNG, A.D., 1989. Boundary Layers. AIAA Education Series ISBN 0930403576

APPENDIX A

Velocity Triangles for Different Operating Conditions

This Appendix presents the velocity triangles for reverse flow through an axial flow compressor.

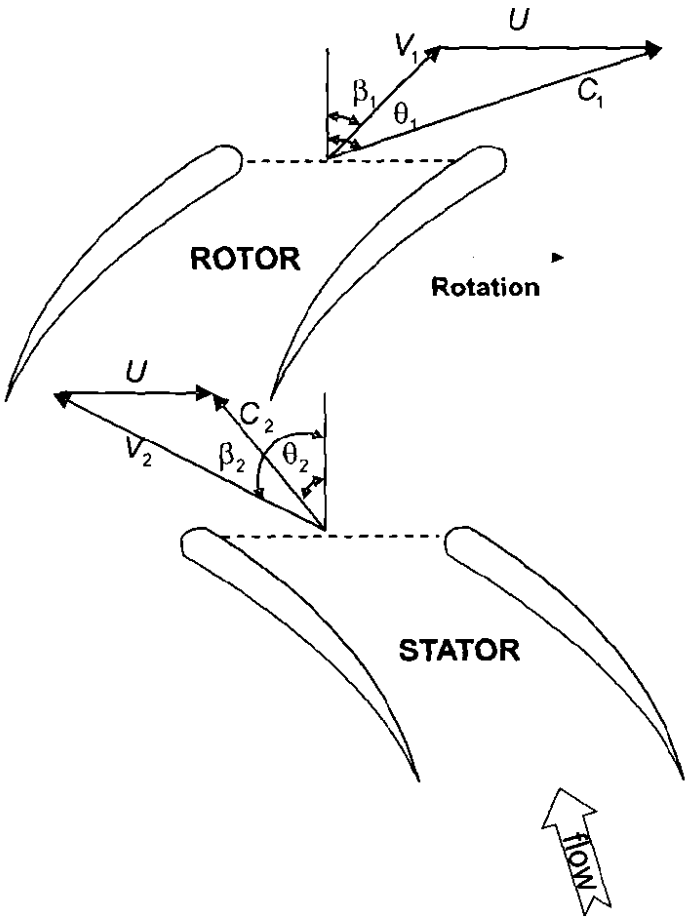

Figure A.1 A compressor stage in reversed flow operation (Bloch and O'Brein, 1992:4)

APPENDIX B

Derivation of an Expression to Determine Choking Incidence

This appendix gives the derivation to estimate the choking incidence with knowledge of throat width and the choking Mach number at the inlet of a blade row. The author defined the chocking incidence as the incidence where the relative velocity would be the highest in the passage throat area with a certain choking Mach number as inlet.

If we assume from continuity:

$$\rho_1 C_{a1} A_1 = \rho_{ps} V_{ps} A_{ps} \tag{B.1}$$

then

$$\rho_1 V_1 \cos\beta_1 A_1 = \rho_{ps} V_{ps} A_{ps} \tag{B.2}$$

where the subscribe ps denotes the values at the cascade throat area.

$$A_{ps} = o\,h \tag{B.3}$$

If we assume that any change in annulus height is negligible, one can divide both sides of (B.2) by annulus height h and define flow width as suggested by Figure B.1. Thus equation (B.2) becomes:

$$\rho_1 V_1 \cos\beta_1 s \cos\beta_1 = \rho_{ps} V_{ps} o \tag{B.4}$$

After some manipulation and taking the inlet values as the values for when a blade row is choked, equation (B.4) becomes:

$$\cos^2\beta_{ch} = \frac{\rho_{ps}}{\rho_{ch}} \frac{V_{ps}}{V_{ch}} \frac{o}{s} \tag{B.5}$$

where s is the blade pitch and o is the throat width. Figure B.1 shows the difference between the flow width and blade pitch. The cascade throat width can be calculated from work done by Raley in 1966 and is presented in Wright and Miller (1991:72). Correlations are given in (3.7) and (3.8) with constants obtained from Figure 3.5.

Lakshminarayana (1996:234) stated that in high subsonic flows, an inflow Mach number called

choking Mach number can be calculated for axial compressor cascades from:

$$\frac{o}{s\cos\beta_1} = M_{ch}\left\{\frac{\gamma+1}{2}\left(1-\frac{\gamma-1}{\gamma+1}M_{ch}^2\right)\right\}^{\frac{1}{\gamma-1}} \tag{B.6}$$

Furthermore, Koch and Smith (1976:411) gave correlations relating the inlet flow conditions with the flow conditions at the passage throat (4.19) etc. If we take the inlet values as the values for when a blade row is choked, the following is obtained:

$$\frac{\rho_{ps}}{\rho_{ch}} = 1-\frac{M_{ch}^2}{1-M_{ch}^2}\left(1-A^*-0.2445\frac{\tan\beta_{ch}}{\cos\beta_{ch}}\sigma\Gamma\right) \tag{B.7}$$

and

$$\frac{V_{ps}}{V_{ch}} = \left[\left(\sin\beta_{ch}-0.2445\sigma\Gamma_{ch}^2\right)+\left(\frac{\cos\beta_{ch}}{A_{ch}^*\frac{\rho_{ps}}{\rho_{ch}}}\right)^2\right]^{0.5} \tag{B.8}$$

where

$$A_{ch}^* = \left(\frac{1-0.4458\sigma\left(\frac{t_{max}}{c}\right)}{\cos\left(\frac{\beta_{ch}+\beta_2}{2}\right)}\right)\left(1-\frac{A_1-A_2}{3A_1}\right) \tag{B.9}$$

and

$$\Gamma_{ch} = \frac{\cos\beta_{ch}\left(\tan\beta_{ch}-\tan\beta_2\right)}{\sigma} \tag{B.10}$$

A_{ch}^* is the annulus area contraction ratio from the inlet to the passage throat and Γ_{ch} is the blade circulation parameter equation. An iterative process is then used to calculate what the inlet flow angle β_{ch} would have to be for choking to occur in the passage throat region. This is done for a fixed rotation speed and mass flow rate. The choking incidence can then be calculated by:

$$i_{ch} = \beta_{ch} - \beta_B \tag{B.11}$$

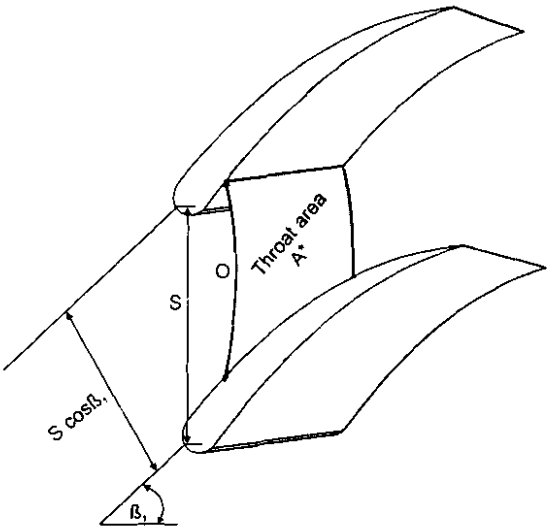

Figure B.1 Calculation of flow width

APPENDIX C

Derivation of a Correctional Slope Factor

Two operational speed lines, 0 r.p.m and 2000 r.p.m. were tested in the experimental work done by Von Backström (2005:P2). It was found that in the fourth quadrant the off-design pressure loss correlations resulted in too high pressure losses when operating at 2000 r.p.m (Figure 7.3).

When the standard off-design pressure loss correlation given by Wright and Miller (1991:72) in equation (4.40) is multiplied with a correctional slope factor denoted by Φ, (4.40) becomes:

$$\left(\frac{\omega}{\omega_i}\right)_{inc} = \Phi\left(\frac{i-i^*}{i^*-i_{ch}}\right)^2 + 1 \qquad \text{(C.1)}$$

Where i_{ch} is the choking incidence derived in Appendix B. The Mach correction slope factor varies the slope of the parabola when a compressor enters the choke side of Figure 4.3. The following three parameters should be considered when examining pressure loss in the choked side of Figure 4.3:

- Increase in pressure loss coefficient with increasing Mach number Figure C.1.
- The decrease in pressure loss coefficient with increasing Reynolds number Figure C.2.
- Change of pressure loss coefficient with thickness to chord ratio t/c and increasing Reynolds number Figure C.1.

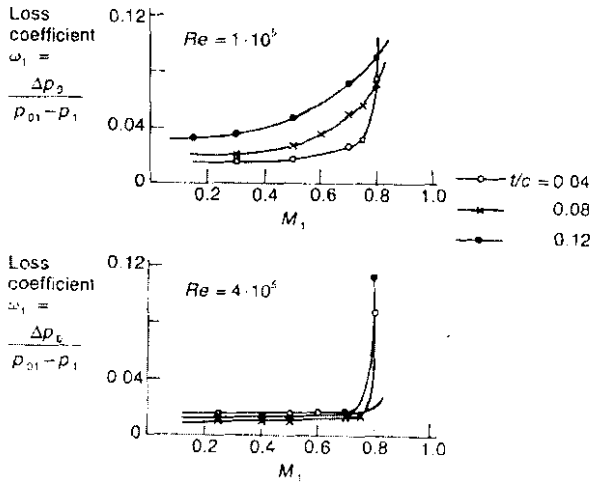

Figure C.1 Pressure loss coefficient versus Mach number for NACA 65 cascades of different thickness at two Reynolds numbers Cumpsty (1989:178)

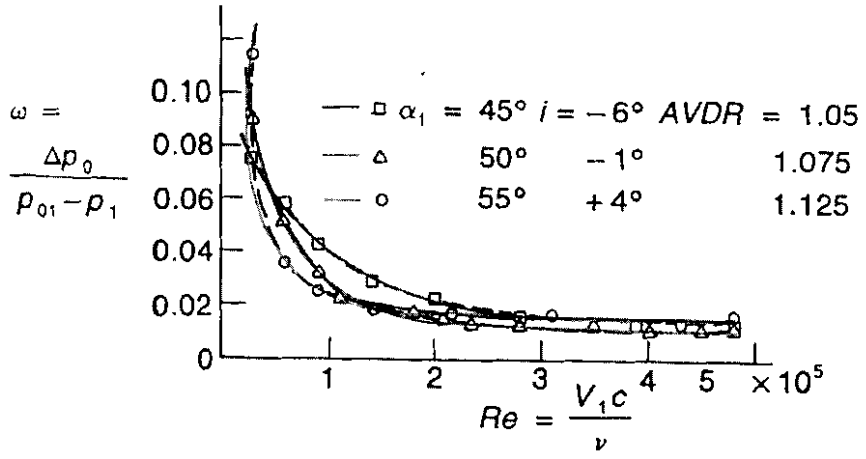

Figure C.2 Loss versus Reynolds number for C4 blades in a cascade. Incidence -1 and inlet Mach number <0.15 Cumpsty (1989:178)

The Mach number and Reynolds number effects on pressure loss coefficient were used to derive a correctional slope factor for off-design analysis. The basic form is defined as:

$$\Phi = \frac{Ma}{\mathrm{Re}} \tag{C.2}$$

When Mach number increases, Φ increases as well in equation (C.2) resulting in an increase in pressure loss coefficient. However, when Reynolds number increases, Φ decreases, resulting in a decreasing pressure loss coefficient. The Re parameter in (C.2) was assumed to be the same as (4.48). However the variation of pressure loss with changing Mach number was assumed to have the shape of a straight line for $M_1 < 0.3$ (Figure C.1). Thus (C.2) becomes:

$$\Phi = \frac{A \cdot Ma + B}{489.8 \cdot \mathrm{Re}^{-0.5}} \tag{C.3}$$

An optimizing simulation code was written in EES to derive answers for constants A and B. The optimizing simulation code is explained in Appendix F.6. Optimization for constants A and B resulted in:

$$\Phi = \frac{0.65 \cdot Ma + 0.01}{489.8 \cdot \mathrm{Re}^{-0.5}} \qquad \text{for } 10^4 < \mathrm{Re}_{chord} < 10^5 \text{ and } Ma < 0.3 \tag{C.4}$$

It can be concluded that a new correctional slope factor was successfully derived. Knowledge gathered from various authors made it possible to make valid assumptions. Experimental work done by Von Backström (2005) enabled the validation of the new empirical slope correctional factor (C.4).

APPENDIX D

Experimental Setup & Results

D.1 THE STANDARD COMPRESSOR RIG

The so-called Rofanco research compressor located at the University of Stellenbosch, is a three-stage axial flow compressor supplied by Royston Fan Co. Ltd. It has 41 rotor blades and 43 stator blades per stage. It was originally fitted with plastic blades of 50% degree of reaction layout, but was later replaced with aluminium blades of approximately 80% degree of reaction. The compressor has a hub diameter of 300 mm and a casing diameter of 420 mm. The nominal blade length is 60 mm and the blade chords are 30 mm. The parameters defining the blade geometry are given in Table D.1. There are no inlet or exit guide vanes in the current experimental setup (Von Backström, 2005:P1,10).

The compressor is shown in Figure D.1 and a section through the compressor is shown in Figure D.2. It is evident that the blade spacing between the rotor TE and stator LE is quite small compared to that between stator TE and rotor LE. The geometrical description of the rotor and stator blade row is presented in Table D.1.

A schematic of the compressor rig operating at positive rotation and positive through-flow can be seen in Figure D.3. The flow enters the compressor goes through a flow straightener entering the venturi, before reaching the adaptor linking the auxiliary fan to the venturi.

Rotor and Stator Blade Row Descriptions

Blade section radial position (mm)	Blade profile stagger angle [ζ] (°)	Blade profile camber angle [θ_{camber}] (°)	Blade row solidity [σ] (c/s)	Blade profile maximum thickness to chord ratio (t_{max}/c)	Maximum camber position (fraction of chord)
ROTOR					
150.0	38.00	31.04	1.3051	0.10	0.5
165.0	45.00	23.48	1.1864	0.10	0.5
180.0	49.40	17.93	1.0876	0.10	0.5
195.0	53.00	13.85	1.0039	0.10	0.5
210.0	56.10	10.90	0.9322	0.10	0.5

STATOR					
150.0	20.38	46.28	1.3687	0.10	0.5
165.0	18.18	43.39	1.2443	0.10	0.5
180.0	16.61	41.05	1.1406	0.10	0.5
195.0	14.90	40.57	1.0529	0.10	0.5
210.0	14.32	40.00	0.9777	0.10	0.5

Table D.1 Rotor and stator blade descriptions

It must be remembered that the setup of the compressor rig was done to obtain data in all four of the quadrants presented in Figure 1.7 (a), where the data only from the first and fourth quadrant is to be used in this thesis.

D.2 MEASUREMENTS AND CALIBRATION

A short description of the measurements from the experimental work done by Von Backström (2005:P2,7) is described below. Further information regarding the commissioning of the compressor rig can be obtained from Von Backström (2005:P2).

D.2.1 Rotational Speed

The rotational speed of the axial-flow compressor is measured by means of a 60-tooth wheel and a magnetic transducer, coupled to a frequency counter. This instrument yields the rotational speed directly in revolutions per minute, that is to say that no calibration was necessary, although the values obtained were compared with those from a handheld tachometer to ensure that the instrument was functioning correctly, and the agreement was always within about 3 r.p.m. Readings were supplemented by a handheld-tachometer when it was discovered that the electromagnetic interference generated by the 3-phase variable speed drive system for the motors of the contra-rotating fans had a detrimental effect on the accuracy of readings from this instrument.

D.2.2 Torque

Torque acting on the compressor was measured by means of a HBS 350Ω load-cell with a nominal load capacity of 20 kg. The load was connected to a HBM Scout-55 bridge-amplifier and the calibration curve can be seen in Appendix F Von Backström (2005:P2). The drive system consists of a direct current motor and control system. Two air bearings support the motor in such a way that the torque on the motor can be determined by attaching weights to a balance arm

connected to the load cell. The motor cooling fan exits through a duct fitted with a honey comb grid to ensure that the cooling air does not exert a torque on the motor.

D.2.3 Pressure and Temperature

Stagnation pressure readings were obtained from seven-hole pressure-rakes inserted into ports at the compressor inlet and exit, corresponding with the axial positions of the static pressure-ports. The pressure-rakes were also each connected to a separate pressure-transducer. Static pressure readings are obtained by connecting pressure-transducers to pressure-tapping in the compressor-casing at the compressor inlet, immediately ahead of the first stage, between stages and at the exit, or after the last stage.

A bank of four AutoTran 705D-215 differential pressure-transducers are used to obtain all the relevant pressure-measurements. The transducers each has an input range of 2 kPa, and an output range of 10 V. All the pressure-transducers, except the one used to measure the pressure-difference across the venturi, had one port connected to their respective pressure-tapping or rake, and one open to the atmosphere. If the ambient atmospheric pressure is higher than the measured pressure, then the high-pressure port would be exposed to the atmosphere, otherwise the low-pressure port would be exposed. This is done so as to remain within the calibrated linear region of the pressure-transducers.

Pressures are measured by means of Auto Tran pressure transducers with a range of 2.5 kPa. The output voltages are recorded through a 22 channel HP data logger to a PC.

D.2.4 Flow

A single differential pressure-transducer is used to determine the pressure-difference across the venturi connected to the compressor outlet, with the high-pressure port connected to static pressure-tappings in the venturi-inlet wall and the low-pressure port to similar tappings at the venturi throat. The maximum pressure drop recorded across the venturi is approximately 100 kPa when the compressor is operated at 2500 r.p.m. This corresponds to a maximum mass flow rate of approximately 2.7 kg/s. Finally, a pressure-transducer is connected to the venturi-throat, so that the density of the gas at this point could be estimated with greater accuracy.

D.2.5 Ambient Conditions

Atmospheric pressure was measured by means of a mercury manometer just outside the lab. All pressures except the differential pressure across the venturi were referenced to the atmospheric

pressure. Air temperature was measured at the compressor inlet by means of a thermocouple.

D.3 EXPERIMENTAL RESULTS

D.3.1 Zero Rotational Speed S-Curve

The measured static-to-static pressure S-curve is shown as a parabolic curve in Figure D.4. The zero speed rotation was obtained by locking the compressor shaft relative to the motor casing, which was floating in air bearings.

Its also represented as a parabolic curve, since the change in the angular momentum of the flow passing through the rotor is proportional to the mass flow times the circumferential deflection of the flow as state by Von Backström (2005:P2,10).

D.3.2 First Quadrant Operation

As previously described in Chapter 1, Figure 1.7 (a), compressor operation may be in the stalled or normal mode of operation in the first quadrant. The first quadrant operation was accessed by running and throttling the compressor normally, but an auxiliary counter-rotating fan in series was required to access the region near the x-axis where the system resistance was too high, described Von Backström (2005:P2,10).

The static-to-static pressure rise can be seen in Figure D.4, where all the results have been scaled to 2000 r.p.m. and a density of 1.20 kg/m^3. Firstly some points where obtained in the stall region of the first quadrant by throttling the compressor and some by running auxiliary fans in opposition to the compressor, but still in the positive flow direction. Secondly data points were obtained in the region between the stall point and x-axis. The normal mode of operation characteristic shows no abnormalities.

The first quadrant torque and power curves are very flat, even in the stall region, but otherwise not particularly remarkable Figure E.5. Von Backström (2005:P2,10) mentioned that the relatively low peak total-to-static efficiency of ±75% can more or less be described by two effects. Firstly since the stator blade chord Reynolds numbers is ± 0.8 x 10^5 and the general lower limit is seen as between 1 and 2 x 10^5, but that conception is based on cascade data. Cumpsty (1989) gives a lower limit for compressors of 0.3 x 10^5. The lower limit in compressors is due to the relatively high turbulence in compressors. In extreme off-design cases with massive flow separation the limit can be expected to be even lower, such as nearing zero rotation. Secondly is bearing power loss, which does not decrease as fast as power input when speed is reduced.

D.3.3 Fourth Quadrant Operation (Right of S-Curve)

Fourth quadrant operation occurs when the compressor exit pressure is lower than its inlet pressure, the pressure rise is less than zero and the flow is in the positive direction. Von Backström (2005:P2,13) describes that this is the normal operating quadrant for a compressor running forwards as a turbine. In this operating mode the compressor operates as an inefficient turbine, since the flow relative to the blade rows is turned away from the axial direction by blades curved the wrong way.

The pressure rise characteristic in the fourth quadrant is a continuation of the normal first quadrant characteristic Figure D.4. The same can be said for the torque and power characteristics Figure D.5 and Figure D.6. Von Backström (2005:P2,13) describes that these experimental measurements agree in principle with the measurements of Bammert and Zehner (1980).Flow and rotation are positive, and pressure rise and torque are negative, so both fluid power and shaft power are negative. Negative efficiency values have no meaning, so a term call non-dimensional power, described in Appendix G, was incorporated to accurately define when the axial compressor is operating as a compressor or a turbine.

D.4 SUMMARY AND CONCLUSIONS

The axial flow compressor characteristics for pressure rise, torque, power and efficiency were measured successfully in four quadrants by Von Backström (2005:P2), using a small laboratory compressor. The experimental results obtained in the first and fourth quadrant right of the S-curve is used in this thesis and is compared to simulated results described in Chapter 7.

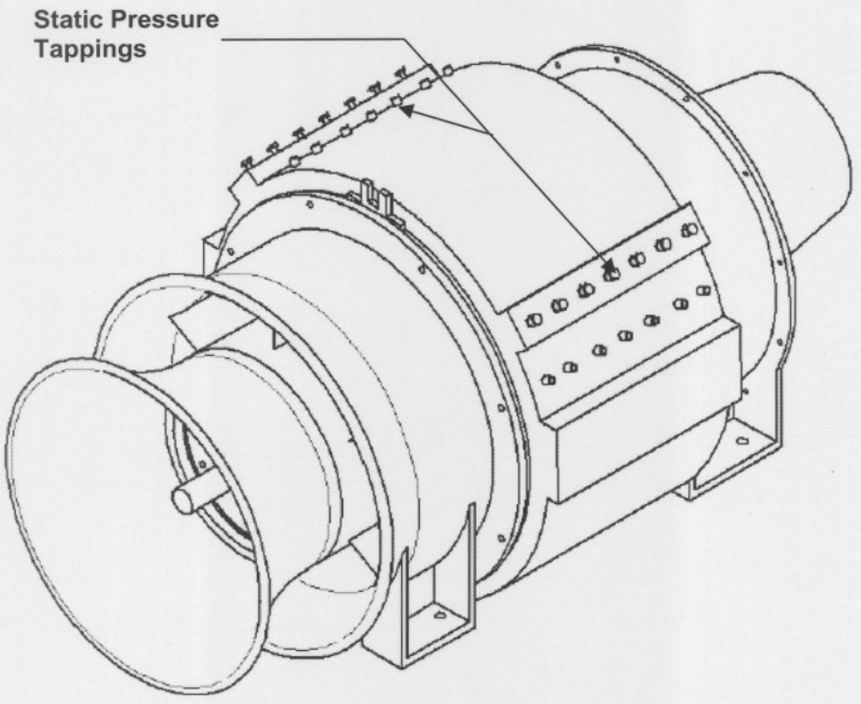

Figure D.1 The Rofanco axial flow compressor

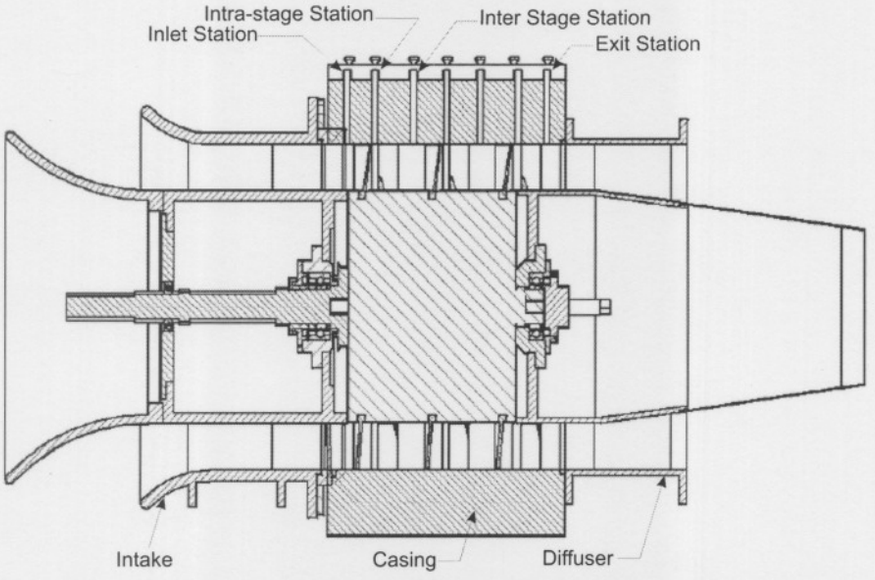

Figure D.2 A section through the Rofanco axial flow compressor

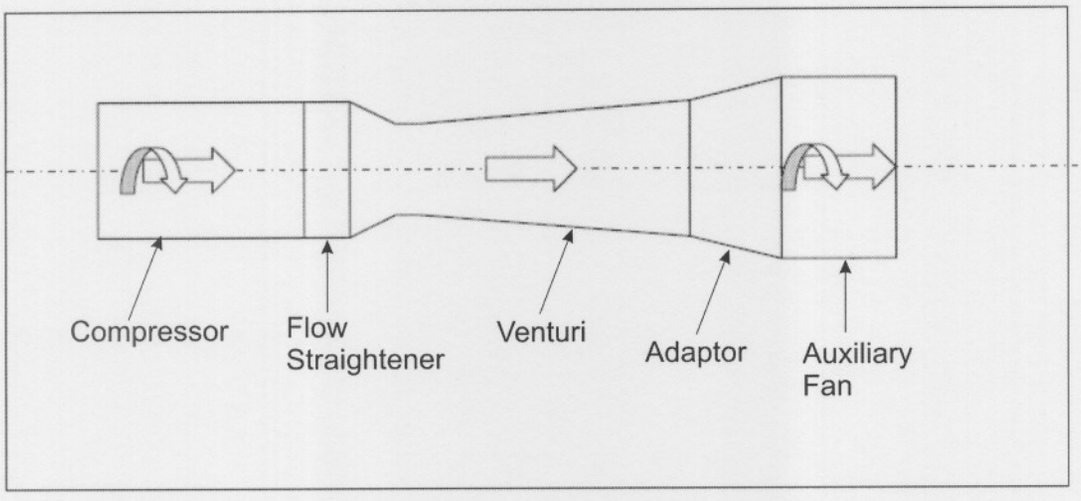

Figure D.3 Schematic of compressor rig (Positive compressor rotation and positive through-flow) Von Backström (2005:P2,17)

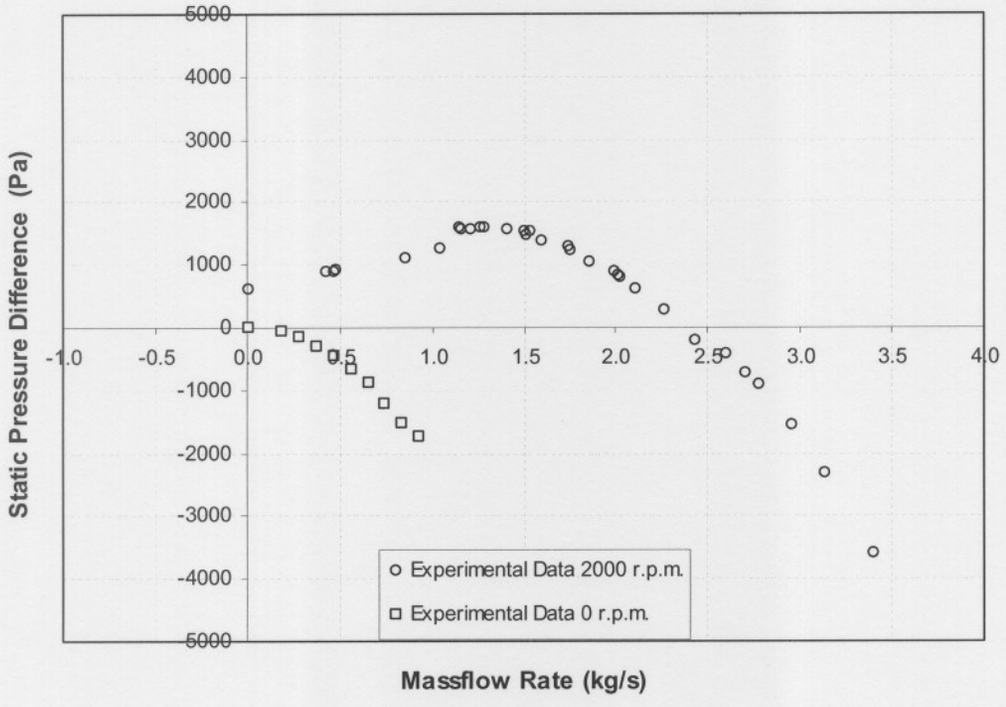

Figure D.4 Experimental results static pressure difference versus mass flow rate

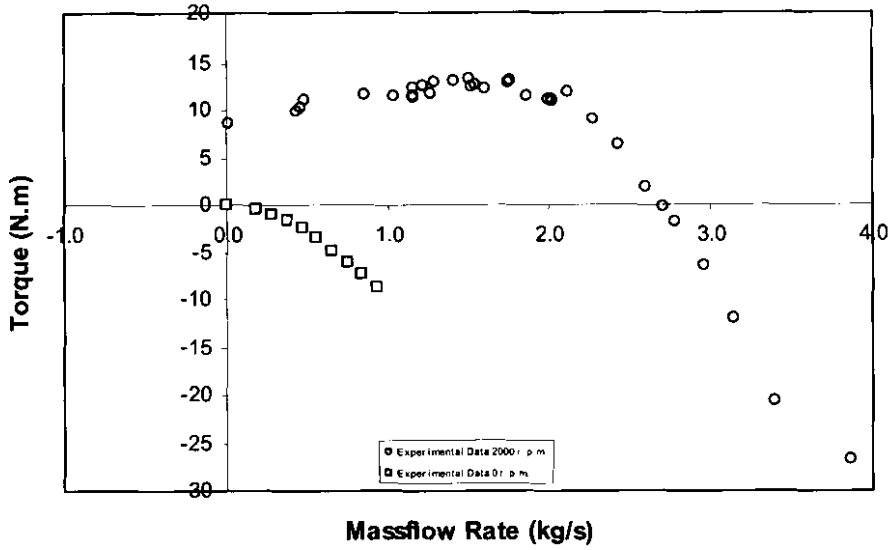

Figure D.5 Experimental results torque versus mass flow rate

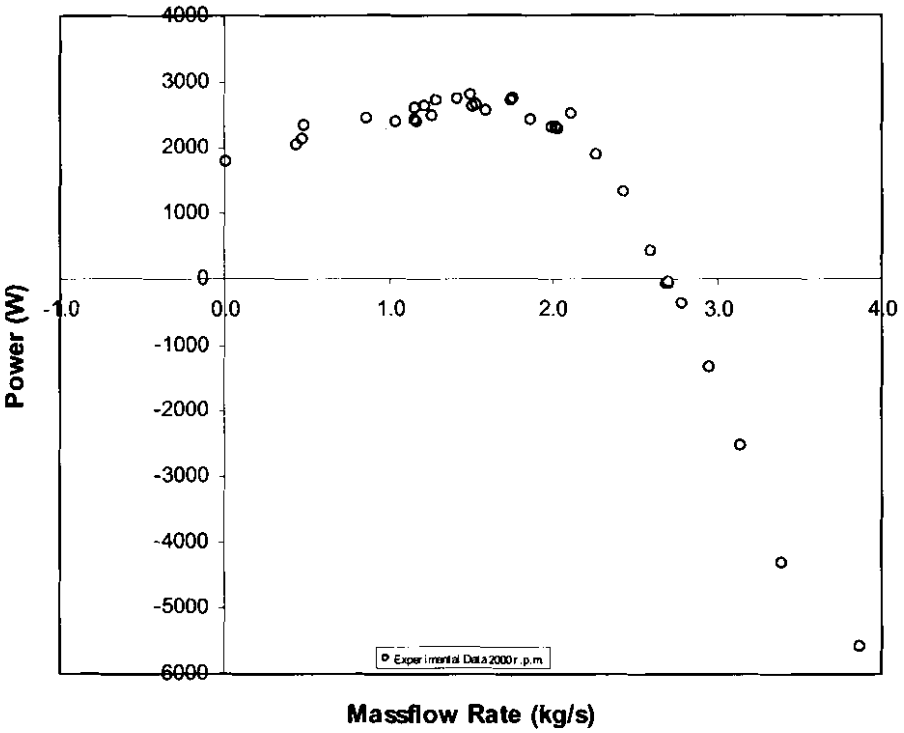

Figure D.6 Experimental results power versus mass flow rate

APPENDIX E

Uncertainty Analysis on Experimental Measurements

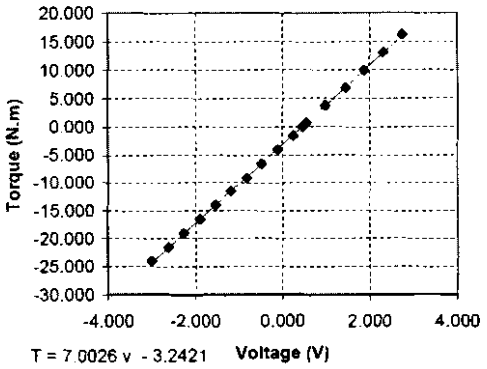

Figure E.1 Torque calibration curve

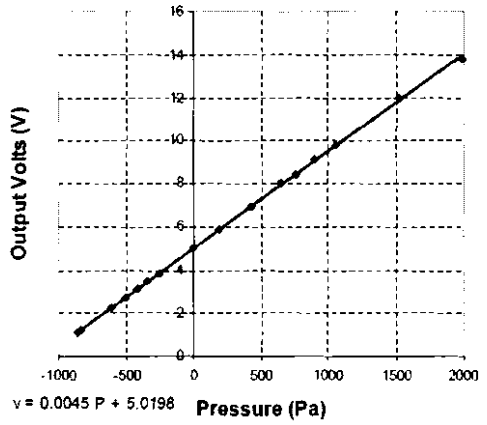

Figure E.2 Pressure transducer calibration curve for total inlet pressure

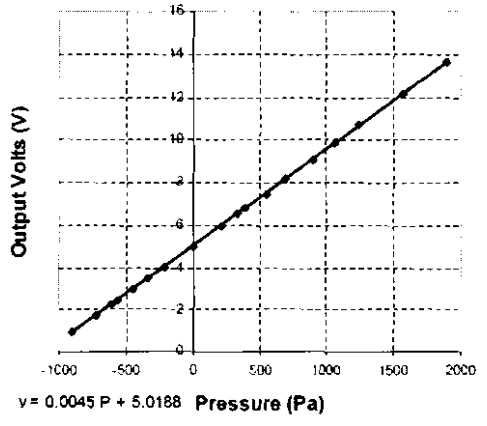

Figure E.3 Pressure transducer calibration curve for static inlet pressure

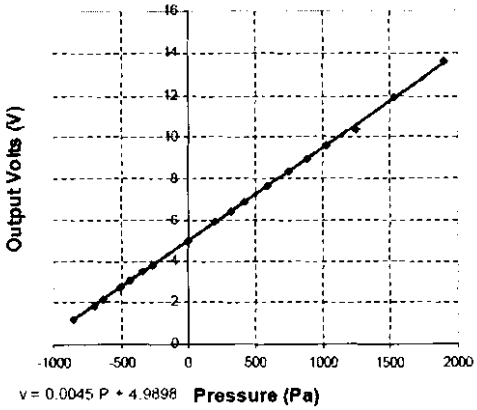

Figure E.4 Pressure transducer calibration curve for total outlet pressure

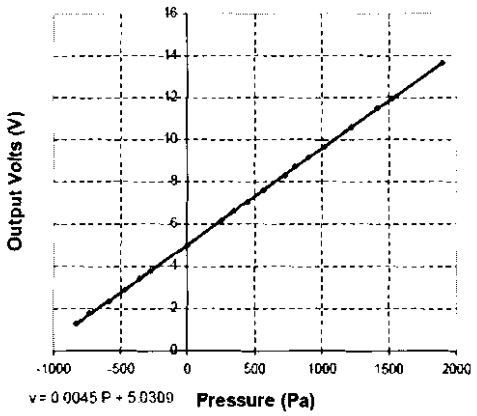

Figure E.5 Pressure transducer calibration curve for static outlet pressure

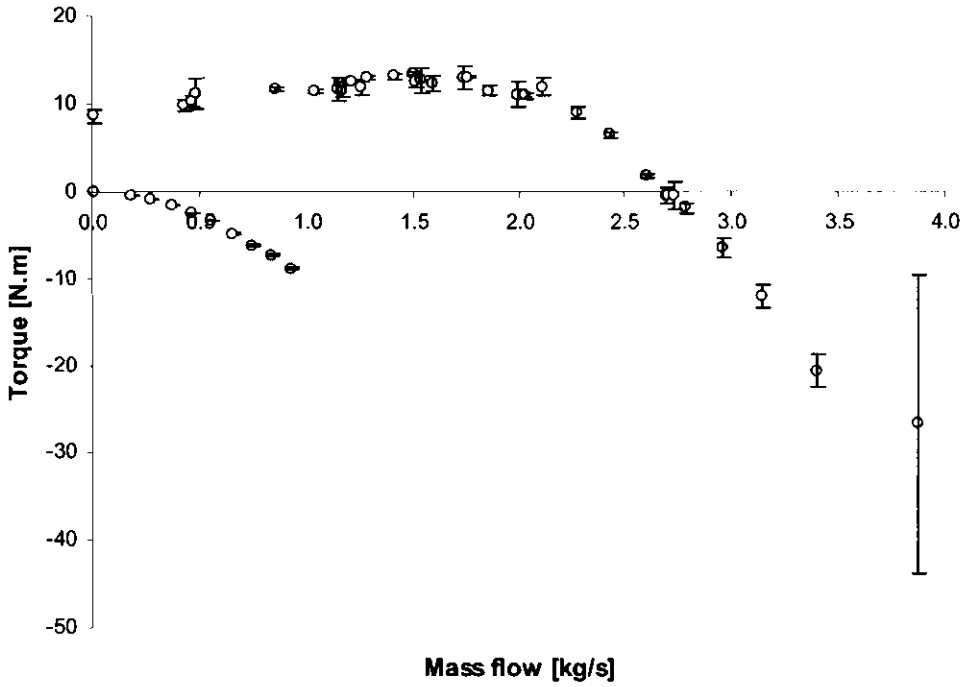

Figure E.6 Experimental data with uncertainty [torque versus mass flow]

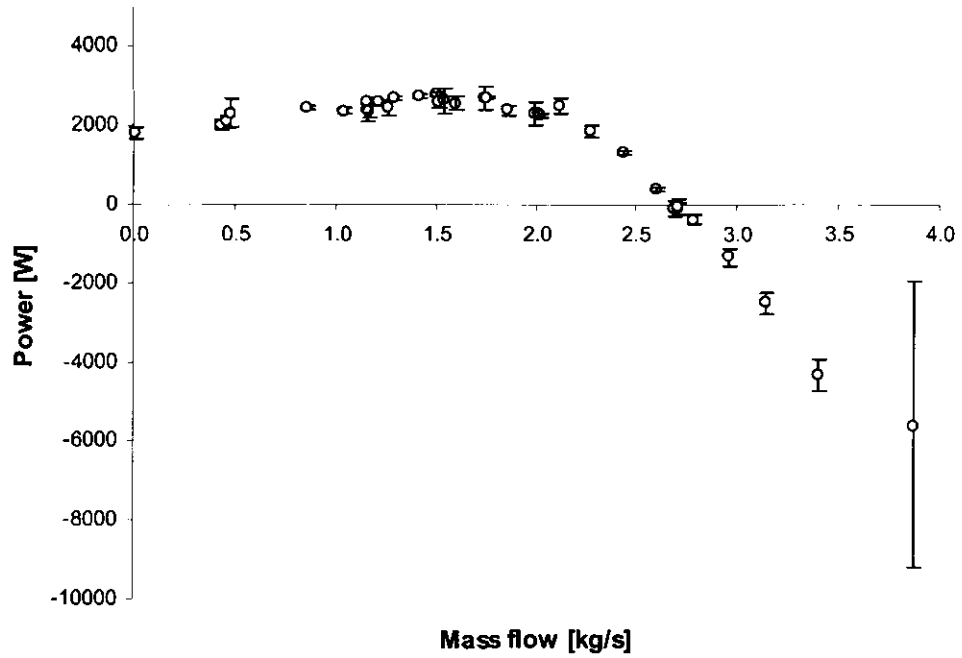

Figure E.7 Experimental data with uncertainty [power versus mass flow]

Mass flow [kg/s]	Torque [N.m]	± Torque [%]	± Torque [N.m]	Power [W]	± Power [%]	± Power [N.m]
0.009	8.561	8.220	0.704	1793.037	8.220	147.386
0.430	9.711	7.202	0.699	2033.951	7.202	146.488
0.464	10.130	6.754	0.684	2121.615	6.754	143.296
0.480	11.110	15.472	1.719	2326.948	15.472	360.021
0.860	11.621	2.148	0.250	2433.965	2.148	52.286
1.040	11.345	2.272	0.258	2376.037	2.272	53.991
1.152	11.525	11.817	1.362	2413.812	11.817	285.252
1.161	12.293	1.621	0.199	2574.654	1.621	41.746
1.162	11.308	6.462	0.731	2368.295	6.462	153.037
1.213	12.465	2.004	0.250	2610.712	2.004	52.312
1.261	11.708	7.217	0.845	2452.154	7.217	176.981
1.288	12.866	1.856	0.239	2694.572	1.856	50.012
1.415	13.052	2.192	0.286	2733.580	2.192	59.928
1.502	13.340	2.028	0.271	2793.819	2.028	56.666
1.514	12.478	5.824	0.727	2613.444	5.824	152.216
1.539	12.572	11.870	1.492	2633.027	11.870	312.552
1.599	12.227	6.939	0.848	2560.755	6.939	177.685
1.743	12.873	10.643	1.370	2696.164	10.643	286.953
1.757	12.979	1.221	0.158	2718.220	1.221	33.189
1.862	11.427	5.070	0.579	2393.357	5.070	121.347
1.996	10.970	12.585	1.381	2297.604	12.585	289.162
2.019	10.983	1.906	0.209	2300.329	1.906	43.838
2.028	10.815	2.615	0.283	2265.004	2.615	59.226
2.117	11.859	7.783	0.923	2483.691	7.783	193.306
2.274	8.892	7.383	0.657	1862.352	7.383	137.506
2.434	6.340	4.748	0.301	1327.875	4.748	63.051
2.603	1.857	12.641	0.235	388.991	12.641	49.171
2.693	-0.481	174.528	0.840	-100.795	174.528	175.916
2.707	-0.424	164.310	0.696	-88.704	164.310	145.750
2.730	-0.500	310.929	0.916	-61.729	310.929	191.934
2.787	-1.827	29.905	0.546	-382.553	29.905	114.403
2.960	-6.432	17.407	1.120	-1347.080	17.407	234.487
3.145	-12.018	10.704	1.286	-2517.109	10.704	269.431
3.400	-20.567	8.845	1.819	-4307.622	8.845	380.989
3.873	-26.641	64.464	17.174	-5579.656	64.464	3596.858
S-curve						
0.006	0.000	0.000	0.000			
0.180	-0.457	2.187	0.010			
0.275	-0.941	0.141	0.001			
0.370	-1.611	1.035	0.017			
0.464	-2.444	1.316	0.032			
0.558	-3.380	1.684	0.057			
0.652	-4.819	1.830	0.088			
0.744	-6.129	1.434	0.088			
0.837	-7.320	1.364	0.100			
0.928	-8.849	1.556	0.138			

Table E.1 Uncertainties and data for torque and power measurements

It was found that the uncertainty on the instruments was the biggest 0.75%.

Mass flow [kg/s]	Δ P s-s [Pa]	± Δ P s-s [%]	± Δ P s-s [Pa]
0.009	595.089	9.18E-07	1.14E-05
0.430	878.176	2.72E-07	3.14E-06
0.464	895.202	3.66E-07	4.20E-06
0.480	920.405	4.29E-07	5.20E-06
0.860	1092.671	1.08E-07	1.46E-06
1.040	1250.395	2.04E-07	3.10E-06
1.152	1595.841	2.25E-08	3.68E-07
1.161	1550.642	1.18E-08	2.25E-07
1.162	1553.340	2.49E-08	3.05E-07
1.213	1567.081	2.88E-08	5.52E-07
1.261	1572.859	1.85E-08	2.25E-07
1.288	1579.676	3.34E-08	6.36E-07
1.415	1569.253	1.50E-08	2.82E-07
1.502	1515.741	5.70E-08	1.03E-06
1.514	1473.711	3.62E-08	3.67E-07
1.539	1524.721	2.98E-08	4.49E-07
1.599	1383.187	3.44E-08	3.04E-07
1.743	1276.376	1.89E-08	2.30E-07
1.757	1222.656	3.89E-05	5.72E-04
1.862	1041.672	2.15E-08	7.78E-08
1.996	877.711	3.20E-08	2.55E-07
2.019	813.812	2.10E-08	2.12E-07
2.028	800.012	3.41E-08	3.38E-07
2.117	621.413	1.02E-08	8.10E-08
2.274	264.397	1.30E-08	5.40E-08
2.434	-209.265	2.95E-08	7.75E-09
2.603	-427.552	1.35E-07	8.94E-07
2.711	-716.769	1.68E-06	2.06E-05
2.787	-927.737	4.61E-07	6.10E-06
2.960	-1570.016	2.30E-09	3.29E-08
3.145	-2323.585	1.68E-09	2.52E-08
3.400	-3591.302	1.37E-09	2.15E-08
3.873	-6460.617	9.03E-10	1.48E-08
S-curve			
0.006	-0.188	1.65E-07	3.10E-10
0.180	-71.224	3.12E-06	2.22E-06
0.275	-166.391	7.81E-06	1.30E-05
0.370	-300.580	2.01E-05	6.04E-05
0.464	-466.744	4.42E-05	2.06E-04
0.558	-673.233	1.38E-04	9.31E-04
0.652	-898.772	1.76E-04	1.58E-03
0.744	-1204.670	1.74E-02	2.10E-01
0.8366	-1510.839	2.19E-04	3.31E-03
0.9275	-1748.805	2.70E-04	4.72E-03

Table E.2 Uncertainties and data for static pressure difference

APPENDIX F.1

Program Algorithm

The basic logical structure of the performance prediction algorithm is presented in Figure F.1.1. Blade row sets are coupled using the array function of EES. Arrows are pointing both ways to indicate that inputs are given when calling and the necessary outputs are provided to the calling structure. Modules, functions and procedures can be updated and changed separable from the main code. The number of stages is decided by the user as long the necessary input variables are given.

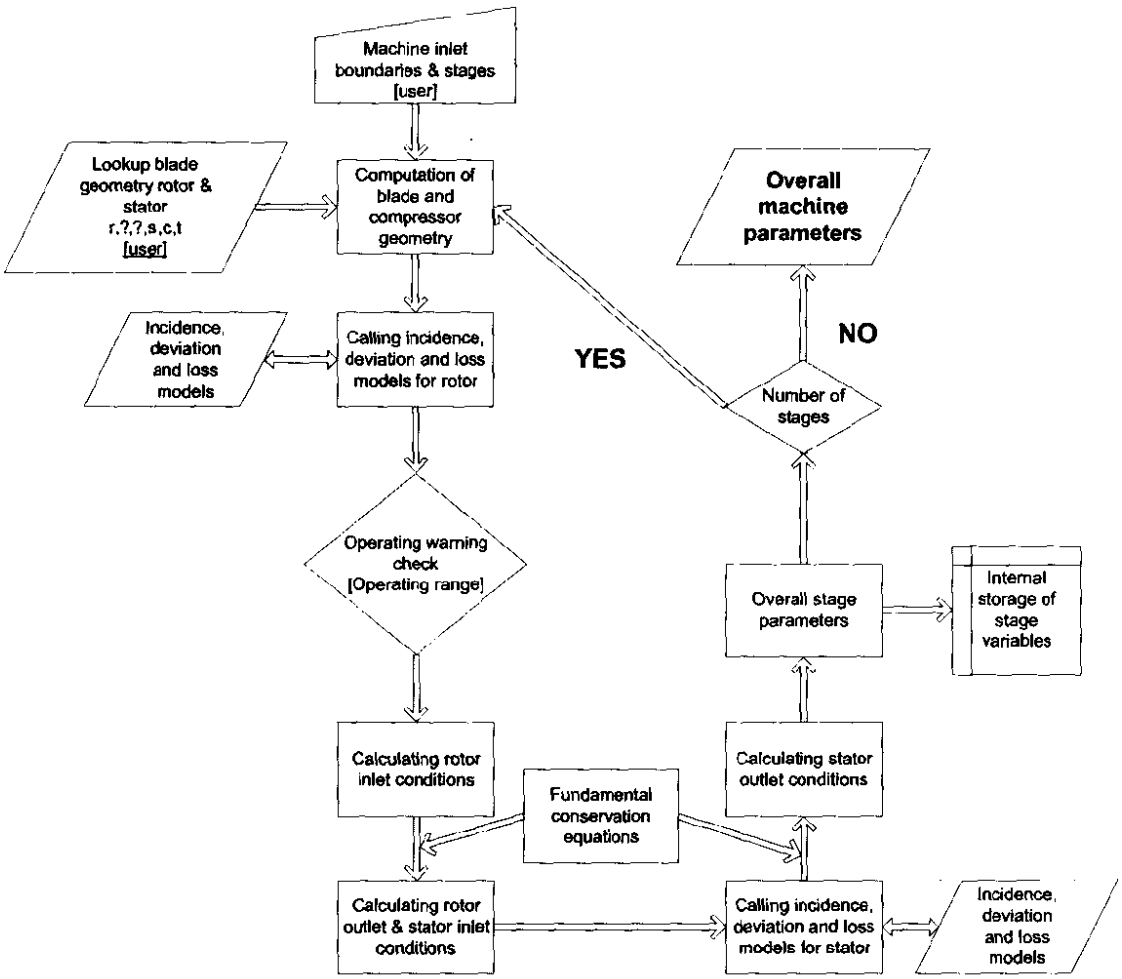

Figure F.1.1 Program algorithm

APPENDIX F.2

User Variable Input

These operating values must be supplied by the user into the main program and a lookup table described in Section 6.3.1. Table F.2.1 describes where certain variable must be supplied.

Table F.2.1 User supplied variables

Compressor user inputs (main program)		
Variable	**Description**	**Unit**
stages	Number of stages in the compressor	-
N	Compressor rotational speed	rpm
P_{01}	Compressor inlet total pressure	kPa
T_{01}	Compressor inlet total temperature	°C
$\dot{m}$	Inlet mass flow rate	kg/s
θ_1	Compressor absolute inlet flow angle – from IGV or zero for no IGV in setup	°
G1$	Operating working fluid – EES variable	-
Compressor user inputs (lookup table)		
r_{t1}	Tip radius at leading edge of rotor	m
r_{t2}	Tip radius at trailing edge of rotor	m
r_{t3}	Casing radius at trailing edge of stator	m
r_{hb1}	Hub radius at leading edge of rotor	m
r_{hb2}	Hub radius at trailing edge of rotor - leading edge of stator	m
r_{hb3}	Hub radius at trailing edge of stator	m
ζ_{rotor}	Rotor stagger angle	°
ζ_{stator}	Stator stagger angle	°
$\theta_{camber,rotor}$	Rotor blade camber angle	°
$\theta_{camber,stator}$	Stator blade camber angle	°
σ_{rotor}	Rotor solidity	-
σ_{stator}	Stator solidity	-
c_{rotor}	Rotor blade chord length	m
c_{stator}	Stator blade chord length	m
$t_{max,rotor}$	Rotor blade maximum thickness	m
$t_{max,stator}$	Stator blade maximum thickness	m

User variable input for compressor operating conditions is changed in the main program as previously mentioned and is displayed in Figure F.2.1 where user inputs supplied to EES lookup tables as mentioned in Table F.2.1 can be seen in Figure F.2.2. The rows representing stage one to three. Each variable consist of three rows meaning input variables for three stages.

MACHINE INLET CONDITIONS

stages = 3 Number of stages

N = 2000 Rotational speed rpm

$$\omega = N \cdot \frac{2 \cdot \pi}{60}$$

p_{0i} = 99.7117 Inlet atmospheric pressure

T_{0i} = 21.517 Inlet atmospheric temperature

$\dot{m}$ = 2.5 Inlet mass flow rate into axial compressor

θ_i = 0 Compressor absolute inlet flow angle - from IGV or zero for no IGV in setup

Figure F.2.1 User variable input for operating conditions in main program

Stage geometry	Experimental Data								
Paste Special	r_{t1} [m]	r_{t2} [m]	r_{t3} [m]	r_{hb1} [m]	r_{hb2} [m]	r_{hb3} [m]	ζ_{rotor} [°]	ζ_{stator} [°]	$\theta_{camber,rotor}$ [°]
Row 1	0.21	0.21	0.21	0.15	0.15	0.15	49.9952	16.3273	17.2554
Row 2	0.21	0.21	0.21	0.15	0.15	0.15	49.9952	16.3273	17.2554
Row 3	0.21	0.21	0.21	0.15	0.15	0.15	49.9952	16.3273	17.2554

$\theta_{camber,stator}$ [°]	σ_{rotor}	σ_{stator}	c_{rotor} [m]	c_{stator} [m]	$t_{max,rotor}$ [m]	$t_{max,stator}$ [m]
40.9710	1.0738	1.1261	0.03	0.03	0.003	0.003
40.9710	1.0738	1.1261	0.03	0.03	0.003	0.003
40.9710	1.0738	1.1261	0.03	0.03	0.003	0.003

Figure F.2.2 EES lookup table for blade geometry in each blade row

APPENDIX F.3

Performance Prediction Formatted Equations

This section presents the main overall multi stage axial compressor formatted equations in EES that calculates the overall performance of the Rofanco multi stage axial compressor. Some calling arguments are also displayed to show where all the sub-programs is called from and with its input variables.

MAIN PROGRAM

Gas Properties

Only air

G1$ = 'Air'

c_p = **Cp** (G1$, T = T_{0i})

c_v = **Cv** (G1$, T = T_{0i})

R_{air} = (c_p − c_v) · 1000

$$\gamma = \frac{c_p}{c_v}$$

g = 9.796 Gravitation of Newton's law

MACHINE INLET CONDITIONS

stages = 3 Number of stages

N = 2000 Rotational speed rpm

$$\omega = N \cdot \frac{2 \cdot \pi}{60}$$

p_{0i} = 99.7117 Inlet atmospheric pressure

T_{0i} = 21.517 Inlet atmospheric temperature

$\dot{m}$ = 2.5 Inlet mass flow rate into axial compressor

θ_i = 0 Compressor absolute inlet flow angle - from IGV or zero for no IGV in setup

$l_{1,r}$ = 0.09 Constant l_1 for rotor Figure 3.5

$l_{1,s}$ = 0.135 Constant l_1 for stator Figure 3.5

INITIALISE STAGE PARAMETERS

$p_{03,0}$ = p_{0i} Pressure

$T_{03,0}$ = T_{0i} Temperature

$\theta_{3,0}$ = θ_i Flow angle

$A_{1,i} = \pi \cdot r_{t1,i}^2 - \pi \cdot r_{hb1,i}^2$ for i = 1 to stages Inlet area rotor

$A_{2,i} = \pi \cdot r_{t2,i}^2 - \pi \cdot r_{hb2,i}^2$ for i = 1 to stages Outlet area rotor - Inlet area stator

$A_{3,i} = \pi \cdot r_{t3,i}^2 - \pi \cdot r_{hb3,i}^2$ for i = 1 to stages Outlet area stator

$r_{t1,i}$ = **Lookup** ('Stage geometry', i, 'r_{t1}') for i = 1 to stages Tip radius at leading edge of rotor

$r_{t2,i}$ = **Lookup** ('Stage geometry', i, 'r_{t2}') for i = 1 to stages Tip radius at trailing edge of rotor

$r_{t3,i}$ = **Lookup** ('Stage geometry', i, 'r_{t3}') for i = 1 to stages Casing radius at trailing edge of stator

$r_{hb1,i}$ = **Lookup** ('Stage geometry', i, 'r_{hb1}') for i = 1 to stages Hub radius at leading edge of rotor

$r_{hb2,i}$ = **Lookup** ('Stage geometry', i, 'r_{hb2}') for i = 1 to stages Hub radius at trailing edge of rotor - leading edge of stator

$r_{hb3,i}$ = **Lookup** ('Stage geometry', i, 'r_{hb3}') for i = 1 to stages Hub radius at trailing edge of stator

$$r_{rms,1,i} = \sqrt{\frac{r_{t1,i}^2 + r_{hb1,i}^2}{2}}$$ for i = 1 to stages Root-mean-square radius inlet rotor

$$r_{rms,2,i} = \sqrt{\frac{r_{t2,i}^2 + r_{hb2,i}^2}{2}}$$ for i = 1 to stages Root-mean-square radius outlet rotor - Inlet stator

$$r_{rms,3,i} = \sqrt{\frac{r_{t3,i}^2 + r_{hb3,i}^2}{2}}$$ for i = 1 to stages Root-mean-square radius outlet stator

$$h_{ratio,rotor,i} = \frac{r_{t1,i} - r_{hb1,i}}{r_{t2,i} - r_{hb2,i}}$$ for i = 1 to stages Height ratio of rotor blade

$$h_{ratio,stator,i} = \frac{r_{t2,i} - r_{hb2,i}}{r_{t3,i} - r_{hb3,i}}$$ for i = 1 to stages Height ratio of stator blade

$\zeta_{rotor,i}$ = **Lookup** ('Stage geometry', i, '$zeta_{rotor}$') for i = 1 to stages Stagger angle rotor

$\zeta_{stator,i}$ = **Lookup** ('Stage geometry', i, '$zeta_{stator}$') for i = 1 to stages Stagger angle stator

$\theta_{camber,rotor,i}$ = **Lookup** ('Stage geometry', i, '$theta_{camber,rotor}$') for i = 1 to stages Camber angle rotor

$\theta_{camber,stator,i}$ = **Lookup** ('Stage geometry', i, '$theta_{camber,stator}$') for i = 1 to stages Camber angle stator

$\sigma_{rotor,i}$ = **Lookup** ('Stage geometry', i, '$sigma_{rotor}$') for i = 1 to stages Solidity rotor

$\sigma_{stator,i}$ = **Lookup** ('Stage geometry', i, '$sigma_{stator}$') for i = 1 to stages Solidity stator

$$space_{rotor,i} = \frac{c_{rotor,i}}{\sigma_{rotor,i}}$$ for i = 1 to stages Blade pitch of rotor

$$space_{stator,i} = \frac{c_{stator,i}}{\sigma_{stator,i}}$$ for i = 1 to stages Blade pitch of stator

$c_{rotor,i}$ = **Lookup** ('Stage geometry', i, 'c_{rotor}') for i = 1 to stages Cord rotor

$c_{stator,i}$ = **Lookup** ('Stage geometry', i, 'c_{stator}') for i = 1 to stages Cord stator

$t_{rotor,i}$ = **Lookup** ('Stage geometry', i, '$t_{max,rotor}$') for i = 1 to stages Maximum blade thickness rotor

$t_{stator,i}$ = **Lookup** ('Stage geometry', i, '$t_{max,stator}$') for i = 1 to stages Maximum blade thickness stator

$$H_{rotor,i} = \frac{r_{t1,i} - r_{hb1,i} + r_{t2,i} - r_{hb2,i}}{2}$$ for i = 1 to stages Mean height of rotor

$$H_{stator,i} = \frac{r_{t2,i} - r_{hb2,i} + r_{t3,i} - r_{hb3,i}}{2}$$ for i = 1 to stages Mean height of stator

$\beta_{1B,i} = \zeta_{rotor,i} + \frac{\theta_{camber,rotor,i}}{2}$ for i = 1 to stages Inlet rotor blade angle

$\theta_{2B,i} = \zeta_{stator,i} + \frac{\theta_{camber,stator,i}}{2}$ for i = 1 to stages Inlet stator blade angle

$\theta_{camber,rotor,i} = \alpha_{2B,i} - \alpha_{1B,i}$ for i = 1 to stages

$\theta_{camber,stator,i} = \theta_{2B,i} - \theta_{3B,i}$ for i = 1 to stages

$\beta_{2B,i} = 180 - \alpha_{2B,i}$ for i = 1 to stages Calculating alpha angle

$\beta_{1B,i} = 180 - \alpha_{1B,i}$ for i = 1 to stages Calculating alpha angle

$\tan(\beta_{m,i}) = \frac{\tan(\beta_{1,i}) + \tan(\beta_{2,i})}{2}$ for i = 1 to stages Calculating mean angle (inlet flow and outlet flow) of rotor

$\tan(\theta_{m,i}) = \frac{\tan(\theta_{2,i}) + \tan(\theta_{3,i})}{2}$ for i = 1 to stages Calculating mean angle (inlet flow and outlet flow) of stator

The calling of the $Total_{Loss}$ sub-section is not shown, because the variable input is to long.

Call **Minimum**$_{incedence}$ ($\beta_{1,1}$, $\sigma_{rotor,1}$, $t_{rotor,1}$, $c_{rotor,1}$, $\theta_{camber,rotor,1}$, $space_{rotor,1}$, $o_{rotor,1}$, $M_{1r,1}$, $\beta_{1B,1}$: $i_{min,r,1}$)

Call **Deviation** ($i_{r,i}$, $i_{min,r,i}$, $\beta_{1,i}$, $t_{rotor,i}$, $c_{rotor,i}$, $\theta_{camber,rotor,i}$, $\sigma_{rotor,i}$: $\delta_{min,r,1}$, $\delta_{r11,1}$, $slope_i$) for i = 1 to stages

Call **Choking** ($l_{1,r}$, $c_{rotor,1}$, $t_{rotor,1}$, $\zeta_{rotor,1}$, $\sigma_{rotor,1}$, γ, $space_{rotor,1}$, $V_{max,rotor,1}$, $V_{1,1}$, $\beta_{2,1}$, $M_{1,1}$, $\rho_{1,1}$, $\beta_{1B,1}$, $\beta_{1,1}$, $ch_{val,r,1}$: $\beta_{ch,r,1}$, $i_{choke,r,1}$, $\sigma_{rotor,1}$, $M_{ch,r,1}$)

Call **Choking**$_{Val}$ ($o_{rotor,i}$, $space_{rotor,i}$, $\beta_{1,i}$: $ch_{val,r}$) for i = 1 to stages

Call **StalledDeviation** ($i_{r,i}$, $\zeta_{rotor,i}$, $\theta_{camber,rotor,i}$, $\sigma_{rotor,i}$, $c_{rotor,i}$, $space_{rotor,i}$, $\rho_{1,i}$, $\rho_{2,i}$, $C_{a1,i}$, $C_{a2,i}$, $t_{rotor,i}$: $i_{st,rotor,1}$, $\delta_{opt,1}$, $\delta_{r,1}$, $l_{p,r,1}$, $i_{opt,r,i}$) for i = 1 to stages

Call **Reynolds**$_{Correct}$ [$|Re_{rotor,i}|$, $c_{rotor,i}$: $w_{correctR,rotor,i}$] for i = 1 to stages

Call **Mach**$_{Critic}$ ($p_{01,1}$ [kPa], $p_{1,1}$, $\rho_{1,1}$, $V_{1,1}$, $V_{max,rotor,1}$, g, γ : $M_{1critic,1}$)

Call **Mach**$_{Correct}$ ($M_{1,i}$, $M_{1critic,i}$: $w_{correctM,rotor,i}$) for i = 1 to stages

Call **Opp**$_{range}$ ($i_{r,i}$, $i_{min,r,i}$, $M_{1,i}$, $\beta_{1B,i}$, $\sigma_{rotor,i}$, $\theta_{camber,rotor,i}$: $\delta_{beta,r,1}$, $\delta_{beta,2,r,i}$) for i = 1 to stages

Call **Blade**$_{Stall}$ (i, $\dot{m}$, $i_{r,i}$, $i_{min,r,i}$, $\delta_{\beta,r,i}$: inop$\$_i$) for i = 1 to stages

Call **Blade**$_{choke}$ (i, PR_i : choke$\$_i$) for i = 1 to stages

ROTOR INLET CONDITIONS

$p_{01,i} = p_{03,i-1}$ for i = 1 to stages

$T_{01,i} = T_{03,i-1}$ for i = 1 to stages

$h_{01,i} = h_{1,i} + 0.001 \cdot 0.5 \cdot C_{1,i}^2$ for i = 1 to stages

$p_{01,i} = p_{1,i} \cdot \left[\left(1 + \left[\frac{\gamma - 1}{2} \right] \cdot M_{1,i}^2 \right)^{\left(\frac{\gamma}{\gamma - 1} \right)} \right]$ for i = 1 to stages

$T_{01,i} + 273.15 = (T_{1,i} + 273.15) \cdot \left[1 + \left(\frac{\gamma - 1}{2} \right) \cdot M_{1,i}^2 \right]$ for i = 1 to stages

$h_{1,i} = \mathbf{h}(G1\$, T=T_{1,i})$ for i = 1 to stages

$\rho_{1,i} = \rho(G1\$, T=T_{1,i}, P=p_{1,i})$ for i = 1 to stages

$s_{1,i} = \mathbf{s}(G1\$, T=T_{1,i}, P=p_{1,i})$ for i = 1 to stages

$\mu_{1,i} = \mathbf{Visc}(G1\$, T=T_{1,i})$ for i = 1 to stages

$Re_{rotor,i} = \frac{\rho_{1,i} \cdot c_{rotor,i} \cdot V_{1,i}}{\mu_{1,i}}$ for i = 1 to stages

$$M_{1,i} = \frac{C_{1,i}}{\sqrt{\gamma \cdot R_{air} \cdot (T_{1,i} + 273.15)}} \quad \text{for } i = 1 \text{ to stages}$$

$$U_{1,i} = \omega \cdot r_{rms,1,i} \quad \text{for } i = 1 \text{ to stages}$$

$$C_{a1,i} = \frac{\dot{m}}{\rho_{1,i} \cdot A_{1,i}} \quad \text{for } i = 1 \text{ to stages}$$

$$\theta_{1,i} = \theta_{3,i-1} \quad \text{for } i = 1 \text{ to stages}$$

$$C_{a1,i} = C_{1,i} \cdot \cos(\theta_{1,i}) \quad \text{for } i = 1 \text{ to stages}$$

$$\frac{C_{w1,i}}{C_{1,i}} = \sin(\theta_{1,i}) \quad \text{for } i = 1 \text{ to stages}$$

$$\frac{V_{w1,i}}{V_{1,i}} = \sin(180 - \alpha_{1,i}) \quad \text{for } i = 1 \text{ to stages}$$

$$\frac{U_{1,i} - C_{w1,i}}{C_{a1,i}} = \tan(180 - \alpha_{1,i}) \quad \text{for } i = 1 \text{ to stages}$$

$$V_{1,i} = \frac{C_{a1,i}}{\cos(180 - \alpha_{1,i})} \quad \text{for } i = 1 \text{ to stages}$$

$$\beta_{1,i} = 180 - \alpha_{1,i} \quad \text{for } i = 1 \text{ to stages}$$

$$i_{r,i} = -\alpha_{1,i} + \alpha_{1B,i} \quad \text{for } i = 1 \text{ to stages}$$

ROTOR AVERAGE CONDITIONS

$$T_{0avgrotor,i} = 0.5 \cdot (T_{01,i} + T_{02,i}) \quad \text{for } i = 1 \text{ to stages}$$

$$p_{0avgrotor,i} = 0.5 \cdot (p_{01,i} + p_{02,i}) \quad \text{for } i = 1 \text{ to stages}$$

$$T_{avgrotor,i} = 0.5 \cdot (T_{1,i} + T_{2,i}) \quad \text{for } i = 1 \text{ to stages}$$

$$p_{avgrotor,i} = 0.5 \cdot (p_{1,i} + p_{2,i}) \quad \text{for } i = 1 \text{ to stages}$$

$$\rho_{avgrotor,i} = 0.5 \cdot (\rho_{1,i} + \rho_{2,i}) \quad \text{for } i = 1 \text{ to stages}$$

$$\mu_{avgrotor,i} = 0.5 \cdot (\mu_{1,i} + \mu_{2,i}) \quad \text{for } i = 1 \text{ to stages}$$

$$C_{avgrotor,i} = 0.5 \cdot (C_{1,i} + C_{2,i}) \quad \text{for } i = 1 \text{ to stages}$$

$$V_{avgrotor,i} = 0.5 \cdot (V_{1,i} + V_{2,i}) \quad \text{for } i = 1 \text{ to stages}$$

The calling of the $Total_{Loss}$ sub-section is not shown, because the variable input is to long.

Call **Minimum**$_{incedence}$ ($\theta_{2,1}$, $\sigma_{stator,1}$, $t_{stator,1}$, $c_{stator,1}$, $\theta_{camber,stator,1}$, $space_{stator,1}$, $o_{stator,1}$, $M_{2,1}$, $\theta_{2B,1}$: $i_{min,s,1}$)

Call **Choking** ($l_{1,s}$, $c_{stator,1}$, $t_{stator,1}$, $\zeta_{stator,1}$, $\sigma_{stator,1}$, γ, $space_{stator,1}$, $C_{max,stator,1}$, $C_{2,1}$, $\theta_{3,1}$, $M_{2,1}$, $\rho_{2,1}$ [kg/m^3], $\theta_{2B,1}$, $\theta_{2,1}$, $ch_{val,s,1}$: $\theta_{ch,1}$, $i_{choke,s,1}$, $o_{stator,1}$, $M_{ch,s,1}$)

Call **Choking**$_{Val}$ ($o_{stator,i}$, $space_{stator,i}$, $\theta_{2,i}$: $ch_{val,s,i}$) for $i = 1$ to stages

Call **Deviation** ($i_{s,i}$, $i_{min,s,i}$, $\theta_{Z,i}$, $t_{stator,i}$, $c_{stator,i}$, $\theta_{camber,stator,i}$, $\sigma_{stator,i}$: $\delta_{min,s,1}$, $\delta_{s11,1}$, $slope_{stator,i}$) for $i = 1$ to stages

Call **BoundryDev** ($\delta_{lib,s,i}$, $\theta_{wake,stator,i}$, $space_{stator,i}$, $\theta_{3,i}$, $i_{s,i}$, $i_{min,s,i}$: $\delta_{boundry,stator,1}$, $\delta_{s111,i}$) for $i = 1$ to stages

Call **StalledDeviation** ($i_{s,i}$, $\zeta_{stator,i}$, $\theta_{camber,stator,i}$, $\sigma_{stator,i}$, $c_{stator,i}$, $space_{stator,i}$, $\rho_{1,i}$, $\rho_{2,i}$, $C_{a1,i}$, $C_{a2,i}$, $t_{stator,i}$: $i_{st,stator,1}$, $\delta_{opt,s,1}$, $\delta_{s,1}$, $l_{p,s,1}$, $i_{opt,s,i}$) for $i = 1$ to stages

Call **Reynolds**$_{Correct}$ [$|Re_{stator,i}|$, $c_{stator,i}$: $w_{correctR,stator,i}$] for $i = 1$ to stages

Call **Opp**$_{range}$ ($i_{s,i}$, $i_{min,s,i}$, $M_{2,i}$, $\theta_{2B,i}$, $\sigma_{stator,i}$, $\theta_{camber,stator,i}$: $\delta_{beta,s,1}$, $\delta_{beta,2,s,i}$) for $i = 1$ to stages

Call **Mach**$_{Critic}$ ($p_{02,1}$ [kPa], $p_{2,1}$, $\rho_{2,1}$ [kg/m^3], $V_{2,1}$, $V_{max,stator,1}$, g, γ : $M_{2critic,1}$)

Call **Mach**$_{Correct}$ ($M_{2,i}$, $M_{2critic,i}$: $w_{correctM,stator,i}$) for $i = 1$ to stages

ROTOR OUTLET CONDITIONS AND STATOR INLET CONDITIONS

$$X_i = \omega \cdot \left(r_{rms,2,i}^{\,2} - r_{rms,1,i}^{\,2} \right) - \left(V_{2,i} \cdot r_{rms,2,i} \cdot \sin(\alpha_{2,i}) - V_{1,i} \cdot r_{rms,1,i} \cdot \sin(\alpha_{1,i}) \right) \quad \text{for } i = 1 \text{ to stages}$$

$$\frac{p_{avgrotor,i}}{p_{0avgrotor,i}} \cdot (p_{02,i} - p_{01,i}) \cdot 1000 + 0.5 \cdot \rho_{avgrotor,i} \cdot C_{avgrotor,i}^{\,2} \cdot \left[\frac{1}{T_{0avgrotor,i} + 273.15} \right] \cdot (T_{02,i} - T_{01,i}) + w_{total,rotor,i} \cdot (p_{01,i} - p_{1,i}) \cdot 1000 = \rho_{avgrotor,i} \cdot \omega$$

$$(h_{02,i} - h_{01,i}) \cdot 1000 = \omega \cdot X_i \quad \text{for } i = 1 \text{ to stages}$$

$$h_{02,i} = h_{2,i} + 0.001 \cdot 0.5 \cdot C_{2,i}^{\,2} \quad \text{for } i = 1 \text{ to stages}$$

$$p_{02,i} = p_{2,i} \cdot \left[\left(1 + \left[\frac{\gamma - 1}{2} \right] \cdot M_{2,i}^{\,2} \right)^{\left(\frac{\gamma}{\gamma - 1} \right)} \right] \quad \text{for } i = 1 \text{ to stages}$$

$$T_{02,i} + 273.15 = (T_{2,i} + 273.15) \cdot \left[1 + \left(\frac{\gamma - 1}{2} \right) \cdot M_{2,i}^{\,2} \right] \quad \text{for } i = 1 \text{ to stages}$$

$$h_{2,i} = \mathbf{h}(G1\$, T = T_{2,i}) \quad \text{for } i = 1 \text{ to stages}$$

$$\rho_{2,i} = \rho(G1\$, T = T_{2,i}, P = p_{2,i}) \quad \text{for } i = 1 \text{ to stages}$$

$$s_{2,i} = \mathbf{s}(G1\$, T = T_{2,i}, P = p_{2,i}) \quad \text{for } i = 1 \text{ to stages}$$

$$\mu_{2,i} = \mathbf{Visc}(G1\$, T = T_{2,i}) \quad \text{for } i = 1 \text{ to stages}$$

$$Re_{stator,i} = \frac{\rho_{2,i} \cdot c_{stator,i} \cdot C_{2,i}}{\mu_{2,i}} \quad \text{for } i = 1 \text{ to stages}$$

$$M_{2,i} = \frac{C_{2,i}}{\sqrt{\gamma \cdot R_{air} \cdot (T_{2,i} + 273.15)}} \quad \text{for } i = 1 \text{ to stages}$$

$$U_{2,i} = \omega \cdot r_{rms,2,i} \quad \text{for } i = 1 \text{ to stages}$$

$$C_{a2,i} = \frac{\dot{m}}{\rho_{2,i} \cdot A_{2,i}} \quad \text{for } i = 1 \text{ to stages}$$

$$C_{w2,i} = U_{2,i} - V_{2,i} \cdot \sin(180 - \alpha_{2,i}) \quad \text{for } i = 1 \text{ to stages}$$

$$\frac{C_{w2,i}}{C_{a2,i}} = \tan(\theta_{2,i}) \quad \text{for } i = 1 \text{ to stages}$$

$$\frac{V_{w2,i}}{V_{2,i}} = \sin(180 - \alpha_{2,i}) \quad \text{for } i = 1 \text{ to stages}$$

$$\frac{C_{a2,i}}{V_{2,i}} = \cos(180 - \alpha_{2,i}) \quad \text{for } i = 1 \text{ to stages}$$

$$\frac{C_{a2,i}}{C_{2,i}} = \cos(\theta_{2,i}) \quad \text{for } i = 1 \text{ to stages}$$

$$\beta_{2,i} = 180 - \alpha_{2,i} \quad \text{for } i = 1 \text{ to stages}$$

$$\delta_{r,i} = \alpha_{2B,i} - \alpha_{2,i} \quad \text{for } i = 1 \text{ to stages}$$

$$i_{s,i} = \theta_{2,i} - \theta_{2B,i} \quad \text{for } i = 1 \text{ to stages}$$

STATOR AVERAGE CONDITIONS

$$T_{0avgstator,i} = 0.5 \cdot (T_{02,i} + T_{03,i}) \quad \text{for } i = 1 \text{ to stages}$$

$$p_{0avgstator,i} = 0.5 \cdot (p_{02,i} + p_{03,i}) \quad \text{for } i = 1 \text{ to stages}$$

$$T_{avgstator,i} = 0.5 \cdot (T_{2,i} + T_{3,i}) \quad \text{for } i = 1 \text{ to stages}$$

$$p_{avgstator,i} = 0.5 \cdot (p_{2,i} + p_{3,i}) \quad \text{for } i = 1 \text{ to stages}$$

$$\rho_{avgstator,i} = 0.5 \cdot (\rho_{2,i} + \rho_{3,i}) \quad \text{for } i = 1 \text{ to stages}$$

$$\mu_{avgstator,i} = 0.5 \cdot (\mu_{2,i} + \mu_{3,i}) \quad \text{for } i = 1 \text{ to stages}$$

$$C_{avgstator,i} = 0.5 \cdot (C_{2,i} + C_{3,i}) \quad \text{for } i = 1 \text{ to stages}$$

STATOR OUTLET CONDTIONS

$$\frac{p_{avgstator,i}}{p_{0avgstator,i}} \cdot (p_{03,i} - p_{02,i}) \cdot 1000 + 0.5 \cdot \rho_{avgstator,i} \cdot C_{avgstator,i}^{2} \cdot \left[\frac{1}{T_{0avgstator,i} + 273.15}\right] \cdot (T_{03,i} - T_{02,i}) + w_{total,stator,i} \cdot (p_{02,i} - p_{2,i}) \cdot 1000 = ($$

$h_{03,i} = h_{02,i}$ for i = 1 to stages

$h_{03,i} = h_{3,i} + 0.001 \cdot 0.5 \cdot C_{3,i}^{2}$ for i = 1 to stages

$$p_{03,i} = p_{3,i} \cdot \left[\left(1 + \left[\frac{\gamma - 1}{2}\right] \cdot M_{3,i}^{2}\right)^{\left(\frac{\gamma}{\gamma - 1}\right)}\right]$$ for i = 1 to stages

$$T_{03,i} + 273.15 = (T_{3,i} + 273.15) \cdot \left[1 + \left(\frac{\gamma - 1}{2}\right) \cdot M_{3,i}^{2}\right]$$ for i = 1 to stages

$h_{3,i} = \mathbf{h}(G1\$, T = T_{3,i})$ for i = 1 to stages

$\rho_{3,i} = \rho(G1\$, T = T_{3,i}, P = p_{3,i})$ for i = 1 to stages

$s_{3,i} = \mathbf{s}(G1\$, T = T_{3,i}, P = p_{3,i})$ for i = 1 to stages

$\mu_{3,i} = \mathbf{Visc}(G1\$, T = T_{3,i})$ for i = 1 to stages

$$M_{3,i} = \frac{C_{3,i}}{\sqrt{\gamma \cdot R_{air} \cdot (T_{3,i} + 273.15)}}$$ for i = 1 to stages

$$C_{a3,i} = \frac{\dot{m}}{\rho_{3,i} \cdot A_{3,i}}$$ for i = 1 to stages

$C_{a3,i} = C_{3,i} \cdot \mathbf{cos}(\theta_{3,i})$ for i = 1 to stages

$C_{w3,i} = C_{3,i} \cdot \mathbf{sin}(\theta_{3,i})$ for i = 1 to stages

$\delta_{s,i} = \theta_{3,i} - \theta_{3B,i}$ for i = 1 to stages

OVERALL STAGE PARAMETERS

$$PR_i = \frac{p_{03,i}}{p_{01,i}}$$ for i = 1 to stages

$Q_i = \dot{m} \cdot (h_{03,i} - h_{01,i})$ for i = 1 to stages

$T_{03s,i} = \mathbf{T}(G1\$, s = s_{1,i}, P = p_{03,i})$ for i = 1 to stages

$h_{03s,i} = \mathbf{h}(G1\$, s = s_{1,i}, P = p_{03,i})$ for i = 1 to stages

$Q_{s,i} = \dot{m} \cdot (h_{03s,i} - h_{01,i})$ for i = 1 to stages

$$\eta_{s,i} = \frac{Q_{s,i}}{Q_i}$$ for i = 1 to stages

OVERALL MACHINE PARAMETERS

$$Z = \dot{m} \cdot \sum_{i=1}^{stages} (X_i) \quad \text{Compressor torque}$$

$$POWER = Z \cdot \omega \quad \text{Compressor power}$$

$$p_{0e} = p_{03,3}$$

$$PR = \frac{p_{0e}}{p_{0i}} \quad \text{Stagnation pressure ratio}$$

$$\Delta P = p_{03,3} - p_{01,1} \quad \text{Stagnation pressure difference}$$

$$\Delta P_{ss} = p_{3,3} - p_{1,1} \quad \text{Static pressure difference}$$

$$CM = \frac{\dot{m} \cdot \left[\sqrt{T_{0i} + 273.15}\right]}{p_{0i}} \quad \text{Corrected mass flow}$$

$$CS = \frac{\frac{N}{60}}{\sqrt{T_{0i} + 273.15}} \quad \text{Corrected speed}$$

$$Q_c = \dot{m} \cdot c_p \cdot (T_{03,3} - T_{0i})$$

$$Q_{star} = \frac{Q_c}{p_{0i} \cdot \sqrt{T_{0i}}} \quad \text{Non-dimensional power}$$

$$h_{0i} = h_{01,1}$$

$$h_{0e} = h_{03,3}$$

$$Q = \dot{m} \cdot (h_{0e} - h_{0i}) \quad \text{Compressor work}$$

$$h_{0es} = h(G1\$, s = s_{1,1}, P = p_{0e})$$

$$Q_s = \dot{m} \cdot (h_{0es} - h_{0i}) \quad \text{Compressor Isentropic work}$$

$$\eta_s = \frac{Q_s}{Q} \quad \text{Isentropic Efficiency}$$

APPENDIX F.4

Performance Prediction Formatted Equations

This section presents the various flow field prediction methods presented in Table 5.1. This equations is the sub-section programs and is called from the main program.

F.4.1 Function to linearly interpolate

Function **Interpol** (A, B, Y1, Y2, X)

If (Y1 >= Y2) Then

$$\text{Interpol} := \frac{\left[A - \left(X + 1.0 \times 10^{-15}\right)\right] \cdot \left[\left|Y1 - Y2\right|\right]}{\left|A - B\right|} + Y1$$

Else

$$\text{Interpol} := -\left[\frac{\left(A - \left[X + 1.0 \times 10^{-15}\right]\right) \cdot \left(\left|Y1 - Y2\right|\right)}{\left|A - B\right|} - Y1\right]$$

EndIf

End **Interpol**

F.4.2 Minimum loss incidence – Lieblein

MINIMUM LOSS INCEDENCE

$i_{0.10.1}=0.02857143*\text{beta}_1$ Figure 3.2 for sigma=0.4

$i_{0.10.2}=-0.01525+0.20391*\text{beta}_1-0.00342769*\text{beta}_12+0.0000862955*\text{beta}_13-7.04167e-7*\text{beta}_14$ Figure 3.2 for sigma=2

$i_{0.10}=\text{Interpol}(0.4,2,i_{0.10.1,i.0.10.2,\text{sigma}})$

$n_1=-0.0522-0.00302*\text{beta}_1-0.0000393*\text{beta}_12$ Figure 3.1 for sigma=0.4

$n_2=-0.011821+0.00017691*\text{beta}_1+0.00000606*\text{beta}_12-6.12e-7*\text{beta}_13$ Figure 3.1 for sigma=2

$n=\text{Interpol}(0.4,2,n_{1,n.2,\text{sigma}})$

$K_{sh}=1$ Shape factor for NACA 65 blades

$K_t=0.001499+18.395*(t/c)-105.283*(t/c)^2+260.4167*(t/c)^3$ Figure 3.3

$i_0=K_{sh}*K_t*i_{0.10}$ Equation 3.2

$i_{min}=i_0+n*\text{theta}_{camber}-1$ Equation 3.3

MODULE **Minimum**$_{incedence}$ (β_1, σ, t, c, θ_{camber}, s, o, M_1, β_{1B} : i_{min})

$$\beta_{1min} = \arccos\left[\frac{o}{s \cdot (0.155 \cdot M_1 + 0.935)}\right]$$ Equation 3.4

$$i_{min} = \beta_{1min} - \beta_{1B}$$

END **Minimum**$_{incedence}$

F.4.3 Stalling -, Optimum Incidence and Deviation – Wright and Miller

Procedure **StalledDeviation** (inc, stagger, θ_{camber}, σ, c, space, ρ_1, ρ_2, C_{a1}, C_{a2}, t_{max}, δ_{Re} : i_{st}, δ_{opt}, δ, l_p, i_{opt})

STALLING -, OPTIMUM INCIDENCE AND DEVIATION WRIGHT AND MILLER

$m := 0.001667 \cdot \theta_{camber} + 0.2133$ Figure 3.12

$m_1 := 0.3333 \cdot \theta_{camber} + 3.667$ Figure 3.12

$m_2 := -0.04742 \cdot \theta_{camber}^2 + 3.319 \cdot \theta_{camber} + 2.55$ Figure 3.12

$\delta_{opt} := 1.13 \cdot m \cdot \left[\theta_{camber} \cdot \sqrt{\frac{space}{c}} + 3 \right] + m_1 \cdot \left[\frac{\rho_1 \cdot C_{a1}}{\rho_2 \cdot C_{a2}} - 1 \right] + m_2 \cdot (t_{max}/c - 0.05) + 0.8$

$A := 0.00002 \cdot stagger^3 - 0.0039 \cdot stagger^2 + 0.255 \cdot stagger + 6.8151$ Figure 3.4

$B := -0.12 \cdot stagger + 8.2$ Figure 3.4

$c := 1.0 \times 10^{-6} \cdot stagger^3 - 0.0002 \cdot stagger^2 + 0.0146 \cdot stagger + 0.0843$ Figure 3.4

$X := 0.00003 \cdot stagger^3 - 0.004 \cdot stagger^2 + 0.3536 \cdot stagger - 2.0266$ Figure 3.4

$Y := -0.0915 \cdot stagger + 6.3$ Figure 3.4

$Z := -4.0 \times 10^{-7} \cdot stagger^3 - 0.00001 \cdot stagger^2 + 0.0073 \cdot stagger + 0.0995$ Figure 3.4

$i_{st} := A + B \cdot \sigma - c \cdot \theta_{camber}$ Equation 3.6

$i_{opt} := X + Y \cdot \sigma - Z \cdot \theta_{camber}$ Equation 3.5

$l_p := \frac{inc - i_{opt}}{i_{st} - i_{opt}}$ abs(inc) to be in contex with parameter

```
If ( stagger > 50 ) Then
   AA := 1
  Else
   If (( stagger <= 50 ) and ( stagger >= 25 )) Then
      AA := 0.08 · stagger - 3
     Else
      AA := -1
   EndIf
EndIf
If ( lp < 0.5 ) Then
   D := 0.7 · exp ( 0.55 · ( lp + AA )) - 0.85   Figure 3.13
  Else
   If (( lp >= 0.5 ) and ( lp < 2 )) Then
      D := 0.4696 · ( lp + AA ) - 0.15
     Else
      If (( lp >= 2) and (lp <= 3)) Then
         D := 0.0213 · ( lp + AA )^5 - 0.1561 · ( lp + AA )^4 + 0.3197 · ( lp + AA )^3 - 0.0755 · ( lp + AA )^2 + 0.1683 ( lp + AA ) - 0.0002
        Else
         D := 1
      EndIf
   EndIf
EndIf
δ := D · ( ist - iopt ) + δopt + δRe
End StalledDeviation
```

F.4.4 Choking incidence – van Antwerpen

CHOKING INCIDENCE AUTHOR

MODULE **Choking** (l_1, c, t_{max}, ζ, σ, gamma1, s_{space}, V_{max}, V_1, β_2, M_1, ρ_1, β_B, β_1, ch_{val} : β_{ch}, i_{choke}, o, M_{ch})

$l_2 = 0.9$ Any constant, $t_{max}/c=0.1$

$$\frac{\rho_{ps}}{\rho_1} = 1 - X \cdot \left[1 - A_{p,STAR} - 0.2445 \cdot \frac{\tan(\beta_{ch})}{\cos(\beta_{ch})} \cdot \sigma \cdot \Gamma \right]$$ Equation B.7

$$V_{ps} = V_1 \cdot \left[(\sin(\beta_{ch}) - 0.2445 \cdot \sigma \cdot \Gamma)^2 + \left(\frac{\cos(\beta_{ch})}{A_{p,STAR} \cdot \frac{\rho_{ps}}{\rho_1}} \right)^2 \right]^{0.5}$$ Equation B.8

$$\Gamma = \cos(\beta_{ch}) \cdot \left[\frac{\tan(\beta_{ch}) - \tan(\beta_2)}{\sigma} \right]$$ Equation B.10

$$A_{p,STAR} = \frac{1 - 0.4458 \cdot \sigma \cdot \frac{t_{max}}{c}}{\cos\left[\frac{\beta_{ch} + \beta_2}{2} \right]}$$ Equation B.9

$$o = c \cdot \left[\frac{\cos(\zeta)}{\sigma} - l_1 - l_2 \cdot \left(\frac{t_{max}}{c} - 0.1 \right) \right]$$ Equation 3.7

$$ch_{val} \cdot \frac{o}{s_{space} \cdot \cos(\beta_1)} = M_{ch} \cdot \left[\left(\left[\frac{gamma1 + 1}{2} \right] \cdot \left[1 - \left(\frac{gamma1 - 1}{gamma1 + 1} \right) \cdot M_{ch}^2 \right] \right)^{\left(\frac{1}{gamma1 - 1} \right)} \right]$$ Equation B.6

$$X = \frac{M_{ch}^2}{1 - M_{ch}^2}$$

$$\cos^2(\beta_{ch}) = \frac{\frac{\rho_{ps}}{\rho_1} \cdot V_{ps} \cdot o}{V_1 \cdot s_{space}}$$ Equation B.5

$i_{choke} = \beta_{ch} - \beta_B$ Equation B.11

END **Choking**

```
Procedure ChokeGraph (c, s_space, ζ : l1, l2)
  func := (s_space / c) · sin(ζ)
  l1 := Interpol (10, 50, l1_one, l1_two, ζ)
  If (ζ >= 50) Then
    If (func <= 0.2) Then
      l2 := 5664 · func^5 - 1671.3 · func^4 + 127.21 · func^3 - 19.94 · func^2 + 0.838 · func + 1
    Else
      l2 := 0.526
    EndIf
  Else
    If (ζ >= 40) Then
      If (func <= 0.4) Then
        l2 := - 3.0425 · func^3 + 0.4618 · func^2 - 0.847 · func + 1.0101
      Else
        l2 := 0.55
      EndIf
```

```
      Else
        If (ς >= 10) Then
          If (func < 0.65) Then
            I2 := 0.8813 · func^4 + 0.4884 · func^3 − 2.5015 · func^2 + 0.4861 · func + 0.9998
          Else
            If ((func >= 0.65) and (func <= 0.82)) Then
              I2 := 0.55
            Else
              I2 := 35.137 · func^4 − 144.79 · func^3 + 222.27 · func^2 − 151.61 · func + 39.363
            EndIf
          EndIf
        EndIf
      EndIf
End ChokeGraph

Procedure Choking_val (o, s_space, β1 : ch_val)
  X := s_space · cos(β1)
  If (o <= X) Then
    ch_val := 1
  Else
    ch_val := 0
  EndIf
```

F.4.5 Test to determine if blade row is chocked

```
Procedure Blade_Choke (i, inc, i_choke : choke$)
TEST TO DETERMINE IF BLADEROW IS CHOCKED
  If (inc < i_choke) Then
    Call WARNING ('Blade row in stage XXXA is..' , i)
    choke$ := 'Stage is choked'
  Else
    choke$ := 'Not choked'
  EndIf
End Blade_Choke
```

F.4.6 Deviation – Lieblein

Procedure **Deviation** (i, i_{min}, β_1, t, c, θ_{camber}, σ : δ_{min}, δ_{lib}, slope,)

DEVIATION LIEBLEIN

$K_t := 0.01277 + 6.386 \cdot \frac{t}{c} + 36.074 \cdot \left[\frac{t}{c}\right]^2$ Figure 3.8

$K_{sh} := 1$ Shape factor for NACA 65 blades

If ((σ >= 0.4) and (σ < 1.2)) Then

$\delta_{0,10,1} := 0.0043 + 0.00629 \cdot \beta_1 + 0.0000374 \cdot \beta_1^2 + 0.00000109 \cdot \beta_1^3$ Figure 3.9 for sigma=0.4

$\delta_{0,10,2} := -0.01483 + 0.0176 \cdot \beta_1 - 0.000214 \cdot \beta_1^2 + 0.00000821 \cdot \beta_1^3$ Figure 3.9 for sigma=1.2

$\delta_{0,10} :=$ **Interpol** (0.4 , 1.2 , $\delta_{0,10,1}$, $\delta_{0,10,2}$, σ)

Else

$\delta_{0,10,1} := -0.01483 + 0.0176 \cdot \beta_1 - 0.000214 \cdot \beta_1^2 + 0.00000821 \cdot \beta_1^3$ Figure 3.9 for sigma=0.4

$\delta_{0,10,2} := -0.0016575 + 0.0102 \cdot \beta_1 + 0.000962 \cdot \beta_1^2 - 0.0000255 \cdot \beta_1^3 + 3.26 \times 10^{-7} \cdot \beta_1^4$ Figure 3.9 for sigma=2

$\delta_{0,10} :=$ **Interpol** (1.2 , 2 , $\delta_{0,10,1}$, $\delta_{0,10,2}$, σ)

EndIf

$\delta_0 := K_{sh} \cdot K_t \cdot \delta_{0,10}$ Equation 3.11

$m := 0.255 + 0.000583 \cdot \beta_1 - 0.00000969 \cdot \beta_1^2 + 2.652 \times 10^{-7} \cdot \beta_1^3$ Figure 3.6

$b := 0.964 - 0.00304 \cdot \beta_1 + 0.0000622 \cdot \beta_1^2 - 0.00000147 \cdot \beta_1^3$ Figure 3.7

$\delta_{min} := \delta_0 + \frac{m}{\sigma^b} \cdot \theta_{camber}$ Equation 3.10

Off minimum loss deviation angle

If ((β_1 <= 70) and (β_1 > 60)) Then

$slope_1 := 1.006 - 1.526 \cdot \sigma + 0.475 \cdot \sigma^2 + 0.276 \cdot \sigma^3 - 0.132 \cdot \sigma^4$ Figure 3.10 for beta$_1$=60°

$slope_2 := 1.003 - 0.903 \cdot \sigma - 0.696 \cdot \sigma^2 + 1.02 \cdot \sigma^3 - 0.289 \cdot \sigma^4$ Figure 3.10 for beta$_1$=70°

$slope :=$ **Interpol** (60 , 70 , $slope_1$, $slope_2$, β_1)

Else

If ((β_1 <= 60) and (β_1 > 50)) Then

$slope_1 := 0.978 - 1.955 \cdot \sigma + 1.49 \cdot \sigma^2 - 0.475 \cdot \sigma^3 + 0.046 \cdot \sigma^4$ Figure 3.10 for beta$_1$=50°

$slope_2 := 1.006 - 1.526 \cdot \sigma + 0.475 \cdot \sigma^2 + 0.276 \cdot \sigma^3 - 0.132 \cdot \sigma^4$ Figure 3.10 for beta$_1$=60°

$slope :=$ **Interpol** (50 , 60 , $slope_1$, $slope_2$, β_1)

Else

$slope_1 := 0.972 - 2.563 \cdot \sigma + 2.685 \cdot \sigma^2 - 1.288 \cdot \sigma^3 + 0.234 \cdot \sigma^4$ Figure 3.10 for beta$_1$=0

$slope_2 := 0.978 - 1.955 \cdot \sigma + 1.49 \cdot \sigma^2 - 0.475 \cdot \sigma^3 + 0.046 \cdot \sigma^4$ Figure 3.10 for beta$_1$=50°

$slope :=$ **Interpol** (0 , 50 , $slope_1$, $slope_2$, β_1)

EndIf

EndIf

$\delta_{lib} := \delta_{min} + (i - i_{min}) \cdot slope$ Equation 3.12

End **Deviation**

F.4.7 Deviation – Csanady

BOUNDRY LAYER DEVIATION CSANADY

Procedure **BoundryDev**(δ_{lib}, θ_{wake}, space, β_2 : $\delta_{boundry}$, δ_{total})

$H_2 := 1.08$ Wake form factor - Lieblein

$\delta_{star} := H_2 \cdot \theta_{wake}$

$$\Delta := \frac{\delta_{star}}{space \cdot \cos(\beta_2)}$$ Equation 3.20

$$\Theta := \frac{\theta_{wake}}{space \cdot \cos(\beta_2)}$$ Equation 3.19

$\beta_{2IN} := \arctan((1 - \Theta - \Delta) \cdot \tan(\beta_2))$ Equation 3.21

$\delta_{boundry} := \beta_2 - \beta_{2IN}$ Equation 3.22

$\delta_{total} := \delta_{lib} + \delta_{boundry}$ Equation 3.23

End **BoundryDev**

F.4.8 Low Reynolds Number Deviation – Roos

DEVIATION DUE TO LOW REYNOLDS NUMBER ROOS

Procedure **ReynoldsDeviation** (Re, θ_{camber}, s_{space}, c, V_1, V_2, V_{w1}, V_{w2}, β_1, β_2, β_{2B}, δ_{cal} : δ, ε_{SB})

$$\sigma := \frac{c}{s_{space}}$$

TF := 0.006

$$D := 1 - \frac{V_1}{V_2} + \frac{V_{w1} - V_{w2}}{2 \cdot \sigma \cdot V_1}$$ Equation 3.25

$$Re_{CB} = \left[\frac{D + 0.4}{7.5 \cdot \sqrt{TF}}\right] \cdot 10^5 + 10000 + 17766$$ Equation 3.30

$\varepsilon_B := \beta_1 - \beta_2$

if ($Re < Re_{CB}$) Then

$delRe_c := Re_{CB} - Re$ Equation 3.29

$$\varepsilon_{SB} := \varepsilon_B - 0.00000172523 \cdot \theta_{camber} \cdot \frac{s_{space}}{c} \cdot delRe_c$$ Equation 3.31

$\beta_2 := \beta_1 - \varepsilon_{SB}$

$\delta := \beta_2 - \beta_{2B} - \delta_{cal}$

Else

$\delta := 0$

$\varepsilon_{SB} := \varepsilon_B$

EndIf

End **ReynoldsDeviation**

F.4.9 Operating Range – Casey

CASEY OPERATING RANGE

Procedure **Opp**$_{Range}$ (i, i_{min}, M_1, β_{1B}, σ_{rotor}, $\theta_{camber,rotor}$: δ_{beta})

If ($M_1 < 0.2$) Then

$K_m := 1$ Equation 4.33

Else

$K_m := 10^{(-2.5 \cdot (M_1 - 0.2)^{4.4})}$ Equation 4.34

EndIf

$$\delta_{beta,i} := 21 + \frac{0.001 \cdot \left[1 + \sqrt{\sigma_{rotor}}\right] \cdot (-40 - 7 \cdot (\beta_{1B} - 45) + 0.25 \cdot (\beta_{1B} - 45)^2 - 0.02 \cdot (\beta_{1B} - 45)^3)}{\sigma_{rotor} \cdot \theta_{camber,rotor}}$$ Equation 4.31

$\delta_{beta} := \delta_{beta,i} \cdot K_m$ Equation 4.30

End **Opp**$_{Range}$

F.4.10 Test to determine if blade row is stalled – Casey

TEST TO DETERMINE IF BLADEROW IS STALLED BY CASEY

Procedure **Blade**$_{Stall}$ (i, $\dot{m}$, i_r, $i_{min,r}$, δ_{beta} : inop$)

if $\left[\left| i_r - i_{min,r} \right| >= 0.8 \cdot \frac{\delta_{beta}}{2} \right]$ Then Equation 1.2

Call WARNING ('The massflow is XXXA' , $\dot{m}$)

Call WARNING ('Blade row in stage XXXA is..' , i)

inop$:= 'Stage is stalled'

Else

inop$:= 'In operating range'

EndIf

End **Blade**$_{Stall}$

APPENDIX F.5

Loss Model Formatted Equations

F.5.1 Blade Profile Losses

BLADE PROFILE LOSS MODELS

$a := 0.0117$ Factor in equation for equivalent diffusion ratio - Lieblein

$H_2 := 1.08$ Wake form factor - Lieblein

Diffusion factor equation Lieblein on-design conditions

$D_{eq}=(\cos(\beta_2)/\cos(\beta_1))*(1.12+0.61*(\cos(\beta_1))^2/\sigma)*(\tan(\beta_1)-\tan(\beta_2))$ Equation 4.14

Diffusion factor equation Lieblein off-design conditions

$D_{eq}=(\cos(\beta_2)/\cos(\beta_1))*(1.12+a*ABS(i-i_{min})^{1.43}+0.61*((\cos(\beta_1))^2/\sigma)*(\tan(\beta_1)-\tan(\beta_2))$ Equation 4.24

Diffusion factor equation Kiapproth

$U_1 := \omega \cdot r_1$

$$K := \tan(\beta_1) - \frac{r_2 \cdot C_{a2}}{r_1 \cdot C_{a1}} \cdot \tan(\beta_2) - \frac{U_1}{C_{a1}} \cdot \left[1 - \frac{r_2^2}{r_1^2}\right]$$ Equation 4.16

$$D_{eq} := \frac{C_{a1} \cdot \cos(\beta_2)}{C_{a2} \cdot \cos(\beta_1)} \cdot \left[1.12 + 0.61 \cdot \frac{\cos^2(\beta_1)}{\sigma} \cdot K\right]$$ Equation 4.15

Diffusion factor equation Wright and Miller

$D_{eq}=(1-(V_2/V_1)+(0.1+(tc)*(10.116-34.15*(tc)))*(s/c)*(V_{w1}-V_{w2})/V_1)*(V_1/V_2)+1$ Equation 4.23

Maksimum velocity in cascade Jansen and Moffatt

$$E := 0.4 + \frac{t}{c}$$ Equation 4.53

$$F := 0.03 + 0.7 \cdot \frac{t}{c}$$ Equation 4.53

$$V_{max} := V_1 \cdot \left[1 + E \cdot \left(\frac{V_{w1} - V_{w2}}{\sigma \cdot V_1}\right) + F\right]$$ Equation 4.52

Wake momentum thickness Casey

$$\theta_{wake} := c \cdot \left[\frac{0.0045}{1 - 0.95 \cdot \ln(D_{eq})} + 0.0025\right]$$ Equation 4.12

$$w_{p1} := 2 \cdot \sigma \cdot \frac{\cos^2(\beta_1)}{\cos^3(\beta_2)} \cdot \frac{\theta_{wake}}{c} \cdot \left[\frac{\frac{2 \cdot H_2}{3 \cdot H_2 - 1}}{\left(1 - \frac{\theta_{wake}}{c} \cdot \frac{\sigma \cdot H_2}{\cos(\beta_2)}\right)^3}\right]$$ Equation 4.11

choking inc

If ($i >= i_{min}$) Then

Off-design correction Casey

$$X := \frac{\left| i - i_{min} \right|}{\frac{\delta_{beta}}{2}}$$ Equation 4.36

$$w_{inc} := 1 + 0.1667 \cdot X + 0.8333 \cdot X^2$$ Equation 4.37

Off-design correction Miller and Wasdell

$w_{inc}=((i-i_{min})/(i_{st}-i_{min}))^2+1$ Equation 4.39

Else

Off-design correction Miller and Wasdell

$w_{inc}=2.25*((i-i_{min})/(i_{min}-i_{choke}))^2+1$ Equation 4.40

Off-design correction Author

$$\Phi := \frac{0.73 \cdot M_1 + 0.01}{489.8 \cdot Re^{-0.5}}$$ Equation C.4

$$w_{inc} := \Phi \cdot \left[\frac{i - i_{min}}{i_{min} - i_{choke}} \right]^2 + 1$$ Equation C.1

EndIf

$$w_p := w_{p1} \cdot w_{inc}$$

ANNULUS LOSS

$$w_a := 0.02 \cdot \sigma \cdot \frac{c}{H} \cdot \frac{\cos^2(\beta_1)}{\cos^3(\beta_m)}$$ Equation 4.43

SECONDARY LOSS

$$w_s := \frac{0.072}{\sigma} \cdot \frac{\cos^2(\beta_1)}{\cos(\beta_m)} \cdot (\tan(\beta_1) - \tan(\beta_2))^2$$ Equation 4.44

TOTAL LOSS

$$w_{total} := w_p \cdot w_{correctR} \cdot w_{correctM} + w_a + w_s \cdot w_{correctR}$$ Equation 4.1

F.5.2 Reynolds Correction – Koch and Smith

REYNOLDS NUMBER CORRECTION FACTOR KOCH AND SMITH

$k_{CLA} := 0.000067$ Centerline average deviation of the roughness particles

$k_s := 6.2 \cdot k_{CLA}$

$Re_c := 200000$ Critical Re_c number $=10^5$

If ($Re <= Re_c$) Then

$$K_{Re} := \left[\frac{Re}{Re_c}\right]^{-0.5}$$ Equation 4.46

$$K_R := \frac{\left[2.635 - 0.618 \cdot \ln\left(\frac{k_s}{c}\right)\right]^{-2.57}}{0.0028}$$ Equation 4.47

Else

$$K_{Re} := \left[\frac{Re}{Re_c}\right]^{-0.166}$$ Equation 4.46

$$K_R := \frac{\left[2.635 - 0.618 \cdot \ln\left(\frac{k_s}{c}\right)\right]^{-2.57}}{0.006}$$ Equation 4.47

EndIf

If ($K_R > K_{Re}$) Then

$w_{correctR} := K_R$

Else

$w_{correctR} := K_{Re}$

EndIf

REYNOLDS NUMBER CORRECTION FACTOR WRIGHT AND MILLER

IF ($Re<10^5$) THEN

$w_{correctR}=489.8*Re^{(-0.5)}$ Equation 4.48

ELSE

IF ($Re>10^5$) AND ($Re<10^6$) THEN

$w_{correctR}=13.8*Re^{(-0.19)}$ Equation 4.48

ELSE

$w_{correctR}=1$ Equation 4.48

ENDIF

ENDIF

F.5.3 Mach Correction – Jansen and Moffatt

MACH NUMBER CORRECTION FACTOR JANSEN AND MOFFATT

MODULE **Mach**$_{Critic}$ (p_{01}, p_1, ρ_1, V, V_{max}, g, γ : $M_{1critic}$)

$$P_{coef} = \left[\frac{V_{max}}{V}\right]^2 - 1 \quad \text{Equation 4.52}$$

$$P_{coef} = \frac{1 - \left[\left(\frac{2}{\gamma + 1} + \left[\frac{\gamma - 1}{\gamma + 1}\right] \cdot M_{1critic}^{\ 2}\right)^{\left(\frac{\gamma}{\gamma - 1}\right)}\right]}{\left[1 + \left(\frac{\gamma - 1}{2}\right) \cdot M_{1critic}^{\ 2}\right]^{\left[\frac{\gamma}{\gamma - 1}\right]} - 1} \quad \text{Equation 4.53}$$

END **Mach**$_{Critic}$

Procedure **Mach**$_{Correct}$ (M, $M_{1critic}$: $w_{correctM}$)

If ($M > M_{1critic}$) Then

$w_{correctM} := 1 + 2 \cdot (M - M_{1critic})$ Equation 4.51

Else

$w_{correctM} := 1$

EndIf

End **Mach**$_{Correct}$

F.5.4 Annulus Blockage Factor

ANNULUS BLOCKAGE FACTOR WRIGHT AND MILLER

SUBPROGRAM **Blockage** (c, β_1, β_2, σ, h, A_{geo}, r_{hb}, r_t, C_{a1}, C_{a2}, ρ_1, ρ_2, μ_1, μ_2, M_1, U_1, U_2, δ_1^{star}, θ_1, γ, τ : δ_2^{star}, θ_2, BF)

$$C_{a,m} = \frac{C_{a1} + C_{a2}}{2}$$

$$\rho_m = \frac{\rho_1 + \rho_2}{2}$$

$$\mu_m = \frac{\mu_1 + \mu_2}{2}$$

$$Re_\theta = \frac{\rho_m \cdot C_{a,m} \cdot \theta_m}{\mu_m}$$

$$U_m = \frac{U_1 + U_2}{2}$$

$$\theta_m = \frac{\theta_1 + \theta_2}{2}$$

$$\tan(\beta_m) = \frac{\tan(\beta_1) + \tan(\beta_2)}{2}$$

$$\theta_2 - \theta_1 = \frac{c \cdot C_f}{2 \cdot \cos(\beta_m)} - \left[\theta_m \cdot (2 + H_m) \cdot \left(\frac{C_{a2} - C_{a1}}{C_{a,m}}\right)\right] + \frac{F_{xs}}{\rho_m \cdot C_{a,m}^{\ 2}} + \frac{F_{xt}}{\rho_m \cdot C_{a,m}^{\ 2}} \quad \text{Equation 4.60}$$

$$\frac{F_{xs}}{\rho_m \cdot C_{a,m}^2} = (C_{Dl} + C_{Ds}) \cdot \frac{h}{2} \cdot \sigma \cdot \cos^2(\beta_m)$$ Equation 4.61

$$\frac{F_{xt}}{\rho_m \cdot C_{a,m}^2} = \frac{0.9 \cdot \tau}{2 \cdot \cos^2(\beta_m)} \cdot \sigma^2 \cdot C_L^{3.1} - \frac{1.7 \cdot \theta_m \cdot \sin(2 \cdot \beta_m)}{2} \cdot (1 - \exp(-\sigma)) \cdot \frac{U_m}{C_{a,m}}$$ Equation 4.62

$$C_{Dl} = 0.97 \frac{\tau}{h} \sigma \cdot C_L^{3.1}$$ Equation 4.63

$$C_{Ds} = \frac{0.04}{2} \cdot \frac{c}{h} \cdot C_L^{4.66}$$ Equation 4.64

$$C_L = \frac{2}{\sigma} \cdot \left[\left|\tan(\beta_1) - \tan(\beta_2)\right|\right] \cdot \cos(\beta_m)$$ Equation 4.65

$$C_f = \frac{0.246 \cdot Re_c^{-0.268} \cdot \exp(-1.56 \cdot H_m)}{1 + 0.6408 \cdot \left[\frac{\gamma - 1}{2}\right] \cdot M_1^2}$$ Equation 4.66

$$H_1 = \frac{\delta^*_1}{\theta_1}$$

$$H_1 = \frac{H^*_1}{H^*_1 - 2}$$

$$H_m = \frac{H^*_m}{H^*_m - 2}$$

$$\frac{1}{c} \cdot (C_{a2} \cdot \theta_2 \cdot H^*_2 - C_{a1} \cdot \theta_1 \cdot H^*_1) = 0.0306 \cdot C_{a,m} \cdot (H^*_m - 3)^{-0.653}$$ Equation 4.68

$$H_2 = \frac{H^*_2}{H^*_2 - 2}$$ Equation 4.67

$$H_2 = \frac{\delta^*_2}{\theta_2}$$

$$H_m = \frac{H_1 + H_2}{2}$$

$$H_m = \frac{\delta_{star,m}}{\theta_m}$$

$$\delta^*_m = \frac{\delta^*_1 + \delta^*_2}{2}$$

$$\delta_{hb} = \delta^*_m$$

$$\delta_t = \delta^*_m$$

$$B^c = 1 - \frac{2 \cdot \pi \cdot (r_{hb} \cdot \delta_{hb} + r_t \cdot \delta_t)}{A_{geo}}$$ Equation 4.70

END **Blockage**

APPENDIX F.6

Optimization Algorithm

An optimization code was created to generate empirical correlations. These empirical constants are used in the correctional slope factor which in turn gives a variation in the gradient of the off-design correction parabola. The optimization code used the same sub-sections presented in Appendix F.4 and F.5 only now using a two dimensional array as input. Experimental data from work done by Von Backström (2005) is read into the optimization program for a specific rotational speed. Simulation results are then compared with experimental data. Using the least square method answers for the desired empirical constants are calculated resulting in the least amount of error between simulation and experimental results. Input data can vary from one to a range of experimental measurements.

APPENDIX G

Derivation Non-Dimensional Power

Problems with using isentropic efficiency arise when calculating work transfer rate for a compressor in all of the relevant quadrants. Thus a new and more generically applicable representation of the work transfer to the compressor element is required. The section below illustrates the derivation of a non-dimensionlal power variable, which is intended for use to calculated compressor power in all of the relevant quadrants.

The relation of pressure and temperature for a compressor is described in Cohen *et al.* (2001:57) and is given by:

$$T_{0e} - T_{0i} = \frac{T_{0i}}{\eta_c}\left[\left(\frac{p_{0e}}{p_{0i}}\right)^{(\gamma-1)/\gamma} - 1\right] \tag{G.1}$$

If one defines the power to a compressor as:

$$\dot{\mathbb{Q}}_c = \dot{m}C_p(T_{0e} - T_{0i}) \tag{G.2}$$

Substitution of (G.1) into (G.2) leads to:

$$\dot{\mathbb{Q}}_c = \frac{\dot{m}C_pT_{0i}}{\eta_c}\left[\left(\frac{p_{0e}}{p_{0i}}\right)^{(\gamma-1)/\gamma} - 1\right] \tag{G.3}$$

When using dimensional analysis, variables involved may be combined to form a smaller and more manageable number of dimensional groups. Cohen *et al.* (2001:173) demonstrated that the important variables used in turbomachinery are:

$$f\left(D, N, \dot{m}, p_{0i}, p_{0e}, RT_{0i}, RT_{0e}\right) = 0 \tag{G.4}$$

When these variables are written in its most useful non-dimensional form, these groups emerge:

$$f\left(\frac{p_{0e}}{p_{0i}}, \frac{T_{0e}}{T_{0i}}, \frac{\dot{m}\sqrt{RT_{0i}}}{D^2p_{0i}}, \frac{ND}{\sqrt{RT_{0i}}}\right) = 0 \tag{G.5}$$

The temperature deferential over a compressor can be presented as follows:

$$\Delta T_{0,c} = T_{0e} - T_{0i} \tag{G.6}$$

By replacing the variable RT_{0e} in (G.4) with $R\Delta T_{0,c}$, (G.5) leads to the following set of non-

dimensional variables:

$$f\left(\frac{p_{0e}}{p_{0i}}, \frac{\Delta T_{0,c}}{T_{0i}}, \frac{\dot{m}\sqrt{RT_{0i}}}{D^2 p_{0i}}, \frac{ND}{\sqrt{RT_{0i}}}\right) = 0 \tag{G.7}$$

Next, consider the new non-dimensional variable formed by multiplying $\frac{\Delta T_{0,c}}{T_{0i}}$ with $\frac{\dot{m}\sqrt{RT_{0i}}}{D^2 p_{0i}}$:

$$\left(\frac{\Delta T_{0,c}}{T_{0i}}\right)\left(\frac{\dot{m}\sqrt{RT_{0i}}}{D^2 p_{0i}}\right) = \frac{\dot{m}\Delta T_{0,c}\sqrt{R}}{D^2 p_{0i}\sqrt{T_{0i}}} \tag{G.8}$$

When one defines the work (power) transfer rate to a horizontally mounted compressor as displayed in (G.2), substitution of (G.2) into (G.8) leads to:

$$\frac{\dot{m}\Delta T_{0,c}\sqrt{R}}{D^2 p_{0i}\sqrt{T_{0i}}} = \left(\frac{R}{c_p}\right)\frac{\dot{\mathbb{Q}}_c}{D^2 p_{0i}\sqrt{RT_{0i}}} \tag{G.9}$$

after some manipulation.

The ratio R/c_p can be rewritten as presented by Cohen *et al.* (2001:66):

$$\frac{R}{c_p} = \frac{\gamma - 1}{\gamma} \tag{G.10}$$

Substitution of (G.10) into (G.9) leads to:

$$\frac{\dot{m}\Delta T_{0,c}\sqrt{R}}{D^2 p_{0i}\sqrt{T_{0i}}} = \left(\frac{\gamma - 1}{\gamma}\right)\frac{\dot{\mathbb{Q}}_c}{D^2 p_{0i}\sqrt{RT_{0i}}} \tag{G.11}$$

Disregarding the influence of the property γ, it follows that $\frac{\dot{m}\Delta T_{0,c}\sqrt{R}}{D^2 p_{0i}\sqrt{T_{0i}}}$ is directly proportional to $\frac{\dot{\mathbb{Q}}_c}{D^2 p_{0i}\sqrt{RT_{0i}}}$. The latter variable can therefore be used to replace the variable $\frac{\Delta T_{0,c}}{T_{0i}}$ in (G.7), leading to the following set of non-dimensional variables:

$$f\left(\frac{p_{0e}}{p_{0i}}, \frac{\dot{\mathbb{Q}}_c}{D^2 p_{0i}\sqrt{RT_{0i}}}, \frac{\dot{m}\sqrt{RT_{0i}}}{D^2 p_{0i}}, \frac{ND}{\sqrt{RT_{0i}}}\right) = 0 \tag{G.12}$$

The isentropic can now be replaced with the non-dimensional work (power) transfer rate variable

$\frac{\dot{Q}_c}{D^2 p_{0i}\sqrt{RT_{0i}}}$. Defining a compressor as a device delivering power to the fluid and a turbine as a device extracting power from the fluid, the sign of $\frac{\dot{Q}_c}{D^2 p_{0i}\sqrt{RT_{0i}}}$ will indicate whether the turbo machine is functioning as a compressor or a turbine. When looking at an axial flow compressor, a positive sign indicates that the turbo machine is in the compressor mode and a negative sign indicates that the turbo machine is in the turbine mode of operation.

Considering a compressor of fixed geometry operating with a specified fluid, R and D may be omitted as done by Cohen *et al.* (2001:174) and the non-dimensionlal power $\dot{Q}$ can be defined by:

$$\dot{Q} = \frac{\dot{Q}_c}{p_{0i}\sqrt{T_{0i}}} \tag{G.13}$$

Traditionally isentropic efficiency of an axial compressor was plotted against two non-dimensionlal variables to obtain a set of curves as showed in (G.14):

$$\eta_c = f\left(\frac{\dot{m}\sqrt{T_{0i}}}{p_{0i}}, \frac{N}{\sqrt{T_{0i}}}\right) \tag{G.14}$$

Instead of using (G.14) for calculating the work (power) transfer rate, the following function can be used to obtain a set of curves:

$$\frac{\dot{Q}_c}{p_{0i}\sqrt{T_{0i}}} = f\left(\frac{\dot{m}\sqrt{T_{0i}}}{p_{0i}}, \frac{N}{\sqrt{T_{0i}}}\right) \tag{G.15}$$

The derivation of non-dimensional power can also be located in the Flownex theory manual – Compressor element (2006:13) under the heading "Dimensionless work transfer rate". "Non-dimensional Power" is replaced by the word "Corrected Work" in the Flownex manual.

APPENDIX H

Percentage Error between Simulation & Experimental Results

Different tables are shown to illustrate the % error in comparing simulation with experimental results. It must be noted that the average percentage error was calculated using experimental results without any uncertainty. The %Error is defined as:

$$\%Error = \frac{\left|X_{Experimental} - X_{Simulation}\right|}{\left|X_{Experimental}\right|} \cdot 100 \qquad \text{(H.1)}$$

H.1 Static Pressure Difference (p_3-p_1)

Experimental Results	0 r.p.m.	Simulation Results	0 r.p.m		
Mass flow [kg/s]	ΔPss [Pa]	Mass flow [kg/s]	ΔPss [kPa]	ΔPss [Pa]	%Error
0.180	-71.224	0.18	-0.09979	-99.79	40.107
0.275	-166.391	0.275	-0.1943	-194.3	16.773
0.370	-300.58	0.37	-0.3308	-330.8	10.054
0.464	-466.744	0.464	-0.5199	-519.9	11.389
0.558	-673.233	0.558	-0.7518	-751.8	11.670
0.652	-898.772	0.652	-1.026	-1026	14.156
0.744	-1204.67	0.744	-1.337	-1337	10.985
0.837	-1510.839	0.837	-1.692	-1692	11.991
0.928	-1748.805	0.928	-2.081	-2081	18.996
				% Average =	16.236%

Table H.1 Pressure %error at 0 r.p.m.

Experimental Results	2000 r.p.m.	Simulation Results	2000 r.p.m		
Mass flow [kg/s]	ΔPss [Pa]	Mass flow [kg/s]	ΔPss [kPa]	ΔPss [Pa]	%Error
1.152	1595.841	1.152	1.659	1659	3.958
1.162	1553.340	1.162	1.665	1665	7.188
1.213	1567.081	1.213	1.684	1684	7.461
1.261	1572.859	1.261	1.671	1671	6.240
1.288	1579.676	1.288	1.661	1661	5.148
1.415	1569.253	1.415	1.619	1619	3.170
1.502	1515.741	1.502	1.565	1565	3.250
1.514	1473.711	1.514	1.558	1558	5.720
1.539	1524.721	1.539	1.542	1542	1.133
1.599	1383.187	1.599	1.482	1482	7.144
1.743	1276.376	1.743	1.316	1316	3.104
1.757	1222.656	1.757	1.297	1297	6.081

1.862	1041.672	1.862	1.141	1141	9.535
1.996	877.711	1.996	0.9062	906.2	3.246
2.019	813.812	2.019	0.8614	861.4	5.848
2.028	800.012	2.028	0.8437	843.7	5.461
2.117	621.413	2.117	0.6599	659.9	6.193
2.274	264.397	2.274	0.3007	300.7	13.730
2.434	-209.625	2.434	-0.1112	-111.2	46.953
2.603	-427.552	2.603	-0.5959	-595.9	39.375
2.711	-716.769	2.711	-0.9327	-932.7	30.126
2.787	-927.737	2.787	-1.182	-1182	27.407
2.960	-1570.016	2.96	-1.791	-1791	14.075
3.145	-2323.585	3.145	-2.522	-2522	8.539
3.400	-3591.302	3.4	-3.697	-3697	2.943
				% Average =	**10.921%**

Table H.2 Pressure %error at 2000 r.p.m.

H.2 Torque

Experimental Results	0 r.p.m.	Simulation Results	0 r.p.m	
Mass flow [kg/s]	**Torque [N.m]**	**Mass flow [kg/s]**	**Torque [N.m]**	**%Error**
0.180	-0.457	0.180	-0.2405	47.382
0.275	-0.941	0.275	-0.5603	40.443
0.370	-1.611	0.370	-1.012	37.168
0.464	-2.444	0.464	-1.589	34.975
0.558	-3.380	0.558	-2.295	32.097
0.652	-4.819	0.652	-3.128	35.084
0.744	-6.129	0.744	-4.067	33.640
0.837	-7.320	0.837	-5.141	29.769
0.928	-8.849	0.928	-6.312	28.673
			% Average =	**35.470%**

Table H.3 Torque %error at 0 r.p.m.

Experimental Results	2000 r.p.m.	Simulation Results	2000 r.p.m	
Mass flow [kg/s]	**Torque [N.m]**	**Mass flow [kg/s]**	**Torque [N.m]**	**%Error**
1.152	11.525	1.152	11.63	0.910
1.161	12.293	1.161	11.67	5.068
1.162	11.308	1.162	11.68	3.292
1.213	12.465	1.213	11.87	4.775
1.261	11.708	1.261	11.86	1.297
1.288	12.866	1.288	11.89	7.583
1.415	13.052	1.415	12.28	5.914
1.502	13.340	1.502	12.39	7.118
1.514	12.478	1.514	12.41	0.547
1.539	12.572	1.539	12.46	0.889

1.599	12.227	1.599	12.41	1.499
1.743	12.873	1.743	12.1	6.007
1.757	12.979	1.757	12.05	7.154
1.862	11.427	1.862	11.54	0.985
1.996	10.970	1.996	10.59	3.466
2.019	10.983	2.019	10.39	5.402
2.028	10.815	2.028	10.31	4.666
2.117	11.859	2.117	9.428	20.498
2.274	8.892	2.274	7.583	14.722
2.434	6.340	2.434	5.337	15.822
2.603	1.857	2.603	2.58	38.912
2.693	-0.481	2.693	0.9547	298.374
2.707	-0.424	2.707	0.6167	245.609
2.730	-0.500	2.73	0.2553	151.060
2.787	-1.827	2.787	-0.8576	53.048
2.960	-6.432	2.96	-4.499	30.051
3.145	-12.018	3.145	-8.958	25.464
3.400	-20.567	3.4	-16.24	21.040
3.873	-26.641	3.873	-33.77	26.760
			% Average =	**34.756%**

Table H.4 Torque %error at 2000 r.p.m.

H.3 Power

If one defines power as $\dot{\mathbb{Q}}_c = \omega Z$ the average % error for torque and power should be the same. The reason for the increase in % error can be due to the fact that scaling the experimental data to 2000 r.p.m was not as accurately done.

Experimental Results	2000 r.p.m.	Simulation Results	2000 r.p.m	
Mass flow [kg/s]	**Power [W]**	**Mass flow [kg/s]**	**Power [W]**	**%Error**
1.152	2413.812	1.152	2436	0.919
1.161	2574.654	1.161	2444	5.075
1.162	2368.295	1.162	2445	3.239
1.213	2610.712	1.213	2485	4.815
1.261	2452.154	1.261	2483	1.258
1.288	2694.572	1.288	2490	7.592
1.415	2733.580	1.415	2571	5.948
1.502	2793.819	1.502	2595	7.116
1.514	2613.444	1.514	2600	0.514
1.539	2633.027	1.539	2609	0.913
1.599	2560.755	1.599	2599	1.494
1.743	2696.164	1.743	2535	5.978
1.757	2718.220	1.757	2524	7.145

1.862	2393.357	1.862	2417	0.988
1.996	2297.604	1.996	2218	3.465
2.019	2300.329	2.019	2176	5.405
2.028	2265.004	2.028	2159	4.680
2.117	2483.691	2.117	1975	20.481
2.274	1862.352	2.274	1588	14.731
2.434	1327.875	2.434	1118	15.805
2.603	388.991	2.603	540.3	38.898
2.693	-100.795	2.693	200	298.422
2.707	-88.704	2.707	129.2	245.653
2.730	-61.729	2.73	53.47	186.620
2.787	-382.553	2.787	-179.6	53.052
2.960	-1347.080	2.96	-942.2	30.056
3.145	-2517.109	3.145	-1876	25.470
3.400	-4307.622	3.4	-3402	21.024
3.873	-5579.656	3.873	-7073	26.764
			% Average =	**35.083%**

Table H.5 Power %error at 2000 r.p.m.

APPENDIX I

Mean-line Applicability

Simulation results where compared with experimental work done by Roos (1995)

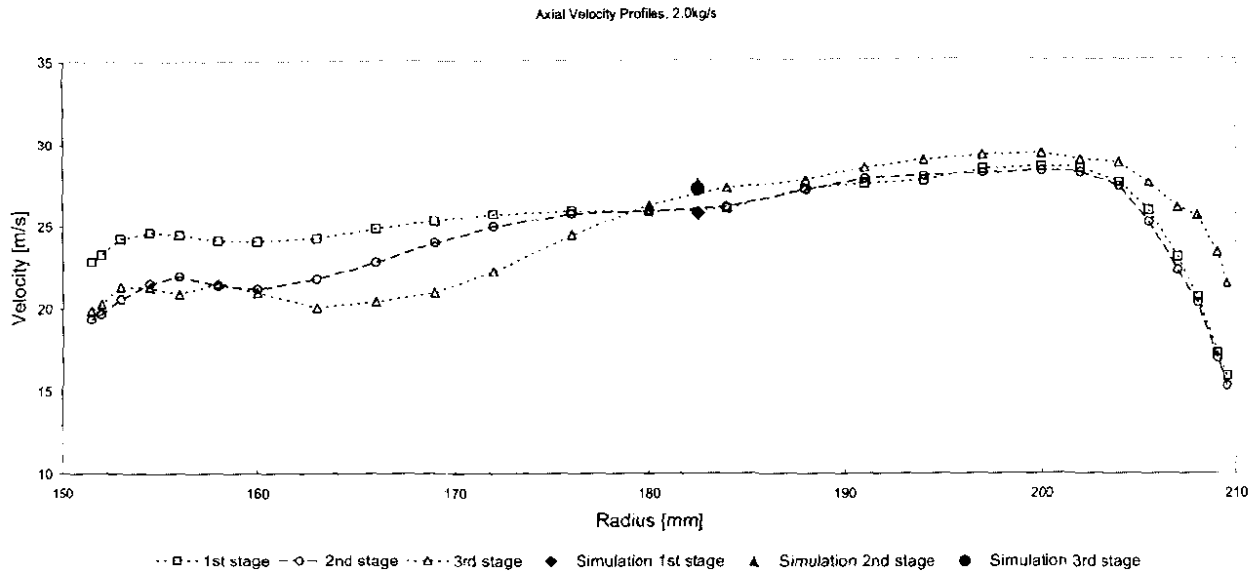

Figure I.1 Axial velocity near surge (Roos, 1995) with simulation results

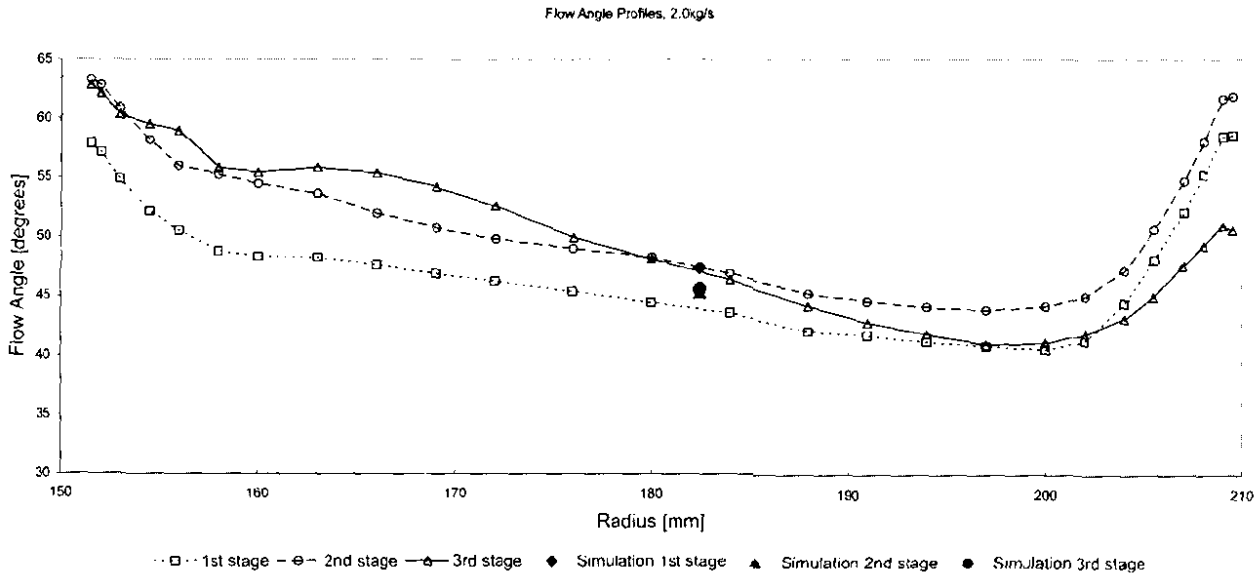

Figure I.2 Flow angles near surge (Roos, 1995) with simulation results

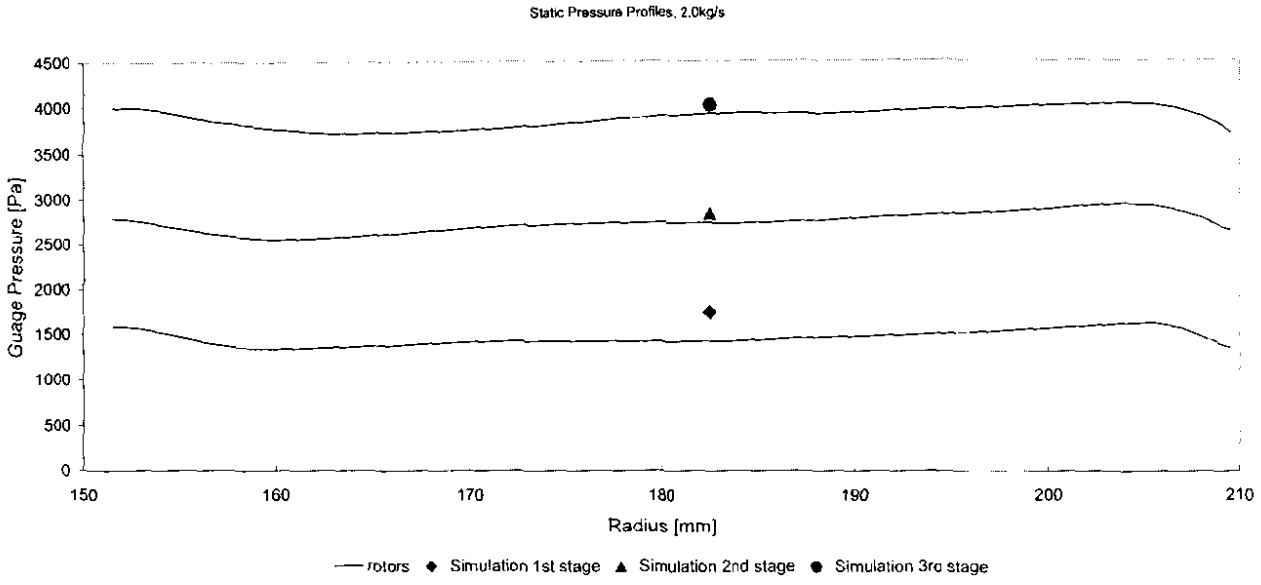

Figure I.3 Total guage pressure near surge (Roos, 1995) with simulation results

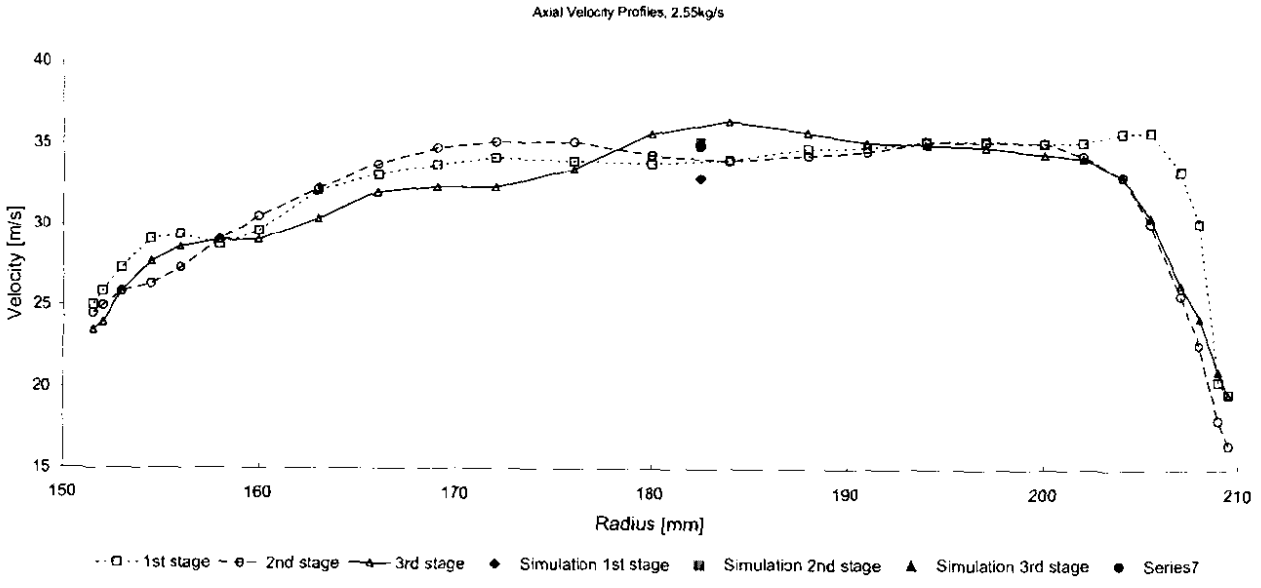

Figure I.4 Axial velocity near design (Roos, 1995) with simulation results

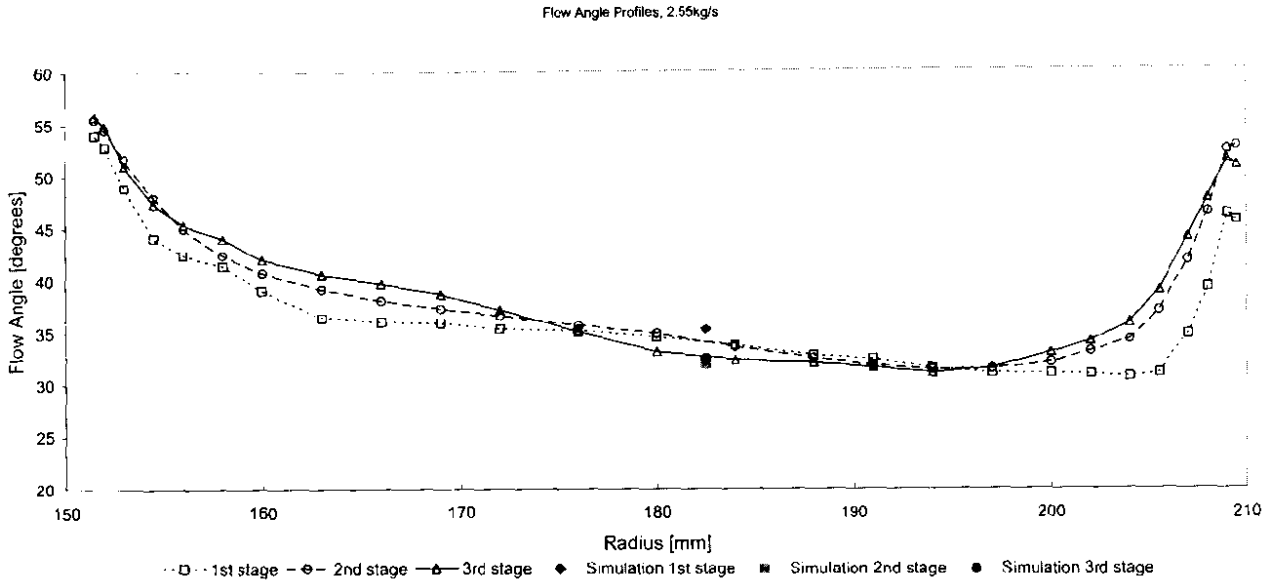

Figure I.5 Flow angles near design (Roos, 1995) with simulation results

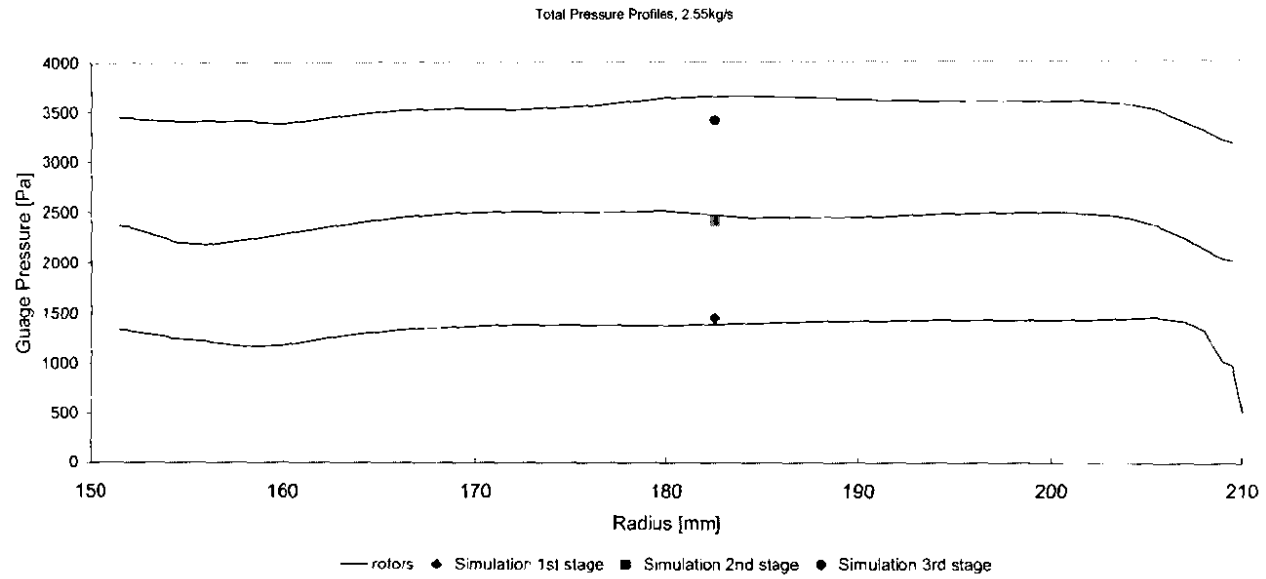

Figure I.6 Total guage pressure near design (Roos, 1995) with simulation results

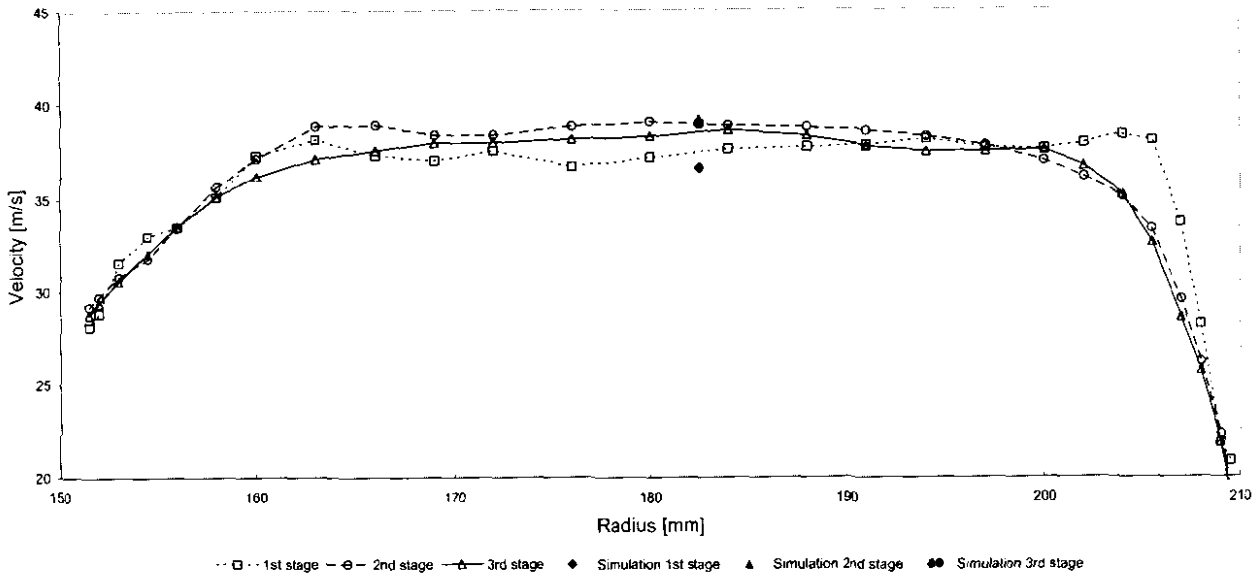

Figure I.7 Axial velocity near choke (Roos, 1995) with simulation results

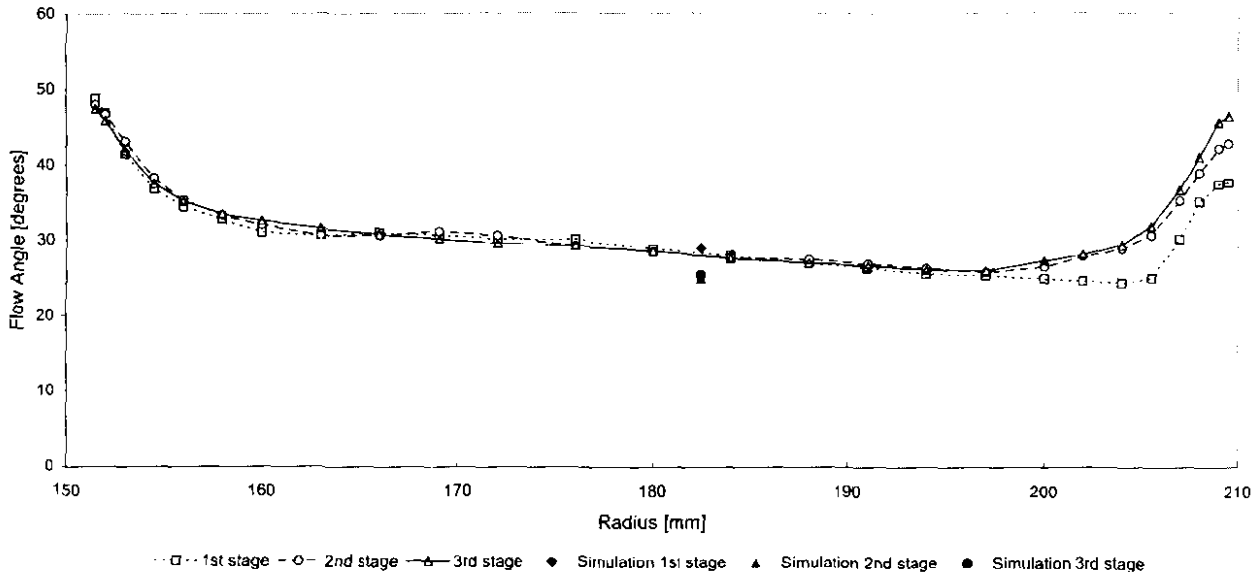

Figure I.8 Flow angles near choke (Roos, 1995) with simulation results

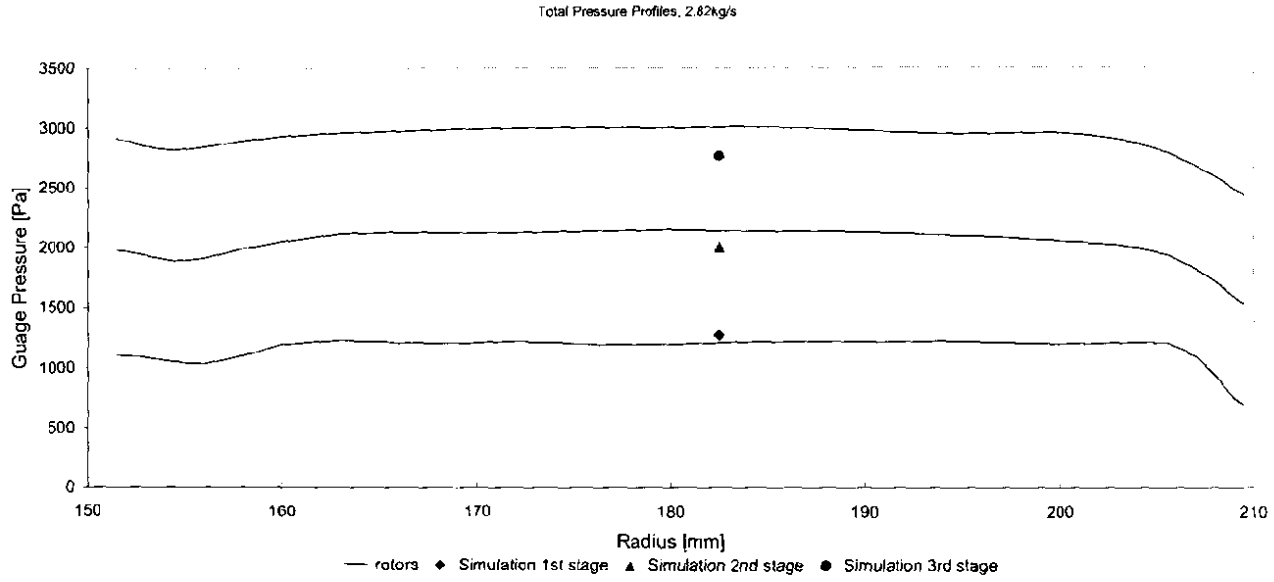

Figure I.9 Total guage pressure near choke (Roos, 1995) with simulation results